

Aus dem Orthopädisch-Unfallchirurgischen Zentrum
der Medizinischen Fakultät Mannheim
Direktor: Prof. Dr. med. Sascha Gravius, MHBA

Mechanical stimulation of mesenchymal stem/stromal cells in a bioreactor
system: An approach to mobilize cells into scaffolds

Inauguraldissertation
zur Erlangung des akademischen Grades
Doctor scientiarum humanarum (Dr. sc. hum.)
der
Medizinischen Fakultät Mannheim
der Ruprecht-Karls-Universität
zu
Heidelberg

vorgelegt von
Jeinmy Carolina Gámez Villamizar

aus
Bogotá, Kolumbien
2020

Dekan: Prof. Dr. med. Sergij Goerd
Referent: Prof. Dr. med. Markus Schwarz

*Dedicada a mi querida familia,
a mis padres y hermanos que con su amor me han enseñado a sonreír
y seguir adelante incluso en los días más grises.*

*Dedicada a Andrés,
por enseñarme que no hay mejor lugar en el mundo que su compañía.*

Dedicada a mí, to the girl I was...

“Caminante no hay camino, se hace camino al andar”, A. Machado.

Table of Contents

1. Introduction	1
1.1. Cartilage tissue	2
1.1.1. Types of cartilage	2
1.2. Cartilage tissue engineering	5
1.2.1. Compressive forces in the knee joint	6
1.2.2. Scaffolds for AC regeneration.....	8
1.2.3. Cell sources for AC regeneration	11
1.3. Mobilization of cells.....	12
1.3.1. Motility of cells in 1D and 2D	12
1.3.2. Motility of cells in 3D	14
1.3.3. Microenvironment and cell mobilization mechanisms	15
2. Aim of the study	17
2.1. General aim	17
2.2. Specific aims	17
3. Animals, material and methods	18
3.1. Animals	18
3.2. Materials.....	18
3.2.1. Cells.....	18
3.2.2. Cell culture reagents.....	18
3.2.3. Scaffold materials.....	18
3.2.4. Antibodies	19
3.2.5. Confocal microscopy.....	19
3.2.6. Bioreactor hardware and software.....	20
3.3. Methods.....	20
3.3.1. Bioreactor specifications	20
3.3.2. Elastic ring preparation	23

3.3.3.	Alginate scaffold preparation	23
3.3.4.	Gelatin and collagen scaffolds	24
3.3.5.	Isolation of porcine bone marrow derived-mesenchymal stromal cells.....	25
3.3.6.	FACS of pBM-MSCs.....	27
3.3.7.	FACS of hBM-MSCs.....	27
3.3.8.	Biomechanical stimulation.....	27
3.3.9.	Viability tests of cells located in the reservoir	29
3.3.10.	Mechanical data analysis.....	30
3.3.11.	Refractive index evaluation.....	30
3.3.12.	Confocal microscopy.....	30
3.3.13.	Pipeline for cell quantification in 3D	31
3.3.14.	Statistical analyses.....	32
4.	Results	34
4.1.	Stiffness tests of elastic ring.....	34
4.2.	Yield of pBM-MSCs isolation	37
4.3.	Immunophenotyping of pBM-MSCs	38
4.4.	Imaging of cells in 3D	41
4.5.	Quantification of cells in 3D	41
4.6.	Continuous and intermittent mechanical stimulation.....	43
4.7.	pBM-MSCs mobilized into alginate and functionalized alginate-Ln scaffolds	44
4.8.	hBM-MSCs mobilized into alginate-Ln scaffolds	45
4.9.	Collagen and gelatin scaffolds fabrication	46
4.10.	Mobilization of hBM-MSCs into collagen scaffolds	49
4.11.	Morphometry of mobilized cells	52
4.12.	Comparison of mechanical stimulation of hBM-MSCs mobilized on different sort of scaffolds	52
4.13.	Analysis of the biomechanical data.....	54
5.	Discussion	57

5.1. Considerations for the established and optimized protocols: Prequel to the mechanical stimulation application on MSCs	58
5.1.1. Bioreactor	58
5.1.2. Alginate scaffolds.....	59
5.1.4. pBM-MSCs isolation and characterization	60
5.1.5. Image analysis pipeline	61
5.2. Mobilization of MSCs into the scaffolds	62
5.2.1. Contrasting our bioreactor system with other studies	62
5.2.2. Culture conditions and continuous vs. intermittent loading.....	63
5.2.3. Scaffold functionalization	64
5.2.4. Image-based analyses	68
5.3. Limitations of the study.....	69
5.4. Conclusions	70
5.5. Outlook.....	71
6. Summary	73
7. References	76
8. Appendix	90
Appendix A	90
Appendix B	92
Appendix C	94
Appendix D	97
Appendix E.....	98
Appendix F.....	99
Appendix G	100
9. Curriculum vitae.....	102
Abbreviations	105
List of figures	107
List of tables	109
Acknowledgments	111

Disclosure: Parts of this thesis have been already published by the author in “**Gamez C**, Schneider-Wald B, Schuette A, Mack M, Hauk L, Khan AUM, Gretz N, Stoffel M, Bieback K, Schwarz ML. “Bioreactor for mobilization of mesenchymal stem/stromal cells into scaffolds under mechanical stimulation: Preliminary results. PLoS One. 2020 Jan 10;15(1):e0227553”. The permission to reuse, reprint, modify, distribute, and/or copy the mentioned article and images was given by PLoS One Journal granted through the CC-BY license.

1. Introduction

Cartilage is considered to not heal. Thus, chondral defects caused by injury or degenerative conditions can be deleterious and harmful and can result in osteoarthritis. The classic surgical therapeutic procedures used for treating lesions in the articular cartilage (AC) are autologous chondrocytes implantation (ACI), mosaicplasty, and microfracture ¹. “The current ACI therapy known as matrix-induced ACI (MACI), consists on isolating the chondrocytes in a first surgery, *in vitro* expansion for several weeks, cell implantation in a matrix, and its implantation in a second surgical procedure ². Mosaicplasty implies the use of osteochondral autologous plugs taken from non-weight bearing regions to transplant them in the defect area. Lastly, microfracture focuses on stimulating the bone marrow through micro-perforations in the subchondral bone, which promotes a blood clot formation in the defect site, containing progenitor cells and growth factors that induces defect healing. Despite their wide application, the clinical outcomes are not fully fulfilled yet, mainly because the repaired tissue is fibrotic with inferior quality biochemical and mechanically in comparison to hyaline cartilage ³” ⁴.
Fragment taken from Gamez C, et al, 2020 with the permission of PLoS One Journal under the CC-BY license.

Impaired AC can lead to joint destruction ⁵ and AC regeneration still remains challenging because the current therapies fail to produce natural-like AC. For instance, the chondrocytes used for *in vitro* expansion dedifferentiate and become senescent after implantation ⁶, mosaicplasty and microfracture can fail or need reoperations ⁷. Therefore, it is relevant to develop approaches that contribute to AC repair.

To have an integral view of the knee joint rather than to examine AC defects as local and isolated entities could provide insights to find complementary or better therapeutic approaches for AC regeneration, i. e., biochemical and mechanical properties of the tissue, neighboring stem cells reservoir and distribution of different nutrient sources.

AC is an avascular viscoelastic tissue with a scarce number of chondrocytes distantly located from each other and contains a complex extracellular matrix (ECM) network that provides functionality and exceptional biomechanical properties for bearing weight ⁸. Nutrients diffuse through the ECM helped by joint motion but the lack of blood supply limits the regeneration potential of AC ^{9,10}.

The main factors to take into account for AC tissue engineering are cell source, scaffolds and bioreactors ¹¹. Therefore, strategies for repairing AC should focus on inducing the mobilization of endogenous stem and progenitor cells, developing scaffolds that provide structure and serve as cell receivers for housing cells while bearing the mechanical environment. Subsequent strategies should assess chondrogenic differentiation of progenitor cells *in situ* and functional physiology of chondrocytes to obtain healthy AC.

An approach *in vitro* is presented here to evaluate whether mechanical stimulation provided by a compression bioreactor induces the mobilization of mesenchymal stromal cells (MSCs) into scaffolds. The hypothesis is based on the microfracture principle of recruiting progenitor cells when the subchondral lamella is opened.

1.1. Cartilage tissue

Cartilage is a connective tissue rich in extracellular matrix (ECM) to the extent of 90 % of its dry weight ¹², mainly composed of collagen and proteoglycans ¹³. Functionality of this tissue depends on the distribution, organization and composition of the ECM.

1.1.1. Types of cartilage

Based on mechanical and histological and properties, cartilage can be classified as elastic, hyaline and fibrous ¹⁴. Elastic cartilage is predominantly composed of elastin, providing support with moderate elasticity. Fibrous cartilage (also known as fibrocartilage) is a tough connective tissue with abundant collagen fibers arranged as bundles, conferring firmness but moderated elasticity ¹⁵. Hyaline is the most abundant type of cartilage in the body. It is present in bronchial tree, nose, developing bones, and in most of the joints or articular surfaces; therefore named as articular cartilage (AC) ¹⁶.

1.1.1.1. Articular cartilage in the knee joint

AC is a resilient viscoelastic connective tissue with limited number of chondrocytes but with a rich and highly organized ECM, composed mainly of collagen and non-collagenous proteins as proteoglycans ¹⁷. AC and fibrocartilage mainly differ from the content collagen type I and

II, being collagen-II the most abundant in AC, whereas fibrocartilage contains more collagen-I¹⁸. AC is smooth, tough and wear-resistant¹⁵; hence, its main function is to distribute loads and decrease friction in the joints and provide lubrication in the diarthrodial joints¹⁹.

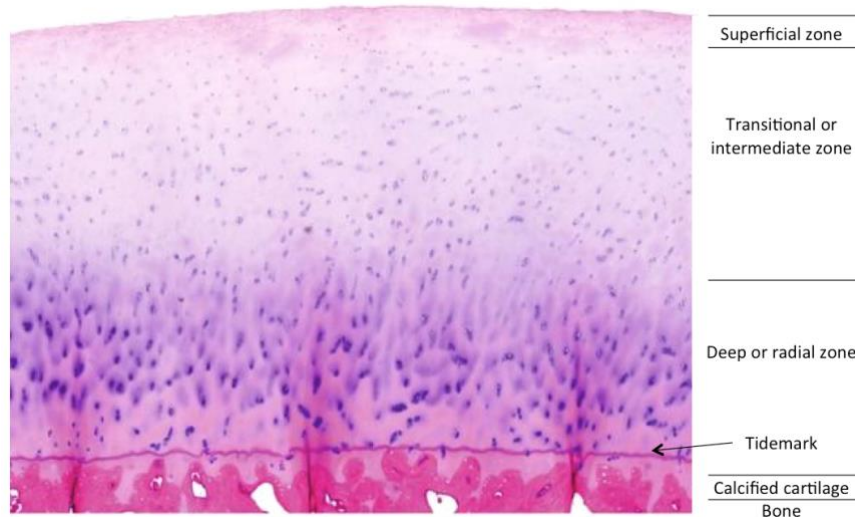


Fig. A1. Histology of articular cartilage. Adult Image AC consists four zones with differential distribution and content in chondrocytes and collagen. Image taken from Ref.²⁰ with the permission of Springer Nature. AC: *Articular cartilage*

Mature AC is anisotropically organized with chondrocytes arranged in columns and three horizontal stratification zones²¹ and the tidemark (Fig. A1). The superficial zone contains flattened, small and immature chondrocytes horizontally constrained and disposed by tangential collagen-II fibers²². The intermediate zone is composed by spherical chondrocytes more loosened within a slightly perpendicular meshwork of collagen fibers. The deep or radial zone contains hypertrophic chondrocytes immersed in big lacunae, which are vertically disposed along the collagen fibers. The tidemark is a mineralized region located between non-calcified and calcified chondrocytes^{14, 22}.

The structural, cellular and biochemical composition of the AC enables compressibility to support weight and to distribute loads of the joints⁸.

1.1.1.2. Articular cartilage injury and disease

Adult normal AC has a thickness of 2 to 4 mm and lacks blood supply, lymphatic vessels and nerves^{23, 24} (Fig. A2). This restricts the direct access to nutrients and limits healing capability

⁹. AC can get naturally degenerated by ageing or impaired as focal defects caused by trauma, which may develop osteoarthritis (OA) if not treated ^{25, 26}.

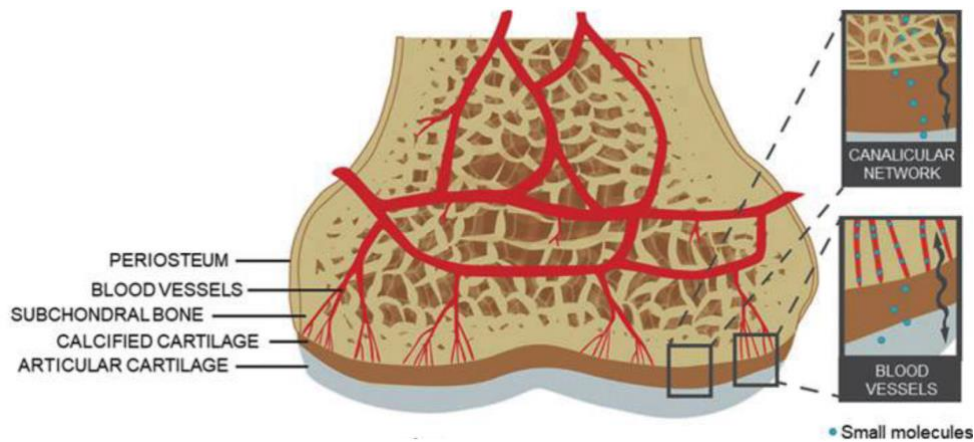


Fig. A2. Blood supply in an osteochondral unit. Blood vessels are located in the bone but not in the cartilage. The small molecules move through the cartilage by diffusion. Image adapted from Ref. ²⁷ with the permission of Mary Ann Liebert, Inc.

1.1.1.3. Current therapies for articular cartilage regeneration

The standard clinical procedures for treating AC defects are autologous chondrocytes implantation (ACI), mosaicplasty, and microfracture (Fig. A3). The current ACI therapy known as matrix-induced ACI (MACI), consists on isolating the chondrocytes in a first surgery, expansion *in vitro* for several weeks, cell implantation in a matrix, and its implantation in a second surgical procedure ². Mosaicplasty implies the use of osteochondral autologous plugs taken from non-weight bearing regions to transplant them in the defect area ²⁸. Lastly, microfracture focuses on stimulating the bone marrow through micro-perforations in the subchondral bone, which promotes a blood clot formation in the defect site, containing progenitor cells and growth factors that induces defect healing ⁵. Despite their wide application, the clinical outcomes are not fully fulfilled yet, mainly because the repaired tissue is fibrotic with inferior quality biochemical and mechanically in comparison to hyaline cartilage ³. Other techniques are focused on inducing chondrogenic differentiation by the use progenitor cells within scaffolds or scaffold-free via cell suspension or intra-articular injection of cells (Fig. A3) ⁵.

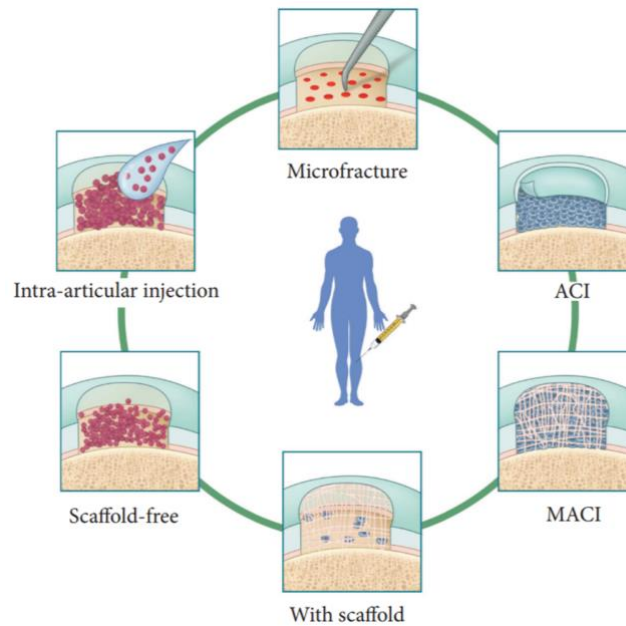


Fig. A3. Therapies for articular cartilage regeneration *in situ*. For microfracture, perforations are done in the subchondral bone to stimulate the bone marrow and to induce the formation of a blood clot rich in progenitor cells and growth factors. ACI and MACI are approaches that involve the use of the chondrocytes. For ACI, chondrocytes from the patient are isolated, expanded *in vitro* and subsequently implanted. MACI uses a matrix of collagen before the implantation. Other approaches address the use of progenitor cells for chondrogenic differentiation by implanting them in scaffolds or in the defect site. Image taken from Ref. ²⁹ with the permission of Hindawi.

An important drawback of use of chondrocytes-based techniques is the donor morbidity, since two surgical procedures are required. In addition, dedifferentiation, cell death, cell leakage, and difficulties to reach a high cell density *in vitro* also has been reported ^{29, 30}. On the other hand, the tissue produced by microfracture is poor in terms of its biochemical and mechanical properties compared to the native AC, therefore known as fibrocartilage ³¹.

1.2. Cartilage tissue engineering

Cartilage tissue engineering (CTE) focuses on the development of strategies that enables regeneration of AC. The backbone of CTE is composed by a scaffold to home the cells, a bioreactor to simulate physicochemical conditions of the native AC and cells source, usually chondrocytes or mesenchymal cells ¹¹. Despite of the enormous advance in cartilage research, there is not a definitive outcome yet; since the developed products still differ from the native AC properties. One of the possible reasons is the lack of mechanical stimulation while culturing the cells ¹¹.

1.2.1. Compressive forces in the knee joint

In an avascular tissue where small molecules are mainly distributed by diffusion, joint motion contributes to the transport rate of solutes¹⁰. Mechanical activity in joints supports the proper functionality of chondrocytes, improves ECM content, promotes glycosaminoglycan synthesis, and fiber organization^{32, 33}. Besides, it also contributes to the synthesis of ECM components by chondrocytes even if isolated from patients with osteoarthritis³⁴. Thus, mechanical loading plays a pivotal role for the nutrients and cytokines delivery from the synovium, waste disposal, repair and AC healthiness³⁵⁻³⁷.

The compression generated on the AC by mechanical loading is more suitably referred as strain, which is defined as the change of the thickness regarding the original value of the height³⁸. Daily normal activities have 0 – 10 % strain, and 5 – 15 % for post-activity; while 50 – 70 % strain is reported to be injurious, and 70 – 90 % to cause cell death³⁹. In the tibiofemoral contact area, peak strains can be 7 – 23 % during walking³⁹.

1.2.1.1. Compression bioreactors

To simulate *in vitro* a realistic biomechanical situation of the joints occurring *in vivo* is challenging, since all the relevant forces and amplitudes on the knee joint acting simultaneously are hard to identify. These mainly depend on the physical activity and particular conditions of the individuals. Nevertheless, bioreactors are biotechnological devices used in CTE to evaluate diverse mechanical stimulation strategies as compression, tension, hydrostatic pressure and shear stress, acting on natural cartilage tissue or cartilage-like constructs⁴⁰⁻⁴³.

The main types of the bioreactors are used in cartilage research are compression, tension, hydrostatic pressure and shear stress bioreactors⁴⁴. Compression bioreactors are used to apply mechanical stimulation on grafts while imitates the physicochemical environment varying the frequency, strain, duration and loading⁴⁵. Of these mechanical stimuli, loading by direct compression has been widely examined, since it simulates the stress exerted on AC by the opposite joint component⁴⁶. Compression bioreactors are usually designed to maintain the samples under confined, semi-confined or unconfined conditions (Fig. A4). In an unconfined situation, the sample is vertically loaded with an unrestricted lateral expansion. A semi-

confined sample is surrounded laterally by walls but the loading is applied through a porous platen. Finally, the sample is fully confined from all sources under hydrostatic pressure and the compressive strains are almost null without compressibility⁴⁷.

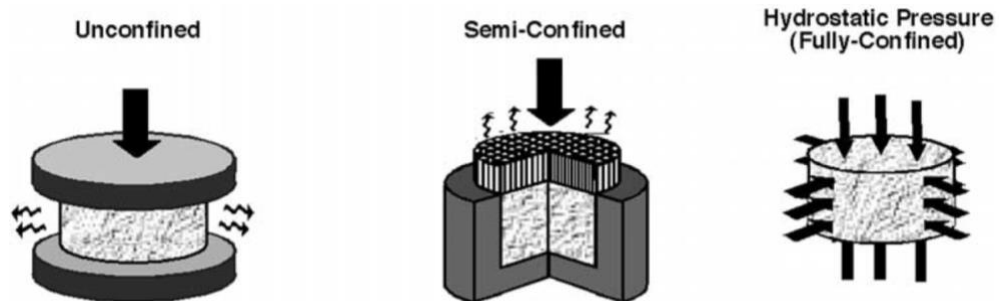


Fig. A4. Types of sample containers in compression bioreactors. In an unconfined bioreactor, the sample has lateral expansion; while in a confined bioreactor, the sample is fully restrained. In a semi-confined bioreactor the sample has limited expansion. Image taken from Ref. ⁴⁷ with permission of Elsevier.

Compressive forces have been applied either under continuous (also known as static) or dynamic (also known as cyclic) conditions, but dynamic stimulation mimics the physiological environment of the AC better. For instance, studies performed applying continuous loading stimulation have shown that this loading pattern hampers proteoglycans synthesis and the transport of large solutes⁴⁸⁻⁵¹. Most of the ECM proteins are down-regulated when continuous loading is applied for 24 hours but up-regulated under dynamic loading regime⁵², as evidenced by the increased synthesis of proteoglycan and collagen-II⁵³. Also, dynamic loading improves the access of soluble growth factors to the isolated chondrocytes within the dense tissue⁴⁹.

Loading can be applied static or dynamically, and under continuous or intermittent regimes (Fig. A5). Intermittent dynamic loading regime has been addressed by several authors in the past⁵⁴⁻⁵⁶. Cyclic is the more frequent loading pattern in the lower limbs joints during locomotion, in which intermittent loading is part of the normal motion scheme since unloaded periods occur between load cycles⁵⁷.

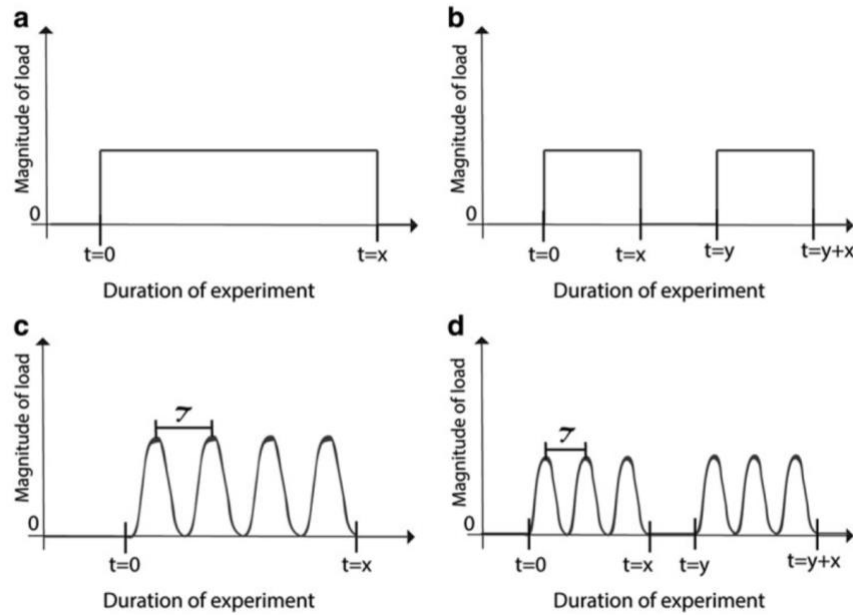


Fig. A5. Regimes of loading application. Loading can be applied as (a) static and continuous, (b) static and intermittent, (c) dynamic and continuous or (d) dynamic and intermittent schemes. Image taken from Ref. ³³ with the permission of Mary Ann Liebert.

1.2.2. Scaffolds for AC regeneration

Tissue-engineered 3D matrices provide support for cells and seem to be better for regeneration as 3D simulates better the natural cell microenvironment ⁵. For instance, chondrocytes in 3D produces hyaline-like tissue as they tend to dedifferentiate less than in monolayer ⁵⁸.

The common biomaterials in CTE used to make scaffolds are hyaluronan, collagen, alginate, gelatin, polyglycolic-, polylactic-, polylactic co-glycolic- acid and polyethylene glycol- acid, or a combination of them, among others ⁵⁹⁻⁶¹.

1.2.2.1. Alginate-based scaffolds

Alginate is an anionic polymer commonly extracted from brown algae or bacterial synthesis widely used in research. In CTE, alginate is used for hydrogels preparation as cell-carrier because of its biocompatibility, reduced cost, low toxicity, mild and relatively easy polymerization ⁶². It is a linear copolymer composed blocks of (1,4)-linked beta-mannuronate (M) and alpha-L-guluronate (G) residues (Fig. A6a). To produce gel structure from a solution,

the alginate chains can be intercrossed by divalent cations with different affinity forces, i. e., $Pb^{2+} > Cu^{2+} > Ba^{2+} > Sr^{2+} > Ca^{2+} > Zn^{2+} > Mn^{2+}$, from which Ca^{2+} is the most commonly used. Ca^{2+} binds the guluronate blocks of one polymer chain to the adjacent chain and produce linear copolymers ⁶³ (Fig. A6b). The crosslinking is influenced by the M/G ratio and divalent cation within the structure.

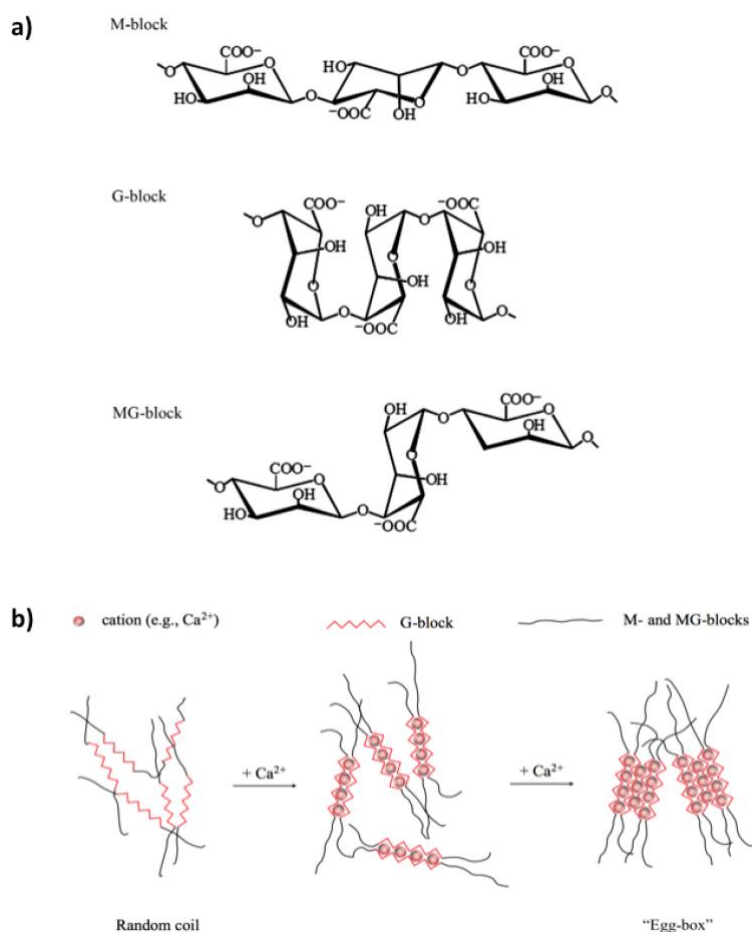


Fig. A6. Chemical structure and ionic gelation of alginate. a) Chemical structures of mannuronate, guluronate, and mannuronate-guluronate blocks. Image taken from Ref. ⁶⁴ with permission of Elsevier, b) Schematic representation of "egg-box" crosslinked alginate by calcium. Only G-blocks conform crumpled tight junction zones in presence of Ca^{2+} . Image taken from Ref. ⁶⁵ with permission of Elsevier. *M*: mannuronate, *G*: guluronate.

1.2.2.2. Collagen-based scaffolds

Collagen is the main component of the ECM in AC and determines the mechanical properties of the tissue ⁵⁹. The classical types of collagen present in mammalian AC are type II, IX, X and XI, of which the fibrillar type-II is the most abundant ⁶⁶.

To produce collagen scaffolds is demanding, in particular when defined morphology of several mm of size is required. Collagen concentration, pH and temperature influence the 3D architecture of the scaffold. For instance, when physiological pH and temperature are used with 2 mg/mL collagen solution, homogeneous scaffolds of 1 μm pore size and reticular fibrils are obtained, whereas decreasing pH or temperature result in bigger pore size but more heterogeneous meshwork ⁶⁷.

Besides of using physical means, collagen fibrils can be crosslinked by chemical agents as 1,4-butanediol diglycidyl ether (BDDGE). BDDGE is a linear molecular which both ends containing epoxide groups that react with the amine groups of collagen (Fig. A7).

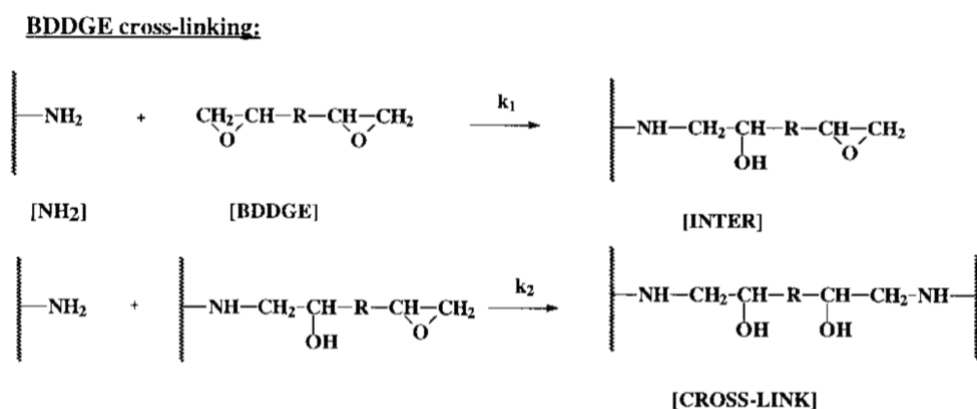


Fig. A7. Collagen crosslinking. Epoxy residues from the BDDGE are hydrolyzed by reacting with the amine groups of the collagen in a second order reaction. The final product is a crosslinked collagen with a diol-ether. Image taken from Ref. ⁶⁸ with the permission of John Wiley and Sons.

BDDGE has been widely used in cosmetics for hyaluronic acid dermal fillers manufacture showing no toxicity with very low levels of unreacted molecules < 2 ppm ⁶⁹.

1.2.2.3. Laminin

Laminins are the main component of the basal membrane. This family of proteins present is composed of the polypeptide chains α , β , γ . There are five different types of chain α , three of β and three of γ , giving a combination of 16 possible molecules that are named according to their chain composition ⁷⁰. Laminins have an important role as scaffold proteins and in

signaling as they are involved in proliferation, migration, differentiation ⁷¹. Laminin-521 (LN521) have been recently used to increase adherence of induced pluripotent stem cells and embryonic stem cells to monolayers and matrices ⁷¹.

1.2.3. Cell sources for AC regeneration

Several types of cells as chondrocytes and stem cells have been experimentally addressed for AC regeneration. Studies show that chondrocytes in culture seem to produce more collagen-II than chondrogenic differentiated stem cells ⁵⁹. Nevertheless, it has also been demonstrated that explanted chondrocytes dedifferentiate and turn into senescent cells after implanted ⁶. Hence, AC research community is enthusiastic about the promising use of stem cells for their proliferative features and chondrogenic differentiation potential.

1.2.3.1. Mesenchymal stromal/stem cells for AC regeneration *in situ*

To maintain tissue homeostasis in the body, stem and progenitors cells can be mobilized from their niches to the injury site for repairing ⁷². Mesenchymal stromal cells (MSCs) are target components for cell-based therapies, e.g., for bone and cartilage injuries, because of their multi-lineage differentiation potential and properties that promote regeneration ⁷³.

MSCs with chondrogenic differentiation potential reside in bone marrow (BM), stroma, synovium, infrapatellar fat pad and periosteum (Fig. A8a) ^{31, 74, 75}. The BM has been the most common reservoir to obtain MSCs in cartilage defects research ⁷⁶, although, AC in the joint is spatially separated from the BM by the subchondral bone lamella.

MSCs located in niches around the knee joint as the BM would colonize the defect site if there is no a physical carrier to pass through and having the appropriate stimuli and microenvironment to stay in place. Such stimuli could be chemicals as chemokines and growth factors or physical factors as mechanical stimulation. When the cells are in the defect site, chondrogenic differentiation might be induced to potentially regenerate AC (Fig. A8a).

In addition, potential strategies for MSCs-based AC regeneration could be given by direct transplantation to allow interaction of MSCs with the adjacent chondrocytes and probably enhancing chondrogenic differentiation (Fig. A8b), via secretome factors provided through conditioned media or components of the stromal cell matrix ⁷⁷.

An approach that induces endogenous mobilization of MSCs, that retains high cell density in the defect site and achieves chondrogenic differentiation *in situ* would be promising for the progress of AC regeneration research.

1.3. Mobilization of cells

Cell migration is a highly organized and complex mechanism involved in physiological processes as tissue development, maintenance, regeneration, wound healing and also in pathophysiological processes as cancer ⁷⁸. The topography of the ECM influences the cell orientation and migration, enabling locomotion of cells in 1D, 2D and 3D.

1.3.1. Motility of cells in 1D and 2D

1D migration refers to a uniaxial movement of cells along collagen fibers, process known as “contact guidance” when the fibers are organized as a bundle and cells migrate through it^{79, 80}.

2D migration, which is the most studied mode of migration on flat surfaces ⁸¹, involve subsequent steps where the cells 1) polarize and cell membrane protrusions are pointed toward the direction of migration, 2) adhere the actin cytoskeleton to the ECM, 3) contract by traction forces that translocate the leading edge forward and disassemble the trailing edge^{80, 82}.

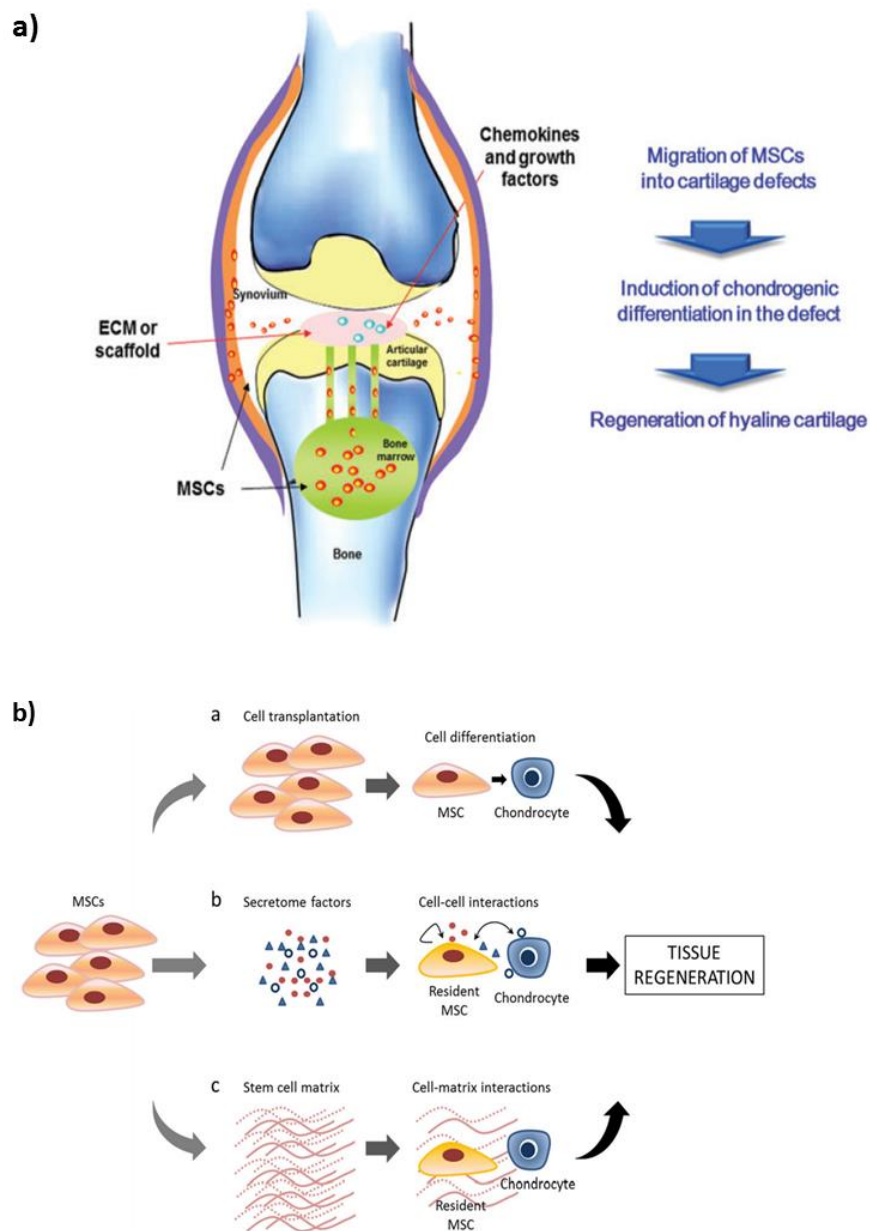


Fig. A8. Potential applications of MSCs for AC regeneration. (a) MSCs located at the bone marrow or synovium niches migrate toward a scaffold by influence of additional stimuli, i.e., chemotactic substances. The induction phase of the chondrogenic differentiation would take place *in situ* and AC would regenerate. Image taken from Ref. ³¹ with the permission of Mary Ann Liebert, Inc. (b) MSCs potentially contribute to the AC regeneration by direct cell transplantation helping on cell differentiation, MSCs-chondrocyte secretome interaction or by MSCs matrix interaction with chondrocytes. Image taken from Ref. ⁷⁷ with the permission of Springer Nature.

1.3.2. Motility of cells in 3D

Different cell locomotion modes occur in 3D environments, as mesenchymal, amoeboid and lobopodial migration (Fig. A9). The 3D mesenchymal is a slow speed migration mode that follows equivalent molecular mechanisms that 2D migration uses depending on focal adhesions⁸³.

For mesenchymal migration, polymerized actin filaments at the leading edge form broad and large cell protrusions named as lamellipodia or spike-like structures known as filopodia⁸². The protrusions are then stabilized when integrins anchor to the ECM and create strong focal adhesions^{79, 84}. Then, the cell contracts through high traction forces driven by actomyosin, and the adhesion focal points are disassembled at the cell rear^{85, 86} (Fig. A9a). Coordinated reactions of Rho GTPases, actin polymerization and myosin-II regulate the adhesion and disassembly dynamics^{82, 86}. Mesenchymal cells align in parallel to the ECM fibers with the microtubule organizing centre located anterior to the nucleus and the leading edge containing protease vesicles ready to digest ECM proteins while the cell migrates (Fig. A9a).

On the other hand, cells can move fast by amoeboid migration since there is not alignment along the ECM fibers, weak and transient adhesion points between cell and the substratum are formed, the microtubule-organizing centre is located posterior the nucleus with cell poor contractility and traction force^{84, 87}. The cell body is highly deformed for actin protrusions or blebs of cell membrane regions containing cytoplasm formed by hydrostatic pressure⁷⁹ (Fig. A9b). Thus, cells that mobilize using amoeboid mechanisms are able to cross the matrix pores by blebbing rather than using protrusion, adhesion, contractility, and enzymatic digestion of the pericellular environment as mesenchymal migration mode does⁸⁸ (Fig. A9a).

Lobopodia migration is a combined mechanism between mesenchymal and amoeboid migration. Lobopodia are formed for an unbalanced intracellular pressure that creates bleb-like protrusions at the leading edge and firmly adhere the cell to the substratum, while intracellular anterior pressure in given the nucleus that acts by a piston and enables the cell to move forward^{79, 89}.

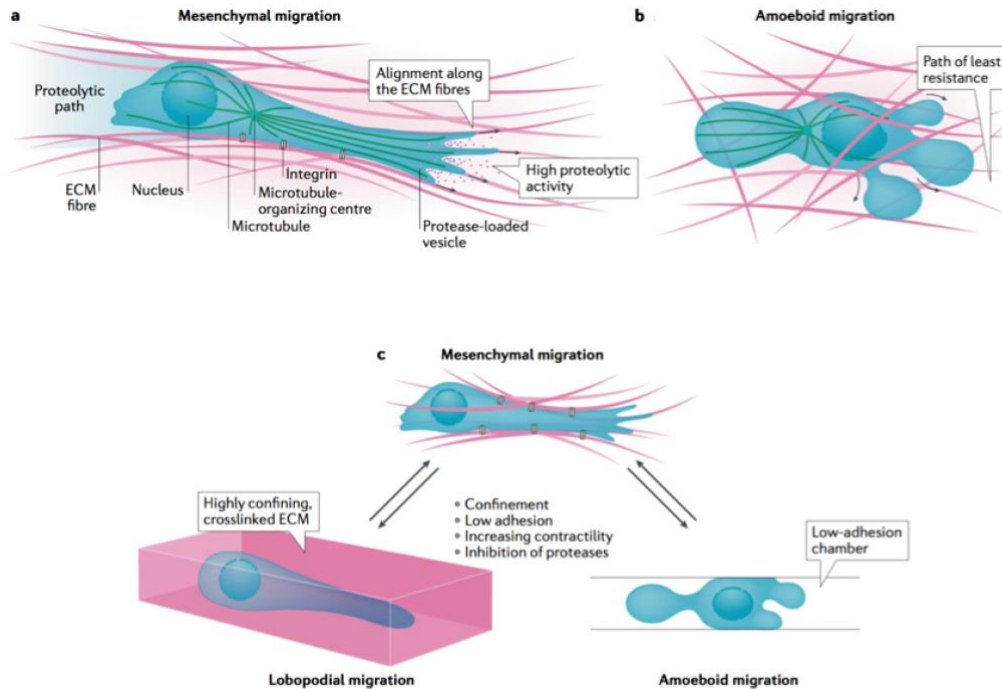


Fig. A9. 3D migration mechanisms. (a) Mesenchymal migration is characterized by cell alignment along the ECM fibers, strong focal adhesions through integrins and substrate, microtubule-organizing centre located anterior to the nucleus, and active enzymatic activity to degrade ECM. (b) For amoeboid migration, the cells protrude the available spaces using weak adhesions and without align to the extracellular fibers. The microtubule-organizing centre is located behind the nucleus. The cell does not produce proteolytic activity to move. (c) Lobopodial migration is a hybrid between mesenchymal and amoeboid migration. Bleb-like protrusions at the leading edge are formed and the cell adheres to the substratum. The cells can exchange of migration mode depending to the ECM content and circumstances, i. e., from mesenchymal to lobopodial or amoeboid migration when confinement increases, adhesion diminishes, contractility increases or metalloproteinase are inhibited. Image taken from Ref. ⁷⁹ with the permission of Springer Nature.

1.3.3. Microenvironment and cell mobilization mechanisms

The mechanism of migration is usually determined by the cell shape and type, e.g., mesenchymal migration is preferably used for fibroblasts and MSCs, whereas amoeboid mode for leukocytes ⁸⁴. Nevertheless, the cells can also change between mesenchymal, lobopodial and amoeboid migration depending on the immediate microenvironment or given circumstances.

Several aspects of the ECM microenvironment influence the mode how the cell mobilize in 3D as its matrix topology, rigidity, adhesion, confinement, biochemical and molecular content, concentration of proteins and fibers within ECM, alignment and distribution of molecules by covalent or non-covalent crosslinking, molecular homogeneity in 3D, pores and micro-channels ^{90, 91}. For instance, lobopodial migration is preferred formed under highly

confined and crosslinked ECM, amoeboid migration in surroundings with poor adhesion or mesenchymal mode in strong adhesion and organized ECM^{79,92} (Fig. A9c).

Tissue functionality is in part given by the composition of the ECM. For instance, the distribution of collagen fibers besides other molecules, contributes to build the dense ECM of the AC and to provide the particular mechanical properties. The cells are able to sense the mechanical neighboring microenvironment through integrin adhesions. As a result, the cell reacts increasing contractility by adding more stress fibers and focal adhesions when exposed to a stiff microenvironment with high collagen content, or reducing cell contractility in soft ambiances with low collagen concentration⁸⁴ (Fig. A10).

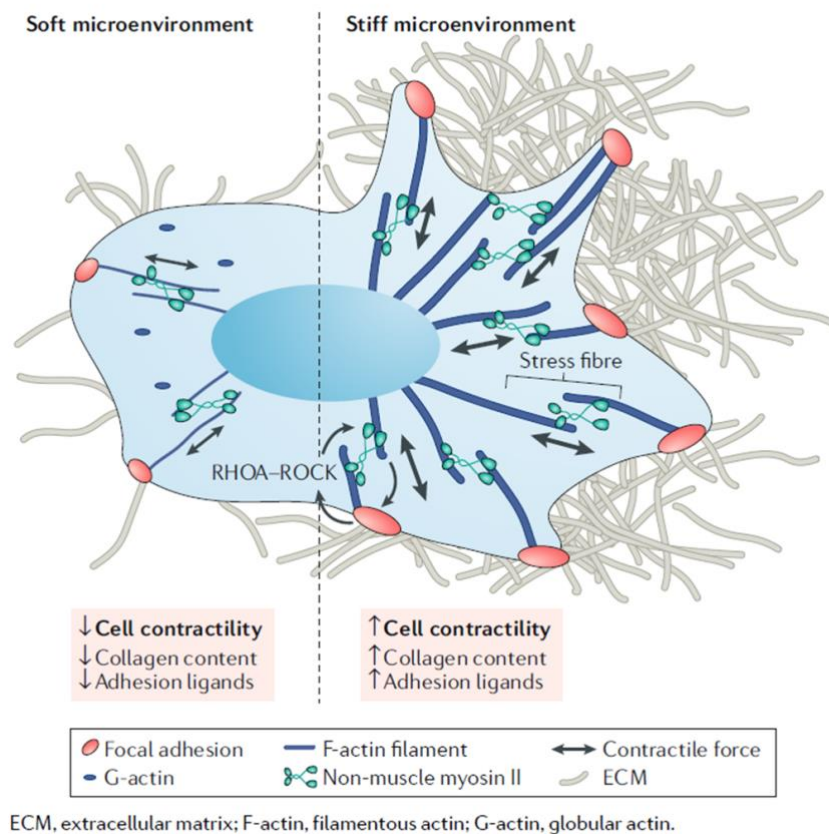


Fig. A10. Cell mechanotransduction. The cell is able to sense the pericellular environment and modify its morphology. The cell responds to a stiff environment, e.i. high collagen content, by increasing contractility, adding more stress fibers and firmly attaching to the ECM through more focal adhesion. Conversely, ECM with low collagen content creates a soft microenvironment and the cell forms less stress fibers and focal adhesions.

Image taken from Ref.⁸⁴ with the permission of Springer Nature.

2. Aim of the study

We hypothesize that mechanical stimuli are involved in endogenous cartilage repair induced by the mobilization of stem cells besides other factors when the subchondral bone is opened. To imitate the process *in vitro*, a compression bioreactor dedicated to cultivate and remodel cartilage replacement material has been modified allowing cell cultivation and load application in the same device ⁹³.

2.1. General aim

To evaluate the role of dynamic of mechanical stimulation on mobilizing mesenchymal stromal cells toward scaffolds in a bioreactor system.

2.2. Specific aims

1. To identify and optimize parameters as frequency, amplitude, time, and strain for the bioreactor operation.
2. To establish and optimize the production of scaffolds that fit in the bioreactor.
3. To establish techniques for cell quantification inside the scaffolds.
4. To evaluate whether mesenchymal stromal cells are mobilized into scaffolds after mechanical stimulation.

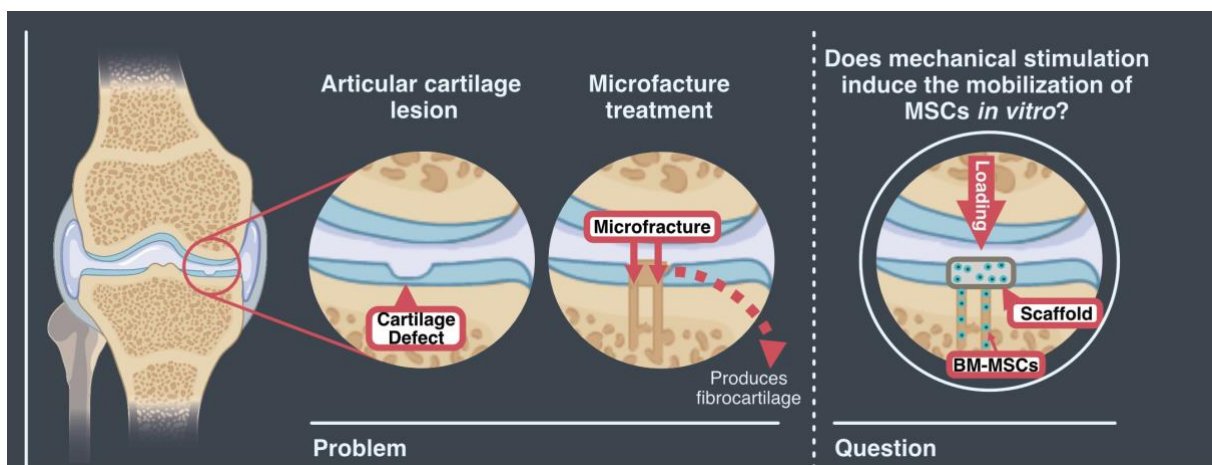


Fig. B1. Problem and experimental question. Current therapeutic options for treating lesions in articular cartilage as microfracture, still fail to produce natural-like tissue. Instead, fibrocartilage of inferior biochemical and mechanical quality is obtained. Therefore, a compression bioreactor that mechanically stimulated an acellular scaffold and a cell reservoir below it was used to evaluate whether mechanical stimulation induced the mobilization of mesenchymal stromal cells toward the scaffold.

3. Animals, material and methods

3.1. Animals

For this study, animal derived products were used. Hind legs from piglets or juvenile pigs (3-5 days or 2-3 months old, respectively) were kindly provided by Prof. Dr. Schmelz (Experimental Pain Research Group, Medical Faculty Mannheim, University of Heidelberg) after being sacrificed for unrelated experiments (animal experimentation approval No. I-17/13). These were used for isolating porcine bone marrow derived-mesenchymal stromal cells (pBM-MSCs).

3.2. Materials

3.2.1. Cells

pBM-MSCs were obtained from hind legs of piglets or juveniles pigs of 3-5 days or 2-3 months old, respectively. Human-bone marrow derived MSCs (hBM-MSCs) were kindly provided by Prof. Dr. Bieback (experimentation approval No. 2015-520N-M, Institute of Transfusion Medicine and Immunology, Medical Faculty Mannheim of the University of Heidelberg).

3.2.2. Cell culture reagents

Stock reagents used for cell culture were Dulbecco's Modified Eagle's Medium – low glucose (DMEM, D5546, Sigma), with Fetal Bovine Serum (FBS, Cat. No. F9665, Sigma), 200 mM L-Glutamine (Cat. No. BE17-605E, Lonza), 1X Penicillin-Streptomycin (A8943,0100, AppliChem), 1X phosphate buffered saline (PBS, Cat. No. BE17-516F, Lonza, Cologne, Germany) and 0.25 % Trypsin-EDTA 1X (Cat. No. 25200-056, Gibco).

3.2.3. Scaffold materials

Alginate scaffolds were made from alginate powder (Keltone LVCR, ISP, US). Functionalized alginate scaffolds contained human laminin-521 (Cat. No. LN521, Biolamina; Stockholm, Sweden). Collagen scaffolds were made from bovine collagen solution (3 mg/mL,

Cat. No. C4243, Sigma-Aldrich, Schnellendorf, Germany) and were cross-linked by 1,4-Butanediol diglycidyl ether (BDDGE, Cat. No. 220892, Sigma). Gelatin scaffolds were made of lyophilized porcine gelatin (G9136, Merck, Darmstadt, Germany).

3.2.4. Antibodies

The antibodies used for flow cytometry were anti-human CD31-FITC, CD34-APC, CD45-PE-Cy7, CD73-PE, CD90-APC and CD106-FITC (Cat. No. 555445, 555824, 557748, 550257, 561971 and 551146, respectively; Becton Dickinson, New Jersey, US); CD29-Alexa Fluor 488, CD140a-PE, CD140b-APC and HLA-DR—APC-Cy7 (Cat. No. 303016, 323506, 323608, and 307618, respectively; BioLegend, San Diego, CA, US); CD44-APC eFluor® 780, CD105 and NG-2 (Cat. No. 47-0441-82, 25-1057-42, and 53-6504, respectively; eBioscience Inc., San Diego, CA, US); CD146 (Cat. No. A07483; Beckman Coulter, Brea, CA, US), HLA-ABC (Cat. No. 130-101-466; Miltenyi, Bergisch Gladbach, Germany); SLA class I and SLA class II DR (Cat. No. MCA2261GA and MCA2314GA, respectively; BioRad, Hercules, CA, US) and F(ab')₂-Goat anti-Mouse IgG PE (Cat. No. A10543; Thermo Fisher Scientific, Waltham, MA, US).

For confocal microscopy, the antibodies Collagen I (COL1A, Cat. No. sc59772, Santa Cruz Biotechnology Inc., Heidelberg, Germany) and secondary Alexa-488 (Cat. No. A28175, Thermo Fisher Scientific, Waltham, MA, US) were used.

3.2.5. Confocal microscopy

DMEM without red phenol (Cat. No. 11570406, Thermo Fisher Sci. GmbH, Dreieich, Germany) and immersion oil type F (Cat. No. 11513859, Leica Microsystems, Wetzlar, Germany) were used as immersion media. Calcein-AM (C-AM) and ethidium homodimer-1 (EthD-1, Live/ Dead kit, Cat. No. L3224, ThermoFisher/Invitrogen) were used for cell viability assessment. C7-PEI dye, used to evaluate cell visualization in the scaffolds was kindly provided by Prof. Gretz group (Medical Research Centre, Medical Faculty of Mannheim of the University of Heidelberg).

Imaging of the scaffolds was done with an upright confocal microscope (TSP8, Leica Microsystems, Wetzlar, Germany).

3.2.6. Bioreactor hardware and software

A compression bioreactor system was composed of different software and hardware software components (Figs. 1 and 2) as detailed:

Table 1. Hardware and software components of the bioreactor. Technical specifications and software used for the construction and operation of the bioreactor.

Item	Specifications
Stepper motor	L4118S1404-T6x1-A25, Nanotec Electronic GmbH & Co, Feldkirchen, Germany
Impermeable membrane	Permeafon PTFE, Berghof Fluoroplastic Technology GmbH, Germany
Motion controller	iPOS3604 MX Intelligent Drive, 144 W, CANopen / EtherCAT; Technosoft SA, Neuchâtel, Switzerland
Digital gauge	DT32P, Sony, Tokyo, Japan
Interpolator	MT11, Sony, Tokyo, Japan
Amplifier	SG-AP, Althen GmbH; Kelkheim, Germany
Connector block	SCB-68A, National Instruments Corporation, Austin, Texas, USA
Nylon mesh	03-160/37, Plastok Associates Ltd, Birkenhead, UK
PC-Card	PCI-6220, National Instruments Corporation, Austin, Texas, USA
Elastic ring	Silicone Rubber high elasticity, Glorex AG, Füllinsdorf, Switzerland
Bioreactor GUI	LabView 2011, National Instruments Corporation, Austin, Texas, USA
EasyMotion Studio	TECHNOSOFT SA, Neuchâtel, Switzerland

3.3. Methods

To evaluate the approach *in vitro* of mechanical stimulation as a mean for cell mobilization into scaffolds, several methods and protocols had to be developed and optimized as follows:

3.3.1. Bioreactor specifications

To evaluate cell recruitment in a 3D model, a compression bioreactor designed and built based on a model that was previously described⁹³ was completed with a lower chamber serving as cell reservoir, assembled below of the target scaffold (Fig. 1). The scaffold was

surrounded by an elastic compressible ring of 2 or 3 mm height with an outer diameter of 30 mm and an inner diameter of 10 mm (Fig. 1b-e).

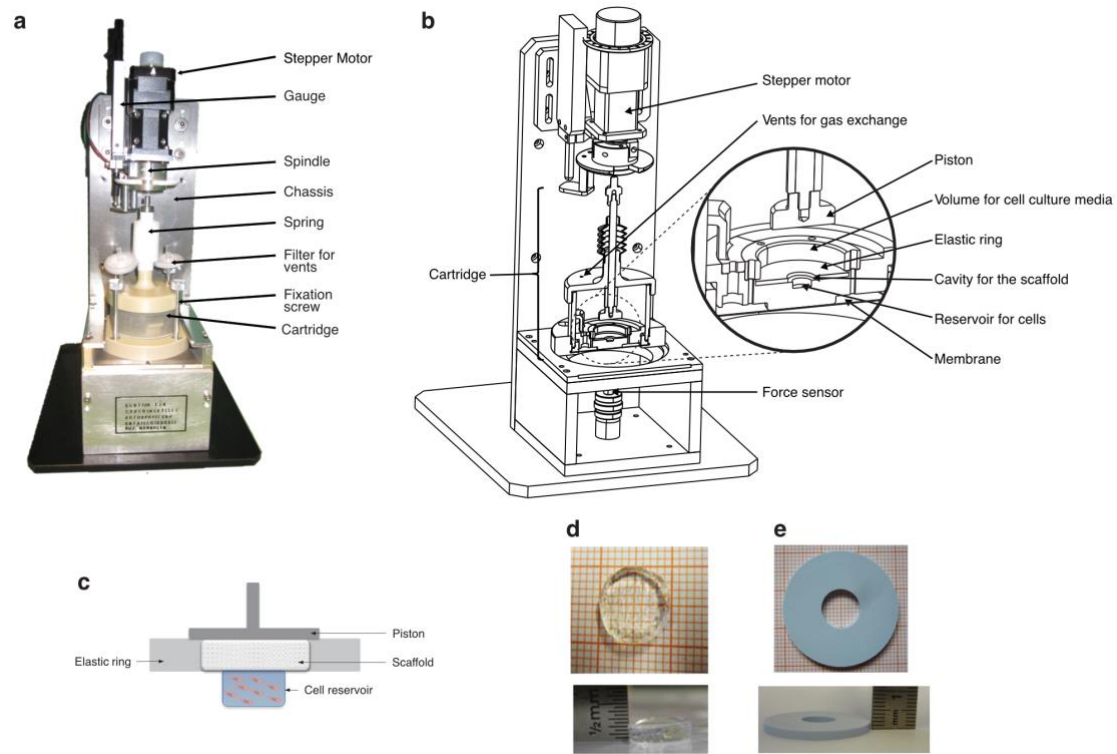


Fig. 1. The compression bioreactor. The picture (a) and technical sketch (b) depict the outer and inner structures of the bioreactor, respectively. A stepper motor drives the piston downward and a spring (covered here by the white bellows) moves it upward. Parallel to the stepper motor, a digital gauge measures independently the vertical displacements of the piston. The cartridge is the housing for cell cultivation and mechanical application of strain to the scaffold. This can be disassembled, assembled and fixed to the bioreactor chassis by fixation screws. The cartridge cap comprises the embedded piston and vents for gas exchange, covered by $0.22\ \mu\text{m}$ filters to protect from the external environment. A non-permeable membrane forms the bottom of the cartridge, isolating the cell cultivation system to protect it from contamination. A force sensor is located underneath the membrane for reliable measurements of the applied forces. (c) The piston simultaneously compresses the scaffold (d) and the elastic ring (e) located over the cell reservoir. Dimensions of the bioreactor: 120 x 150 x 400 mm (width, depth, height). Adapted image from Ref. ⁴ with the permission of PLoS One, license CC-BY.

An upper positioned piston (20 mm diameter) was moved vertically downwards driven by a stepper motor (Fig. 1a and b). The displacement of the piston induced compression acting simultaneously on the scaffold and the elastic ring (Fig. 1c). A force sensor was located underneath the cells reservoir to measure the induced forces (Fig. 1b).

The bottom of the cartridge was covered by a impermeable membrane to isolate the external environment and to communicate the displacements of the scaffold holder to the force sensor below via a rod.

The compression bioreactor had to be dimensioned to be able to set it up in a CO₂ incubator (Fig. 2). Parameters as the piston displacement were set by the custom-made software EasyMotion Studio, which handled the stepper motor through a motion controller. When an examination was about to start, the motion controller synchronized the information with EasyMotion software.

A digital gauge and its interpolator were placed for measuring independently the vertical displacements given by the piston, providing a resolution of 5 μm and an accuracy of $\pm 5 \mu\text{m}$ according to the information of the manufacturer.

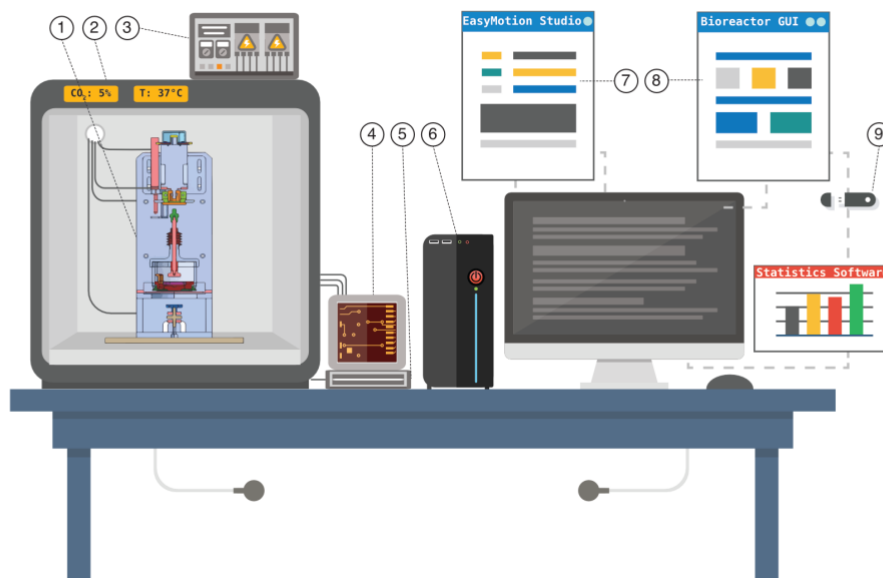


Fig. 2. Bioreactor system. The system of the bioreactor is designed as standalone unit. The bioreactor (1) connected to a power supply (3) is placed inside a CO₂ incubator (2) to allow conditions for cell cultivation. The connection wires from the bioreactor are plugged over an electronic box (4) that contains a motion controller, an amplifier of the force sensor and the interpolator for the digital gauge. The motion controller receives the information from the stepper motor, and the signals of the force sensor generated by the loading are processed by the amplifier. The electronic box (4) is plugged to the connector block (5), which communicates with the PC card in the computer (6). The PC card synchronizes the beginning of the experiment with the motion controller software “EasyMotion” (7), where the settings are established for the experiments. Data as force, displacement of the piston and time are visualized and registered at a rate of 50 Hz by the custom-made software “Bioreactor”, programmed in LabView 2011. Finally, the data can be exported (9) and analyzed by statistical software such as Origin 9.0G, which was used in this study. Image taken from Ref. ⁴ with the permission of PLoS One, license CC-BY.

The signals of the force sensor generated by the displacement were processed by an amplifier. The amplified force signal was plugged to the connector block, communicating the information to the PC-Card for data acquisition (Fig. 2).

Once the tests were running, the position of the piston, forces, and time were visualized and registered by the custom-made data acquisition software Bioreactor, programmed in LabView 2011 at a rate of 50 Hz. The data were then exported and analyzed with the statistical software Origin 9.0G (Fig. 2).

3.3.2. Elastic ring preparation

Silicone rubber was used to prepare the elastic rings following the instructions of the manufacturer. However, the obtained rings were not appropriated in consistency or shape. Therefore, the protocol was optimized and 1.5 g of silicone rubber was mixed with 7 drops of catalyst. Then, the silicone mixture was cast in a custom-made plastic mold with the dimensions of 30 mm diameter, 2 mm height and a pin of 10 mm diameter in the middle. It was placed overnight for hardening at room temperature. Rings were demoulded and sterilized by autoclaving at 120°C.

3.3.3. Alginate scaffold preparation

Lyophilized sodium alginate was dissolved in 0.9 % NaCl and filtered in a 0.22 µm syringe. The scaffolds were produced in a custom-made sterile mold mixing 1.5 % alginate solution, with or without 15 µM LN521, named as “alginate-Ln” or “alginate” scaffold, respectively. Ionic polymerization of the alginate was induced by 0.1 M CaCl₂ for 7 minutes (Fig. 3). NaCl was the solvent for the alginate because the scaffolds were easily dissolved in PBS.

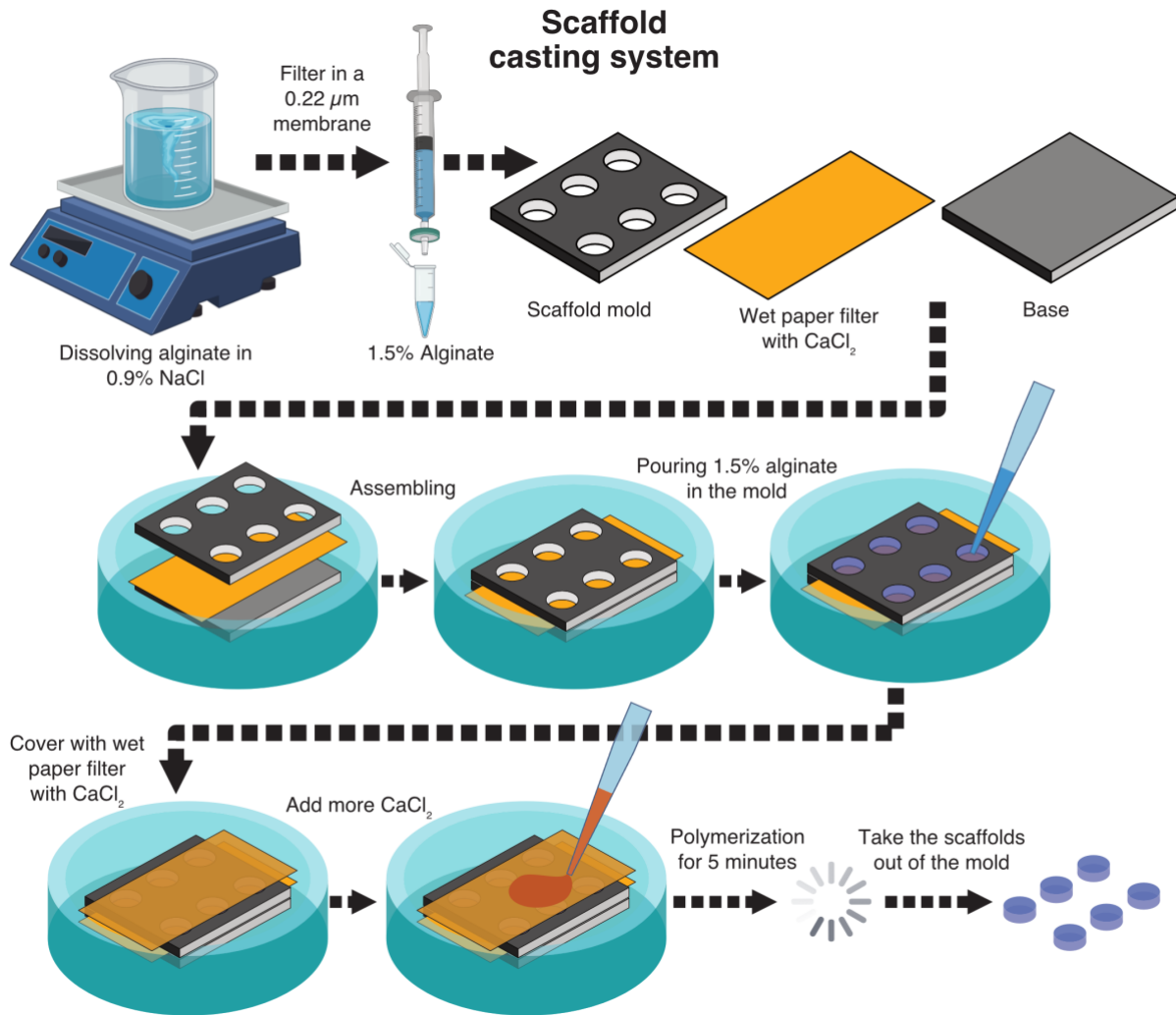


Fig. 3. Alginate scaffold casting system. Lyophilized alginate was dissolved in 0.9 % NaCl by stirring and warming. The viscous solution was then filtered with 0.22 μm membrane. A customized and sterilizable mold was built, consisting of an upper plate with holes for scaffolds of 10 mm in diameter and 2 or 3 mm height, and a metal plated that served as a base. 0.1 M CaCl₂ was used for ionic cross-linking of the alginate. Thus, the mold was assembled with a sterile paper filter in between moistened with CaCl₂ to avoid leakage from the alginate. The alginate solution was poured in the holes and an additional wet paper filter was placed over the mold. CaCl₂ was gently poured on the wells to let polymerize for 5 minutes. Lastly, the scaffolds were taken out and rinsed with 0.9 % NaCl.

3.3.4. Gelatin and collagen scaffolds

Different solutions composed of collagen, gelatin or a combination of them were tested to make suitable scaffolds in shape and composition. The evaluated solutions were divided in four different groups as described in Table 2. 1,4-Butanediol diglycidyl ether (BDDGE) was used as cross-linker at 10 % according to Shankar et al.⁹⁴, or 20 %. Gel polymerization of all groups was tested at 4°C, room temperature (RT) or 37°C with pH 5.0, 7.2, or 9.0 for 2 days. The scaffolds were evaluated in 48-well plates.

Table 2. Collagen and gelatin scaffold fabrication. Four different groups with solutions of collagen, gelatin or a combination of them for scaffolds manufacturing were tested. The polymerization of all groups was evaluated at 4°C, room temperature (RT) and 37°C; and pH 5, 7, and 9. *BDDGE:1,4-Butanediol diglycidyl ether.*

Group	Reagents
A	Collagen (2.4 mg/mL) 10 % BDDGE
B	Collagen (2.1 mg/mL) 20 % BDDGE
C	Collagen (1.2 mg/mL) 4.5 % Gelatin 10 % BDDGE
D	4.5 % Gelatin 10 % BDDGE

3.3.5. Isolation of porcine bone marrow derived-mesenchymal stromal cells

pBM-MSCs were isolated from femora of piglets or juvenile pigs. The dissection of the hind limbs was done using sterile instruments under surgical technique application. Briefly, all soft tissues including skin, muscles, fat and connective tissue were removed with new scalpels. Then, femora bones were sterilized by immersing them in 70 % ethanol for 3 minutes as previously described ⁴. For the juvenile pig legs, an intertrochanteric or intercondylar hole located close to the metaphysis region was made using a punching machine previously developed in the group ⁹⁵ to remove a compact bone plug and to penetrate to the bone marrow (Fig. 4).

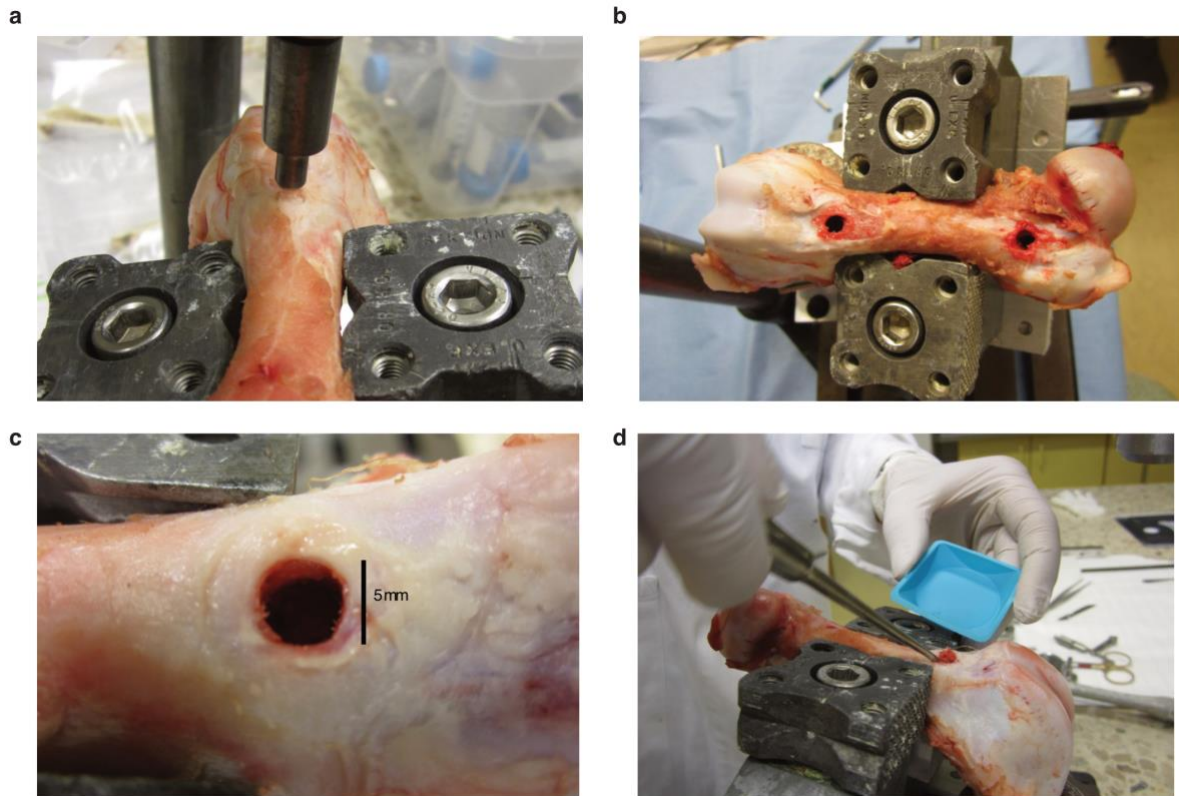


Fig. 4. Isolation of pBM-MSCs from juvenile pigs. (a-c) BM-derived cells were isolated from 2-3 months old pigs by removing soft tissues, immersing the bone 3 minutes in 70 % ethanol, and opening holes of 5 mm diameter at intertrochanteric and intercondylar regions of the bones. (d) The bone marrow was scrapped out using a sharp spoon, and the biological material was collected in 1X PBS supplemented with 1 % penicillin/streptomycin. All surgical tools and punching machine pieces that were in contact with the biological material were previously sterilized by heating them continuously at 180°C for 8 hours.

When pBM-MSCs were isolated from piglets, a sterile scalpel was used to cut the transversely the bone at the intercondylar region. Once the femora were open either for piglets or juvenile bones, the bone marrow was scraped out using a sterile surgical sharp spoon and harvested in 1 X PBS with 1 % penicillin/streptomycin. The suspension was centrifuged at 1000 rpm for 5 minutes and RBC lysis buffer was added for 5 minutes under continuous constant stir. The lysis buffer was removed by centrifugation at 1000 rpm for 5 minutes and the pellet was washed with 1X PBS three times. The cells were then cultivated and expanded using supplemented-DMEM (10 % FBS, 2 mM glutamine, 1 % penicillin, and 1 % streptomycin) at 37°C and 5 % CO₂. After 24 hours of seeding, the cells were washed with 1X PBS and fresh medium was added. The medium was changed every other day and 0.25 % trypsin/EDTA solution was used for passaging. 500 cells per cm² were plated in 75 cm² cultivation flasks until the cells grew to 70 - 80 % confluence.

3.3.6. FACS of pBM-MSCs

pBM-MSCs were characterized at passage 1 by their adherence to cell culture flasks, fibroblastic-like morphology and the identification of surface markers CD44⁺, CD90⁺, CD29⁺, CD45⁻, SLA-1⁺ and SLA-DR⁻ was done by flow cytometry analysis (FACS Canto II, BD Biosciences). Passages 2 and 3 were used for the experiments. Cells isolated from intercondylar or intertrochanteric regions were analyzed independently.

Briefly, the cells were split at 70 – 80 % confluence, 1×10^6 cells were resuspended in 1 mL FACS buffer, 1×10^5 cells were added per FACS tube in 100 μ L FACS buffer, 10 μ L FCR blocking reagent was added per tube, mixed and incubated for 5 minutes. The antibodies CD44 (1:40), CD90 (1:40), CD45 (1:100), SLA-DR (1:50), SLA-1 (1:50) and CD29 (1:100), and corresponding secondary antibodies (1:200) were added and incubated at 4°C for 20 minutes, protected from light.

Then, a wash was done by adding 2 mL of cell wash solution per tube, centrifuged for 4 minutes at 420 g and the supernatant was discarded. The secondary antibody was added in 100 μ L of FACS buffer, and incubated for 20 min at 4°C, protected from light. The cells were washed twice using 2 mL of cell wash solution each time. 100 μ L of the Sytox blue solution 1:2000, prepared in FACS buffer were added per tube. Finally, the experiments were analyzed using the FACS Canto II cytometer and the MSCfacs software.

3.3.7. FACS of hBM-MSCs

hBM-MSC were provided by Prof. Bieback group, isolated and characterized as described in ⁹⁶.

3.3.8. Biomechanical stimulation

We hypothesize that mechanical loading may mobilize MSCs from their bone marrow niche into a scaffold. For the biomechanical tests, 1.0×10^5 pBM-MSCs were seeded in the cell reservoir in a mixture of supplemented-DMEM and 0.5 % alginate or collagen, and covered by the respective scaffold, which was held in place by the elastic ring and a permeable

membrane on top with a mesh pore size of 160 μm . The reservoir had a volume of 42 mm^3 . Then, 2 mL of supplemented-DMEM were added onto the scaffold.

For continuous mechanical stimulation, a regime of periodic dynamic compression was applied at 0.3 Hz frequency ⁹⁷ for 24 hours with 10 % compression strain ⁹⁷ relating the height of the scaffold of 2 or 3 mm.

For intermittent mechanical stimulation, the amount of cells, strain, frequency and total time of the examination were applied as with the continuous regime. However, 2 mL of supplemented-DMEM were added over the arrangement of scaffold and elastic rings. To allow nutrient and gas exchange and waste disposal, the piston released the surface level of the scaffold and the elastic ring for 10 seconds every 180 cycles (i. e. after 10 minutes of loading), which was named as “lift” maneuver. A mesh with 160 μm of pore size was placed on top of the scaffold and elastic ring to held the scaffold in place during the unloaded phase. To avoid hydrostatic disturbance between the gas atmosphere and the liquid during the lift maneuver, the released piston kept immersed in culture medium ⁴. This protocol was developed through various optimization steps, involving several trial runs to determine the optimal bioreactor setup of hardware and software components. A new cartridge was built, composed of an anchor ring with a permeable membrane that allowed intermittent mechanical stimulation. In addition, the software was updated in order to operate the new intermittent program.

The generated force by the applied periodical compression was recorded continuously for the whole duration of the test. For executing the examinations, the starting position point of the piston was set by manual approximation until the piston touched the surface of the scaffold and the elastic ring, which was marked by a rise of the force value ⁴.

Unloaded scaffolds were used as controls prepared in parallel under the same conditions in another structurally identical cartridge.

After biomechanical testing, the scaffolds were demounted and used a) to assess cell numbers mobilized into the scaffold, b) cell viability and c) scaffold architecture, as described below.

3.3.9. Viability tests of cells located in the reservoir

Counting and viability of the cells located in the cell reservoir after the application of continuous or intermittent dynamic mechanical loading was measured by trypan blue exclusion assay after 24 hours. Independent experiments were made in triplicate from the same donor⁴.

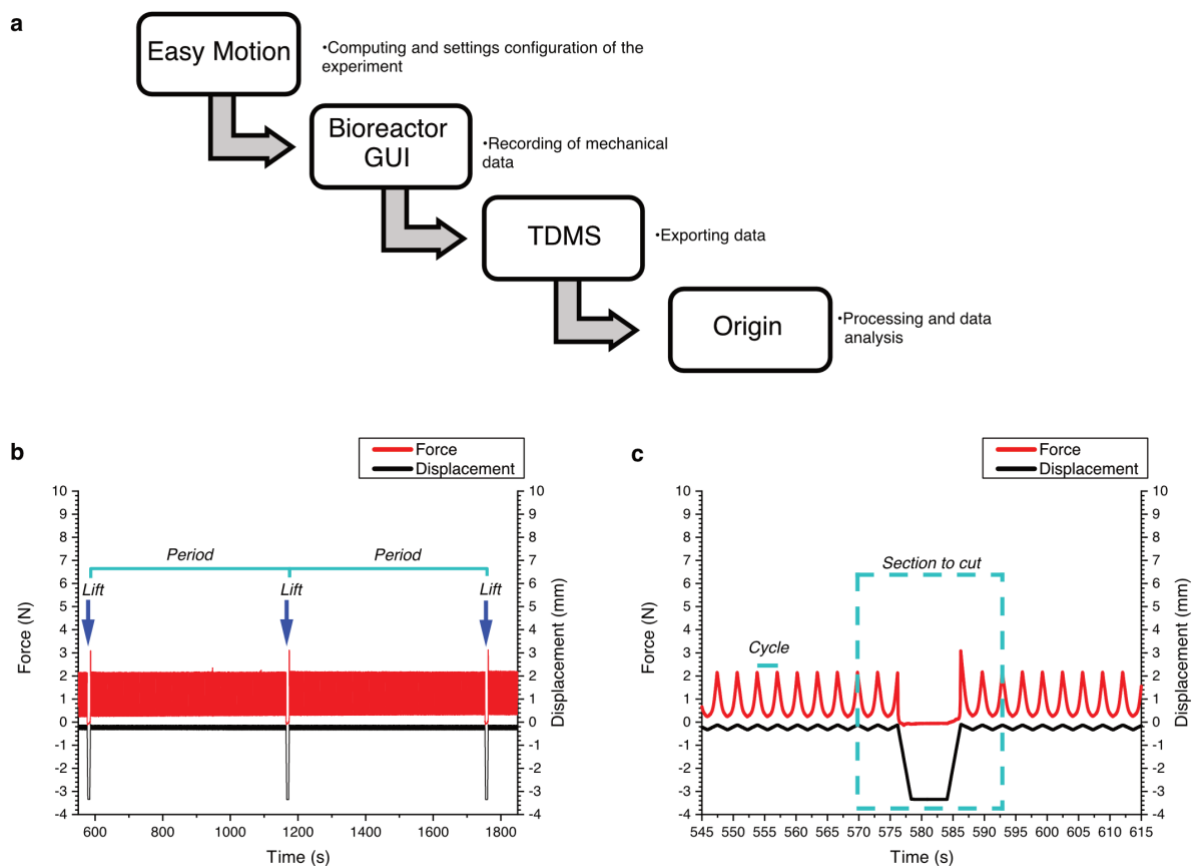


Fig. 5. Mechanical data processing and analysis. (a) Workflow of data handling along the experiment. Settings of the experiment were set up in the Easy Motion controller; mechanical data as displacement, force and time were recorded in Bioreactor GUI at 50 Hz; and the data were exported to Origin software to processing and analysis. (b) Processing of the data consisted on removing the values of the lifts maneuvers for the force and displacement calculations. (c) Detail of the removed section between periods for force and displacement amplitudes calculation. The lifts maneuvers with ± 2 cycles between every lift were cut out. The first and last periods of the whole examination were also removed, corresponding to the position of the piston when started and finished the mechanical stimulation.

3.3.10. Mechanical data analysis

Force and piston displacement values during mechanical stimulation were recorded in the “Bioreactor” Graphical User Interface (GUI) (Fig. 2). Then, data were imported in Origin software for processing and analysis. Briefly, the unload phases ± 2 cycles during intermittent stimulation were detected and removed for descriptive statistics calculation of force amplitude and displacement (Fig. 5). In addition, the first and last periods of the whole examination were also removed for the calculations, corresponding to the position of the piston when started and finished the mechanical stimulation.

3.3.11. Refractive index evaluation

Refractive indexes of the scaffolds were evaluated using an analog refractometer following the manufacturer’s instructions (Cat No., AR4, Kruess Optronic GmbH, Hamburg, Germany).

3.3.12. Confocal microscopy

To analyze numbers and viability of MSCs mobilized into the scaffold, we used confocal microscopy. Scaffolds with embedded cells were stained with 0.5 mg/mL C7-PEI dye detected by the red laser (Ex 654 nm /Em762 nm), 7 μ M C-AM (Ex 494 nm / Em 517 nm) and 5 μ M EthD-1 (Ex 528 nm /Em 617 nm), autofluorescence was evaluated at 488 nm.

After 24 hours of intermittent dynamic load (or unload for controls), the cells were stained by immersing the scaffolds in a solution of 0.9 % NaCl with 7 μ M C-AM and 5 μ M EthD-1 for BM-MSCs viability evaluation in 3D. Cells that mobilized into the scaffolds after stimulation were detected by confocal microscopy and counted by LAS X software. Viable and non-viable were identified by C-AM and EthD-1 staining, respectively.

For the confocal microscopy, the scaffolds were placed in a custom-made holder. Then, DMEM-without red phenol was used as immersion media. 10X magnification immersion objective and green and red channels (Alexa 488 and Texas Red, respectively) were used to visualize the cells. The whole scaffold was initially scanned manually to find the cells. A resolution of 2048 x 2048 pixels was used in all cases at 600 Hz and bidirectional scanning.

0.9 % NaCl was applied as immersion medium when using 10X immersion objective and immersion oil type F as immersion medium when 20X objective was used.

Staining of collagen scaffold structure was carried out using 1:200 COL1A antibody overnight at 4°C and 1:400 IgG Alexa Fluor 488 for 1 hour at RT. Collagen-I was imaged by confocal microscopy using a 63X objective.

3.3.13. Pipeline for cell quantification in 3D

Detection and quantification of the cell number in the scaffolds was done by image analysis using Leica Application Suite X (LAS X) from Leica Microsystems. An initial validation for cell quantification in 3D given by the software was performed as a comparison between known numbers of cells seeded in scaffolds and the quantified cells obtained by another experimenter in a blind test. For this, 1.5 % alginate solution was mixed with 32, 45, and 64 cells/mm³ called as “expected values”, and then scaffold polymerization was carried out with CaCl₂ as previously described and kept in culture in 24-well plates for 24 hours. Then, cells were stained (as described in the section 3.3.6), visualized immediately imaged by confocal microscopy. Viable cells were identified at 494/517 nm (Ex/Em) and non-viable cells at 596/615 nm (Ex/Em). The imaged Region of Interest (ROI) was in the middle of the scaffold with volumes of 0.6-0.7 mm³. Processing of the 3D images was prepared for quantification, called as “counted values”.

A customized pipeline in LAS X was applied for the quantification of cells⁹⁸. The “counted values” were processed for cell segmentation, counting and statistical analysis using the same pipeline as shown in Fig. 6. The ‘Analysis’ tab in the software GUI allowed creating a custom image analysis pipeline based on algorithms. The background noise reduction was obtained using 3D median filtering using sphere having a radius of 3 voxels as a structuring element in every case. Adjust threshold option was used to distinguish the objects (cells) from the background, using values from 6 to 9. Binary data were then processed using morphological filters such as 3D hole filling and opening filter with radius sphere of 2-3 voxels. Unusually large or irregular objects (1-3 in each case) were removed using binary image editing feature in the software by clicking on them. Based on the shape and intensity, 30 different features were calculated by LAS X. These features were subsequently used to generate histograms for features of preference. Objects with diameters between 8 and 25 μm were selected for analysis, assuming that MSCs are within that range as previously reported^{99, 100}.

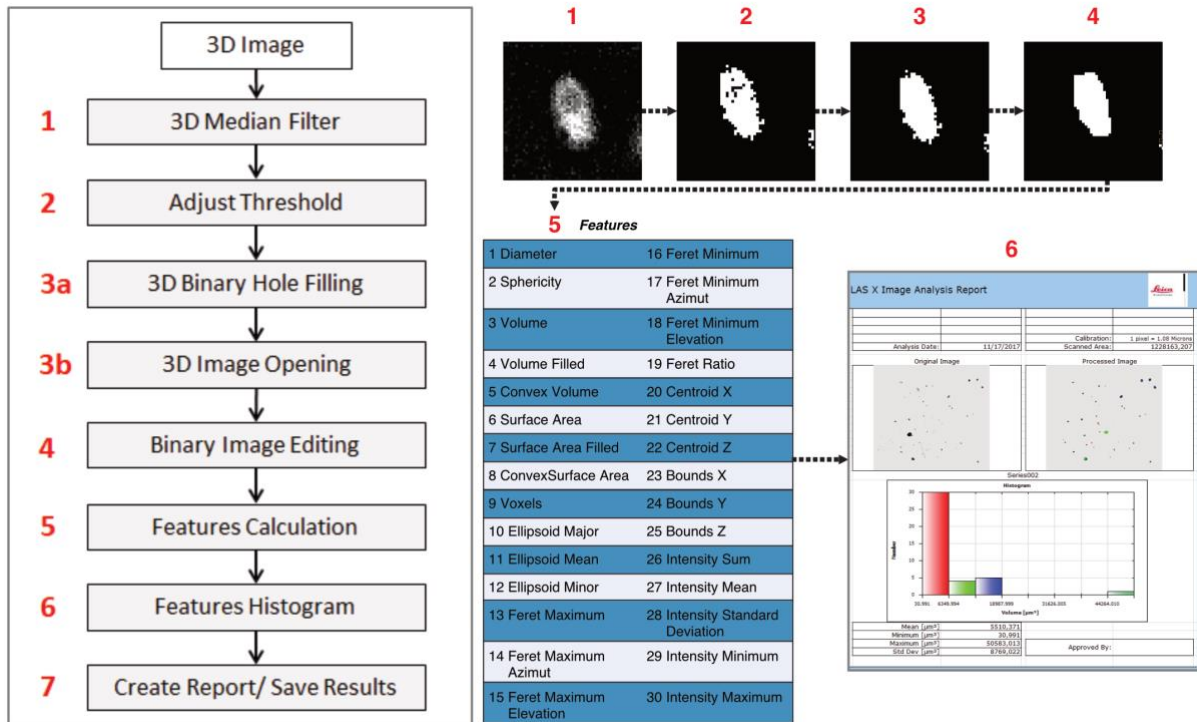


Fig. 6. Pipeline for cell quantification in 3D. The ‘Analysis’ tab in the software GUI allowed to create a custom image analysis pipeline using algorithms. Briefly, the applied pipeline consisted on 3D median filtering, threshold 3D adjusting, binary holes filling, 3D-image opening, binary image editing, and features calculation. The results including cell features, histograms, statistics and image data were then saved in excel sheets on the hard drive in case of further statistical analysis.

3.3.14. Statistical analyses

Descriptive statistical analyses were performed using Origin version 9.0G for Windows (OriginLab Corporation, Northampton, USA).

For the stiffness and selection analysis of the elastic rings, a comparison of the mean force was performed as follows: 1) only data collected after sterilization were used, 2) the mean force across replicates was estimated, 3) followed by computing the Pearson correlation coefficient between the mean force of every ring pair and 4) visualized by a heatmap, showing the correlation coefficient.

Polynomial curves were fitted using the function “stat_smooth” from the R package ggpubr, using the smoothing method “loess” and applying the formula “y ~ log(x)”. The plots were

made in R Core Team 2019 (Foundation for Statistical Computing, Vienna, Austria) using the data obtained from Origin and SAS.

A two-sided Wilcoxon rank sum test was performed to evaluate the difference in cell density in pigs when extracted from intertrochanteric or intercondylar location.

Analysis of variance (ANOVA) was performed using SAS 9.4 (Business Analytics und Business Intelligence Software, Cary, NC, US). The GLM procedure was used to fit general linear models with the least squares method, obtaining a p-value for the whole model. To test the relationship among the factors and their levels in the model, the least square means were estimated in a paired fashion, and adjusted for multiple comparisons using the method Sidak. Several models were built to test the relationship between the groups “Alginate vs. Collagen”, “Loading vs. No Loading”, and “Viable vs. Non-viable”. P-values lower than 0.05 were taken as statistically significant.

4. Results

In order to setup the system, a variety of pretests were run to establish several specifications, such as elastic ring and scaffold fabrication, cell isolation, mechanical program setup and optimization and cell visualization and quantification.

4.1. Stiffness tests of elastic ring

As the mechanical stimulation compresses simultaneously the elastic ring and the scaffold, it was important to determine if the stiffness of the elastic rings alone or with the scaffolds were measurable with our force sensor (up to 10.9 N). This is, stiff rings would have disabled the loading application on the scaffold. Furthermore, since sterility was mandatory for the following experiments with cells, it was critical to evaluate whether it would be possible to sterilize the elastic rings and how much their stiffness would change.

The force exerted on the system as result of the loading applied on elastic rings by the piston was measured in the bioreactor in triplicates for 10 different elastic rings before and after sterilization (Fig. 7). The piston displaced every 30 μm , exerting load while compressing the rings. The forces produced of such displacements were measured up to 10.9 N, which was the maximum limit allowed of the force sensor. Since 10 % strain was chosen as one of the biomechanical set points to apply in the study, 300 μm corresponded to the value to be further analyzed.

The mean force applied on rings before and after sterilization was 5.39 ± 3.34 and 7.18 ± 2.16 N at 300 μm of compression, respectively (Table 3, Fig. 7a). As the variation between the rings seemed to be high in terms of their stiffness values (Fig. 7a), the 10 rings were compared between them to select those with similar stiffness behavior after being sterilized for further stiffness evaluations with scaffolds (Fig. 7b). A heat map was done to compare all the 10 rings between them. The array showed 3 main clusters of rings with similar stiffness, grouping the rings 1, 3, 4 and 8 in cluster A; rings 2, 6 and 7 in cluster B; and rings 5, 9 and 10 in cluster C. From cluster A, the rings 1, 3 and 4 were chosen for further analysis. Their stiffness was compared with alginate scaffolds or alginate scaffolds with embedded cells (Fig. 7c).

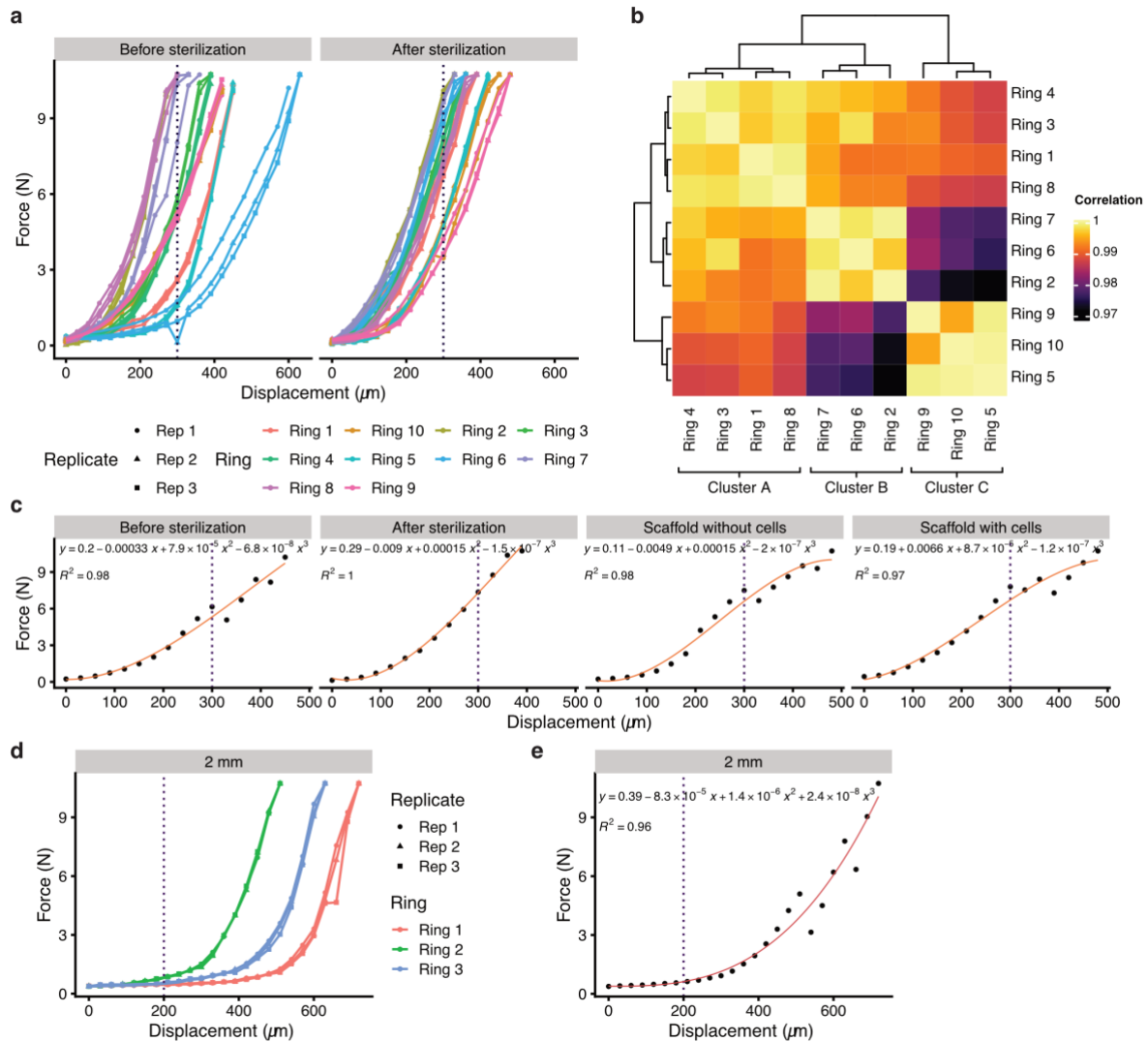


Fig. 7. Stiffness test of silicone rings. (a) The stiffness of 10 different elastic rings made following the same protocol was tested before and after sterilization at 120°C. The force obtained after compressing the rings every 30 μm by displacing the bioreactor piston was measured in the bioreactor. Dashed rows represent 10 % strain regarding the original scaffold height. (b) Heat map showing the correlation of the stiffness between all sterilized rings. The rings were grouped in three main clusters (A-C). (c) Polynomial curves of alginate scaffolds stiffness for rings 1, 3 and 4 showed similarity between the conditions. At 10 % strain, the force was close to 7 N. (d) Stiffness of three different rings of 2 mm of height is shown in triplicates or as a polynomial curve (e). With rings of 2 mm of height, the load applied over the elastic rings slightly affected the force of the system. Therefore, it was the proper height of silicone rings to be used for the subsequent experiments.

Table 3. Descriptive statistics of the force at 10 % strain for elastic rings of 3 mm height. The force was measured every 30 μm that the piston was displaced to compress the elastic rings. 10 % strain is seen at 300 μm of displacement. These values represent the descriptive statistics of the dashed line in Fig. 7.

Condition	Displacement (μm)	n total	n missing	Force Mean (N)	Std Dev (N)	Min (N)	Median (N)	Max (N)
3 mm elastic rings before sterilization	210	30	0	2.64249	1.70912	0.48069	2.43288	5.89581
	300	28	2	5.39165	3.34519	0.11772	5.13063	10.73214
3 mm elastic rings after sterilization	210	30	0	3.50217	1.34063	1.41264	3.88476	5.3955
	300	27	3	7.18452	2.15782	3.46293	7.49974	10.09449
3 mm elastic rings after sterilization, + scaffold	210	9	0	3.29616	2.31576	0.72594	3.06072	6.30783
	300	9	0	5.20771	2.84083	2.69775	5.30721	10.73214
3 mm elastic rings after sterilization, + scaffold, + cells	210	9	0	4.17143	2.06684	1.23606	4.96386	6.1803
	300	9	0	7.80113	2.98731	3.58065	8.77014	10.73214

The selected rings from cluster A showed a mean force of 5.20 and 7.04 N before and after sterilization at 10 % strain (300 μm of compression), respectively. The stiffness of the sterile ring with the empty scaffold was 6.74 N and 6.76 N for those scaffold with cells, respectively. This indicates that neither the empty scaffold alone nor the scaffold with cells alter the stiffness shown by the elastic rings alone.

The arrangement with elastic ring and scaffold with cells was stiffer compared to the same with an empty scaffold, having forces of 7.80 ± 2.99 N and 5.21 ± 2.84 at 300 μm of compression, respectively (Table 3, Fig. 7).

Due to some of the tests reached the maximum limit even before 300 μm compression (seen as missing values in Table 3) or were close to it, the original size of the elastic ring and scaffolds was reduced to 2 mm. Therefore, 200 μm was the new key compression that corresponded to 10 % strain. The mean of the force measured for 210 μm of the compression for the same rings was 2.64 ± 1.71 before sterilization, and 3.50 ± 1.34 after sterilization. Extrapolating from Fig. 7c, it was seen that at 200 μm of compression, the estimated forces were 2.95 and 4.01 N before and sterilizing, respectively.

Three new elastic rings were made with the height of 2 mm and their stiffness was tested accordingly (Table 4). At 210 μm of compression, the force was 0.628 ± 0.181 N, and the

extrapolated force at 200 μm was 0.9692 N (Fig. 7e). Therefore, 10 % strain (200 μm of compression) influences minimally the force of the system using 2 mm elastic rings.

Table 4. Descriptive Statistics of the force at 10 % strain for elastic rings of 2 mm height. The force was measured every 30 μm that the piston was displaced to compress the elastic rings. These values represent the descriptive statistics of the values close to the dashed line in Fig. 7.

Condition	Displacement (μm)	n total	n missing	Force Mean (N)	Std Dev (N)	Min (N)	Median	Max (N)
2 mm elastic ring	180	9	0	0.56026	0.12471	0.45126	0.50031	0.76518
	210	9	0	0.62784	0.18142	0.45126	0.54936	0.87309

The results allowed to determine that scaffolds and elastic rings of 2 mm high were preferred rather than 3 mm for the mechanical loading experiments, since the force sensor was able to measure every value of the curve and never reached the maximum (10.9 N) as happened with 3 mm elastic rings.

4.2. Yield of pBM-MSCs isolation

The pBM-MSCs were isolated from the bone marrow by opening the femora at the intertrochanteric or intercondylar region, and expanded as previously described in the methods section. When the cells reached to 70 – 80 % confluence, the amount of adherent cells was quantified and the amount of tissue collected from bone marrow was correlated. We analyzed whether the tissue source affected cell numbers and growth. First, the density of cells that were harvested at subconfluence with respect to the initial amount of isolated bone marrow was evaluated, showing no linear correlation between variables for all conditions since the R^2 coefficients were small (Fig. 8a). Nonetheless, a negative trend was seen for cells isolated from juvenile pigs. Second, the density of cells was also compared to the time the culture took to reach to subconfluence. A Wilcoxon rank sum test was performed to evaluate the difference in cell density in pigs when extracted from intertrochanteric or intercondylar location. No significant difference was found between both conditions (p-value = 0.4363). The cells from piglet showed shorter time to reach subconfluence (Fig. 8b).

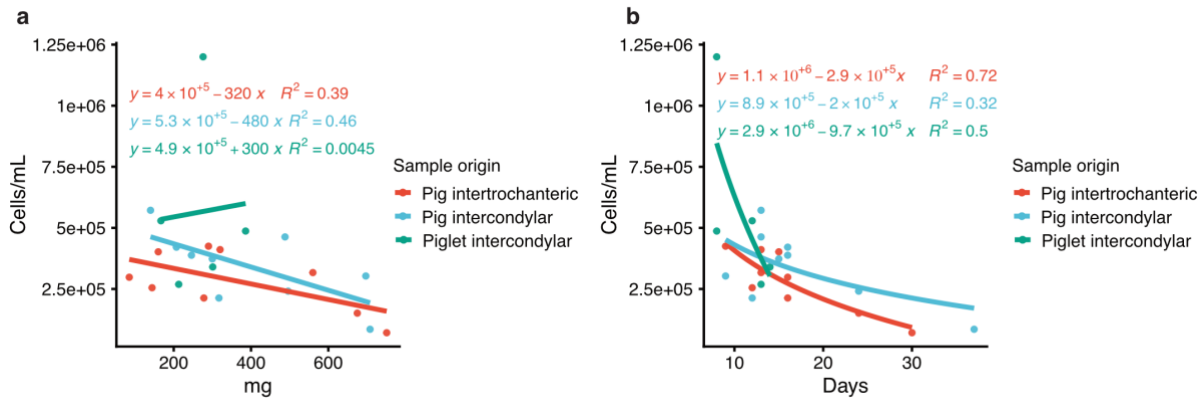


Fig. 8. Yield of pBM-MSCs isolation. Cell density was compared to the amount of material initially isolated from the bone marrow and the duration to grow to subconfluence. **(a)** Correlation between the cell density obtained per mg isolated from different sources. pBM-MSCs were isolated either from intertrochanteric or intercondylar region of femora of juvenile pigs, or intercondylar femora of piglets. No linear correlation was seen between the two variables compared. **(b)** Correlation between the cell density and time to reach subconfluence for cells according to source of isolation. Cells isolated from piglets seemed to grow faster.

4.3. Immunophenotyping of pBM-MSCs

Immunophenotyping of pBM-MSCs was done by staining of surface markers CD29⁺, CD44⁻, CD45⁻, CD90⁺, SLA-1⁺ and SLA-DR⁻ as previously described¹⁰¹ with porcine antibodies (Fig. 9a). Cross-reactivity of human antibodies with porcine antigens was also tested, providing similar detection levels as porcine antibodies with the exception of HLA, which was specific for human cells (Fig. 9b). The observed human surface markers were CD73⁻, CD31⁻, CD34⁻, CD146⁻, NG2⁻, CD104a⁻, CD105⁻, CD106⁻, HLA-ABC⁻ and HLA-DR⁻ and CD104b⁺. The Fig. 9 shows a representative FACS analysis of pBM-MSCs from a juvenile pig.

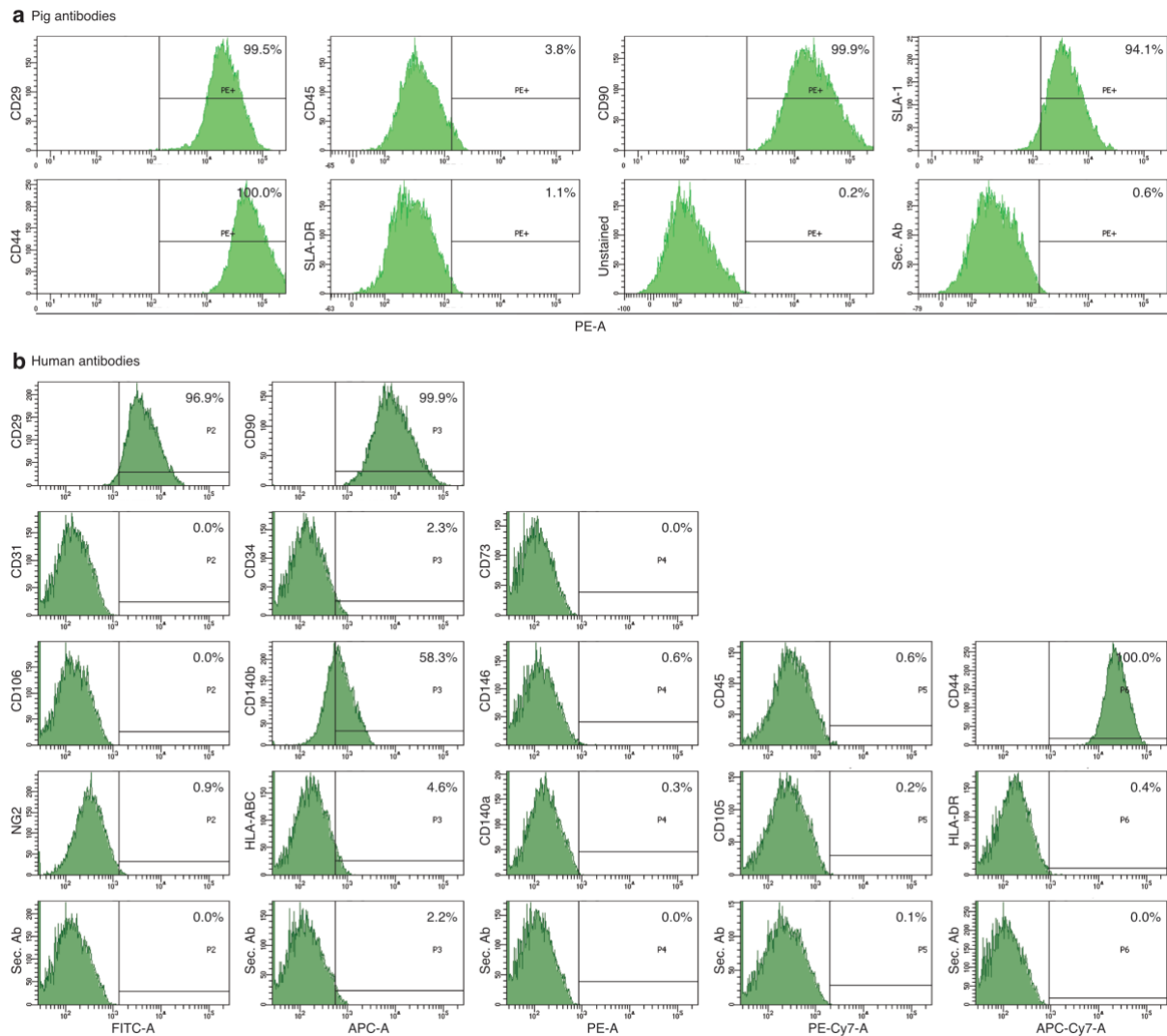


Fig. 9. Surface markers of pBM-MSCs. Representative histograms of porcine antibodies (a) and human antibodies (b) tested on pBM-MSCs. Gating was performed on unstained cells, classified as negative. Values indicate percent positivity for the respective marker. The figure shows the FACS analysis performed on cells from a juvenile pig.

The immunophenotype of porcine cells was similar independently if isolated from intertrochanteric or intercondylar regions (Fig. 10) or from right or left legs (Fig. 11).

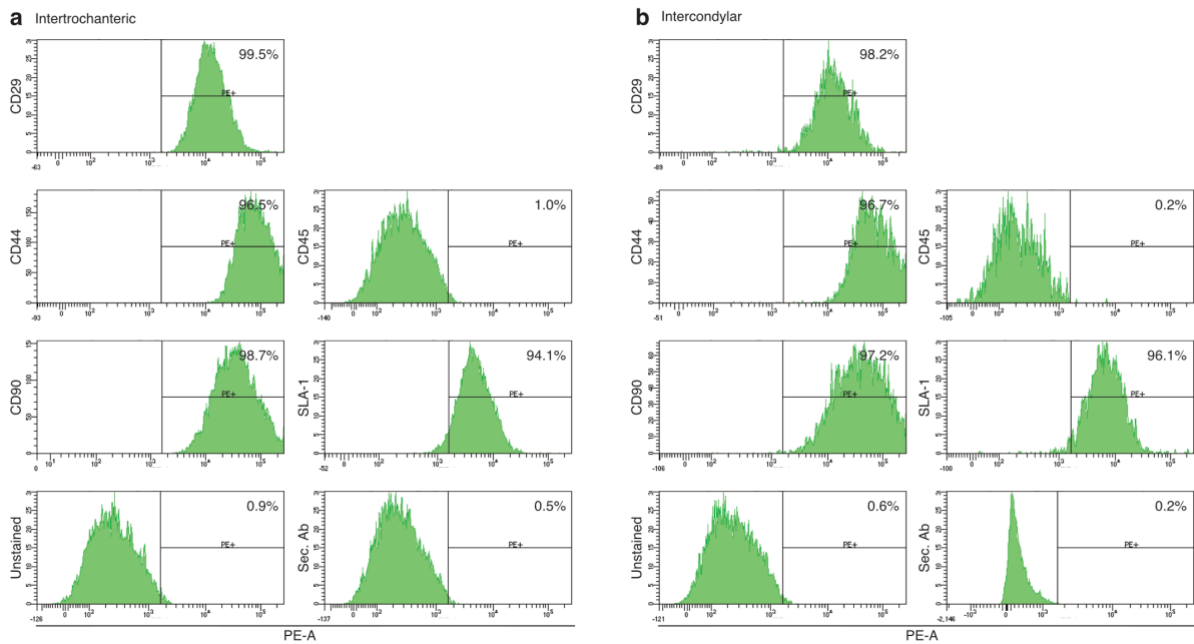


Fig. 10. Immunophenotype of pBM-MSCs isolated from different regions of the same femur. Representative histograms of porcine antibodies tested on pBM-MSCs isolated from intertrochanteric (a) or intercondylar regions region (b) exhibit comparable results.

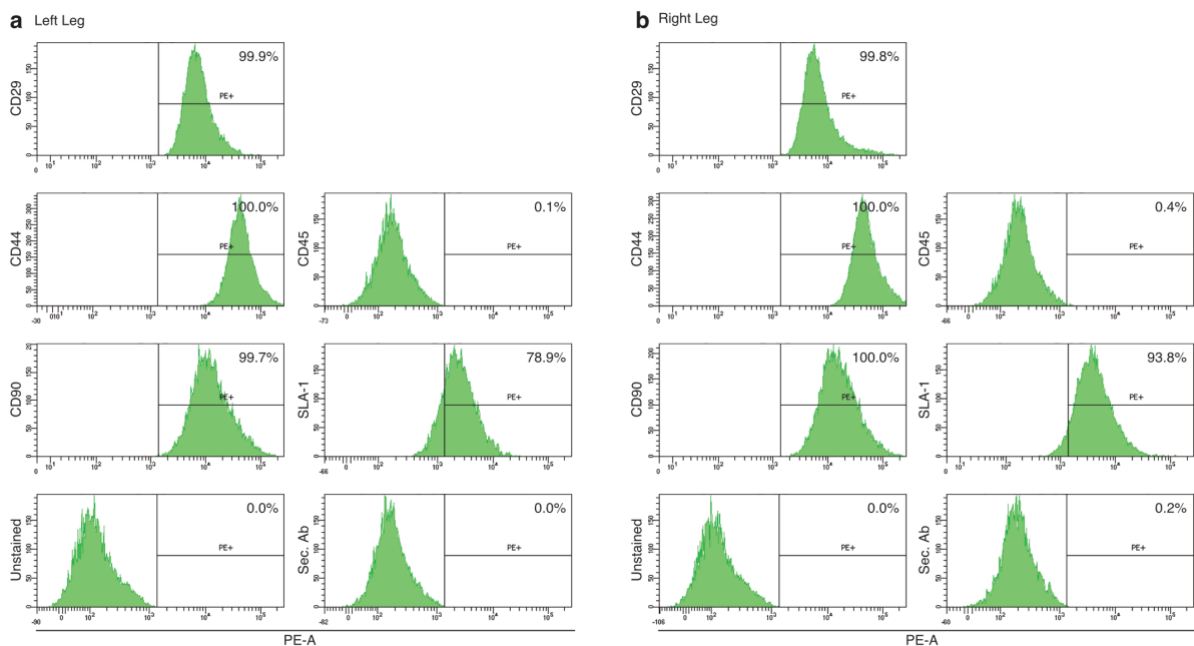


Fig. 11. Immunophenotype of pBM-MSCs isolated from different legs. Representative histograms of porcine antibodies tested on pBM-MSCs isolated from right (a) of left (b) legs from the same animal.

The FACs analysis showed similar behavior was seen in the staining of the antibodies from intertrochanteric, intercondylar, right or left legs (Figs. 10 and 11). This indicates that taken

together as a population, the cells were similar with respect of their characterization of surface markers regardless of their isolation location.

4.4. Imaging of cells in 3D

After having setup the bioreactor and isolated and characterized pBM-MSC, the next step was to establish a method to image cells in the 3D scaffolds. The refractive index of alginate scaffold was 1.3340 at 22.1°C, this is an important value to select the appropriate immersion medium. Therefore, 0.9% NaCl was used as immersion medium for confocal microscopy using 10X immersion objective. Embedded cells in alginate scaffolds of 2 mm height were visualized by confocal microscopy. Cell autofluorescence was detected in green channel (Fig. 12a, left) down to 350 μm depth (Fig. 12a, right). Similarly, cells stained with Cy7-PEI were also detected in a depth of about 400 μm (Fig. 12b). Staining with C-AM and EthD-1 allowed for deeper cell visualization down to 1 mm depth. Examination of cell viability was also possible (Fig. 12c). Thus, the preferred staining method for the confocal microscopy was to stain with C-AM and EthD-1 because these dyes it was possible to visualize and distinguish between viable and non-viable cells, better quality for the images were obtained, higher penetration from the lasers was seen.

4.5. Quantification of cells in 3D

To detect and quantify the number of cells present in each sample, we established an image analysis pipeline was done to detect and quantify the number of cells present in each sample. Quantification of cells was initially validated by embedding known numbers of cells of 32, 45, and 64 cells/ mm^3 , named as “expected value” and comparing these to the values quantified by LAS X, called as “counted value”. The quantification was performed semi-automatically as elucidated in section 3.3.9. The counted values corresponded to 33, 49, and 56 cells/ mm^3 , which correlated very well to the expected counterpart with a Pearson correlation coefficient equal to 0.946 (Fig. 13).

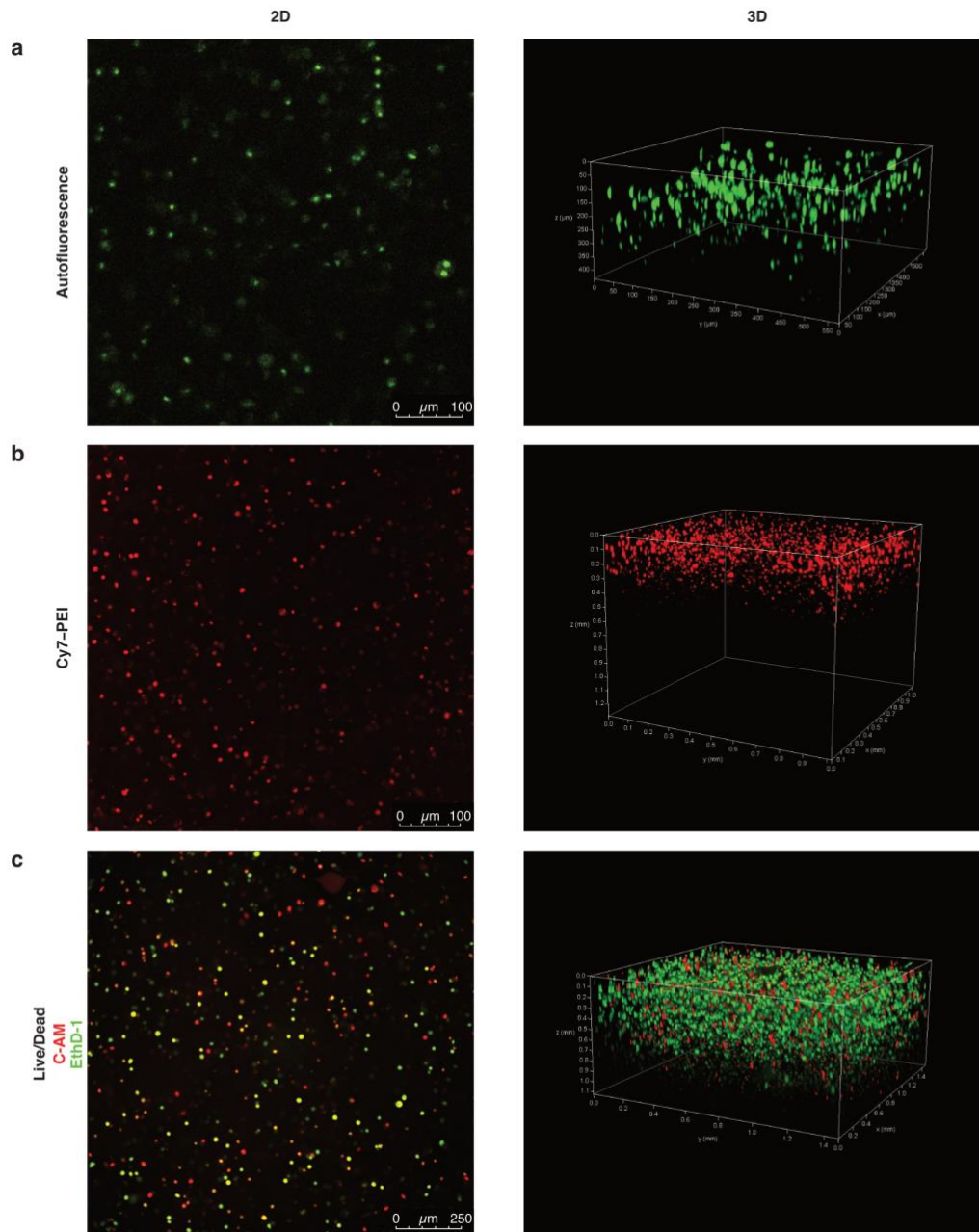


Fig. 12. Staining optimization for cell visualization in 3D. Cells could be detected down to 350 μm by autofluorescence (a), 400 μm by Cy7-PEI (b), and about 1 mm when staining with C-AM and EthD-1 (c). Moreover, viable cells were seen in green and non-viable in red. Images in z-axis were taken until the cells were detected. Z-plane dimension was 0.450 mm in a), 1.2 mm in b) and 1.1 mm in c). *Cy7-PEI*: Cyanine polyethyleneimine, *C-AM*: Calcein-AM, *EthD-1*: Ethidium homodimer-1.

4.6. Continuous and intermittent mechanical stimulation

Having established a pipeline for image analysis, we proceeded to perform mechanical loading experiments. The cartridges were prepared with a suspension of 1×10^5 pBM-MSCs in DMEM in the cell reservoir, the alginate scaffold over it and the elastic ring to hold the scaffold in place. Dynamic mechanical loading was applied continuously for 24 hours to one of the cartridges, whereas the correspondent control was not mechanically stimulated. Subsequently, the viability of the cells in the reservoir was analyzed, obtaining about 35 % (median of 34.4 %, ranging from 32.5 to 36.5 %) of viable cells after applying continuous dynamic loading continuously (Fig 14a).

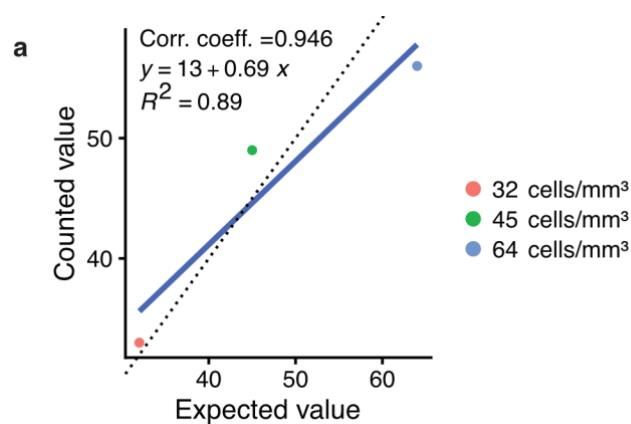


Fig. 13. Validation of cell quantification in 3D. Known numbers of cells (expected value) were correlated to the counts obtained by following an image analysis pipeline (counted value) using LAS X. The ROI was visualized through a depth of 500-600 μm . Independent experiments for every condition were made in triplicates from the same donor. The blue line represents the linear regression of the expected value with respect to the counted value. The dashed line follows the function $y=0+x$.

A modification of the mechanical program as well as the cartridge was necessary to allow nutrients supply. Cell culture medium was provided from the most upper position of the arrangement (Fig. 14c). Therefore, the cartridge was complemented with a mesh (Fig. 14b, 5) and an anchored ring (Fig. 14b, 6), which held the scaffold in position for mechanical stimulation applied as an intermittent scheme (Fig. 14b).

After 24 hours of intermittent dynamic loading, the viability of cells located at the cell reservoir was about 70 % (median of 69.3 %, ranging from 60.0 to 71.1 %) (Fig. 14a).

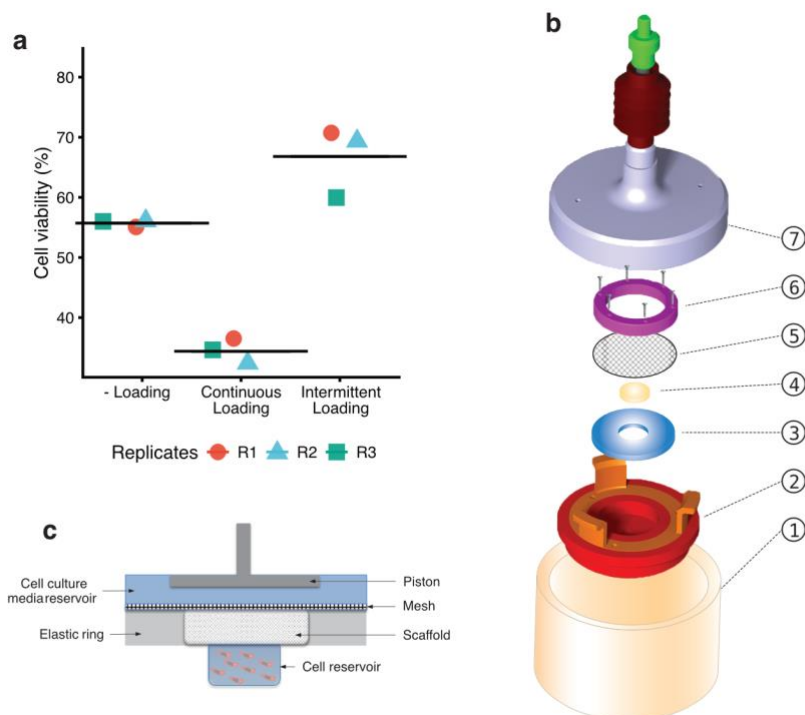


Fig. 14. From continuous to intermittent mechanical stimulation. (a) After 24 hours of mechanical stimulation, the viability of the cells located in the cell reservoir was evaluated by trypan blue exclusion assay. Dynamic continuous loading provided the lowest cell viability values. The intermittent regime comprised interruptions with unloaded phases of 10 seconds after each 180 cycles for 24 hours, providing the highest cell viability percentages. Control scaffolds were prepared simultaneously in a separated and identically constructed cartridge, but no mechanical loading was applied. The results are shown as triplicates of pBM-MSCs from the same donor; Δ , \circ , \square = replicates. (b) The sketch shows parts of a disassembled cartridge. The scaffold holder (2) contains the reservoir in the middle where the cells were placed. A scaffold (4) is placed over them, which is held in place by the elastic ring (3) and a mesh above it (5). The mesh is kept in place by a ring anchored to the construction using screws (6). The scaffold holder is placed as an independent movable unit within the cylindrical container (1) and it is covered up by a cap (7) containing the piston and spring. The cartridge is made of sterilizable materials. (c) Schematic drawing showing the cross-section of the parts of an assembled scaffold holder without the upper anchored ring. (d) Schematic drawing showing the cross-section of the parts of an assembled scaffold holder without the upper anchored ring used for intermittent mechanical loading. The mesh aimed to prevent the scaffold from moving up during the lift maneuvers. Adapted image from Ref. ⁴ with the permission of PLoS One, license CC-BY.

4.7. pBM-MSCs mobilized into alginate and functionalized alginate-Ln scaffolds

After 24 hours of intermittent mechanical stimulation, 13 ± 2 cells/mm³ (median of 13 cells/mm³, ranging from 11 to 15 cells/mm³, and 66.7 % cell viability) were found in the scaffolds, and 24 ± 11 cells/mm³ (median of 30 cells/mm³, ranging from 11 to 31 cells/mm³, and 73.7 % cell viability) in the unloaded alginate scaffolds control. However, when the alginate scaffolds were functionalized by supplementing with LN521 (alginate-Ln scaffolds), 48 ± 21 cells/mm³ were found in the unloaded scaffolds (median of 56 cells/mm³, ranging from 24 to 63 cells/mm³, and viability of 83.8 %), and 194 ± 39 cells/mm³ (median of 202 cells/mm³ ranging from 152 to 230 cells/mm³, 89.7 % cell viability) were present after

loading (Fig. 15). In all cases, the cells in the scaffold were found in regions close to the adjacent cell reservoir.

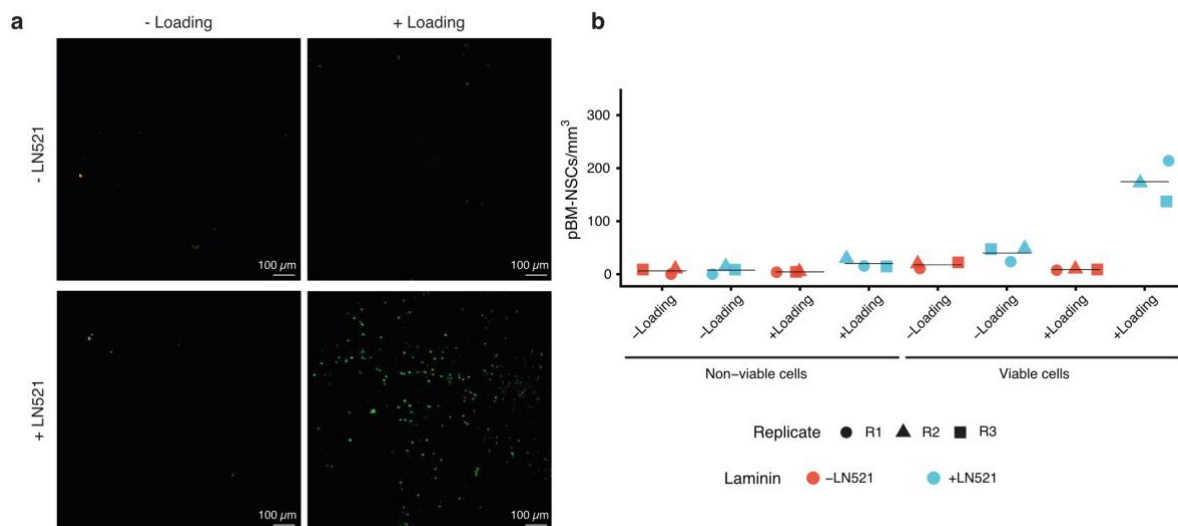


Fig 15. pBM-MSCs mobilized into alginate or alginate-Ln scaffolds. (a) Representative confocal microscopy images of alginate and alginate-Ln scaffolds, with or without mechanical stimulation. Calcein-AM is seen in green and represents viable cells; ethidium homodimer-1 is seen in red and represents non-viable cells. A few non-viable cells were seen in the scaffolds. Bar scale=100 μm. (b) Quantification of viable and non-viable cells found in the scaffolds after biomechanical stimulation or control. LN521 seemed to have improved the alginate scaffold in terms of cell intake. The combination of LN521 in the scaffolds and the intermittent mechanical loading enhanced the number of cells found in the scaffolds. The results for every condition are shown as 3 independent replicates with pBM-MSCs from the same donor. Mechanical dynamic loading regime consisted on 10 % strain, 0.3 Hz frequency, breaks of 10 seconds every 10 minutes. Red color indicates scaffolds without LN521 (alginate scaffolds) and blue indicates the use of LN521 (alginate-Ln scaffolds); Δ, O, □ = replicates. Adapted image from Ref. ⁴ with the permission of PLoS One, license CC-BY.

4.8. hBM-MSCs mobilized into alginate-Ln scaffolds

As more pBM-MSCs were present in the alginate-Ln scaffolds when applying intermittent mechanical loading, the same experimental conditions were tested on hBM-MSCs. 8 ± 5 viable cells/mm³ were counted in loaded scaffolds (Table 5), whereas 4 ± 2 viable cells/mm³ in the unloaded alginate scaffolds (p-value = 0.0447, Fig. 16a). Despite that more cells seem to have been mobilized to the scaffolds, they were mostly observed on the scaffold surface, adjacent to the cell reservoir (Fig. 16b). Analytical statistics is detailed in the Appendix A.

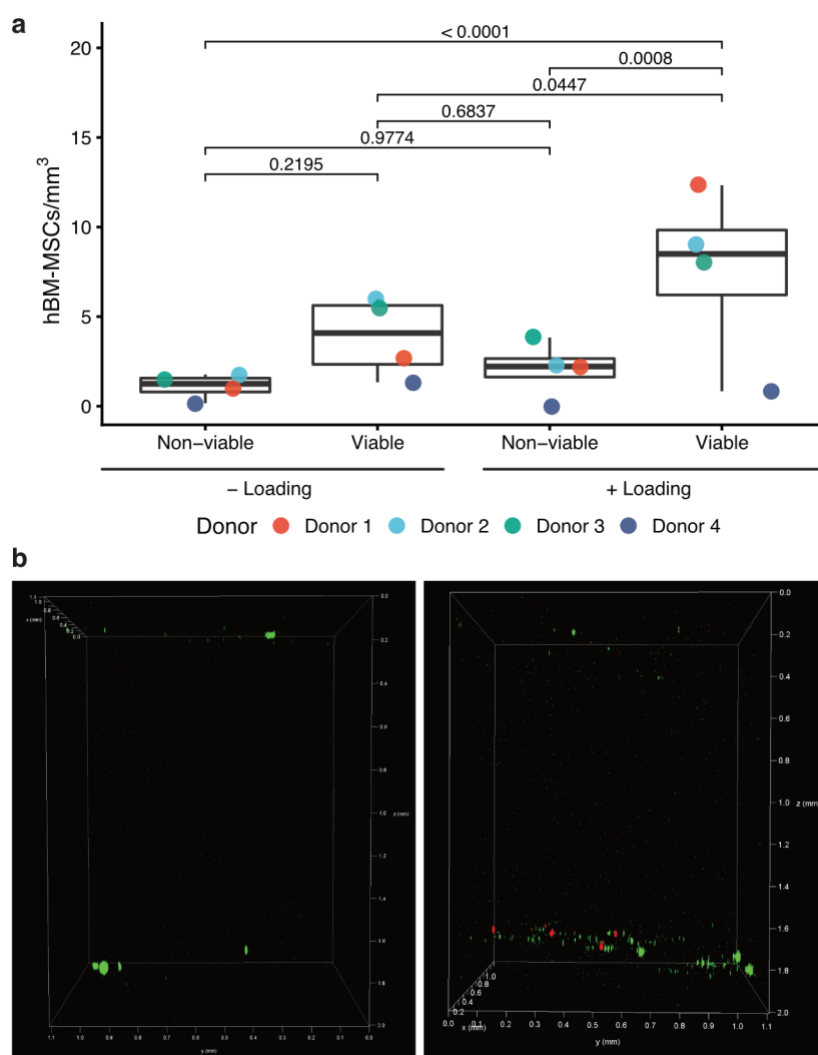


Fig 16. hBM-MSCs mobilized into alginate-Ln scaffolds. (a) The scaffolds were visualized by confocal microscopy after 24 hours of intermittent mechanical stimulation or no loading application for the controls. More cells were found in the loaded scaffolds compared to the control. **(b)** 3D image of the scaffolds. The cells seem to be distributed on the scaffold surface. The examinations were done using cells from four different donors; every dot represents the mean of a technical triplicate. ANOVA test was done adjusting multiple comparisons by Sidak. The dimensions of the axes are 1.1 cm (x), 1.1 cm (y) and 2.0 mm (z).

4.9. Collagen and gelatin scaffolds fabrication

To develop scaffolds better mimicking the local milieu, we decided on collagen and gelatin scaffolds. Different solutions composed of collagen, gelatin or a combination of them with BDDGE as cross-linker were tested to make suitable scaffolds in shape and composition. The evaluated solutions were divided in group A (collagen, 10 % BDDGE), B (collagen; 20 % BDDGE), C (collagen and gelatin; 10 % BDDGE) and D (gelatin; 10 % BDDGE) as described in Table 2. The examinations were performed at 4°C, RT or 37°C, and pH 5.0, 7.2, or 9.0. The polymerization was maintained under the respective temperatures for 48 hours.

Table 5. Descriptive statistics of hBM-MSCs mobilized into alginate-Ln scaffolds. Human cells that mobilized into functionalized alginate-Ln scaffolds after intermittent mechanical stimulation (+ Loading) or no stimulation (-Loading) for the controls were quantified and the descriptive statistics was calculated. More viable cells were seen in Ln-alginate and the cell viability was not affected in any condition. N= number of donors. It is the mean of the technical triplicates within every donor.

Group	Viability	N	Mean (cells/mm ³)	Std Dev	Min	Median	Max	% viability
-Loading	Non-viable	4	1	1	0	1	2	77.76
-Loading	Viable	4	4	2	1	4	6	
+Loading	Non-viable	4	2	2	0	2	4	78.49
+Loading	Viable	4	8	5	1	9	12	

First, we addressed scaffold stability. The scaffolds with gelatin (groups C and D) were immediately polymerized at 4°C but became liquid after some minutes at RT, while all the rest remained liquid. After 24 hours, only the groups with gelatin at 4°C were solid. After 48 hours, all the scaffolds with only collagen (A and B) at pH 5.0 were solid, regardless of the temperature; but not at pH 7.2 or 9.0. Scaffolds with gelatin (C and D) were solid at 4°C, regardless the pH. The combination of collagen and gelatin was solid at 4°C when the pH was 7.2 or 9.0, and at RT with pH 7.2 (Fig. 17).

As collagen polymerized at pH 5.0 under the evaluated temperatures and the scaffolds also seemed to be stable in shape (Fig. 18a), further analyses were performed for groups A and B. The scaffolds were observed by optical microscopy with 10X (Fig. 18b left) and 40X (Fig. 18b right) magnification, showing a gel indicating that polymerization of the collagen solution occurred. When completely solidified, the refractive index was 1.3362 at 22.0°C. Then, the collagen network was observed by confocal microscopy with specific staining of COL1A antibody (Fig. 18c).

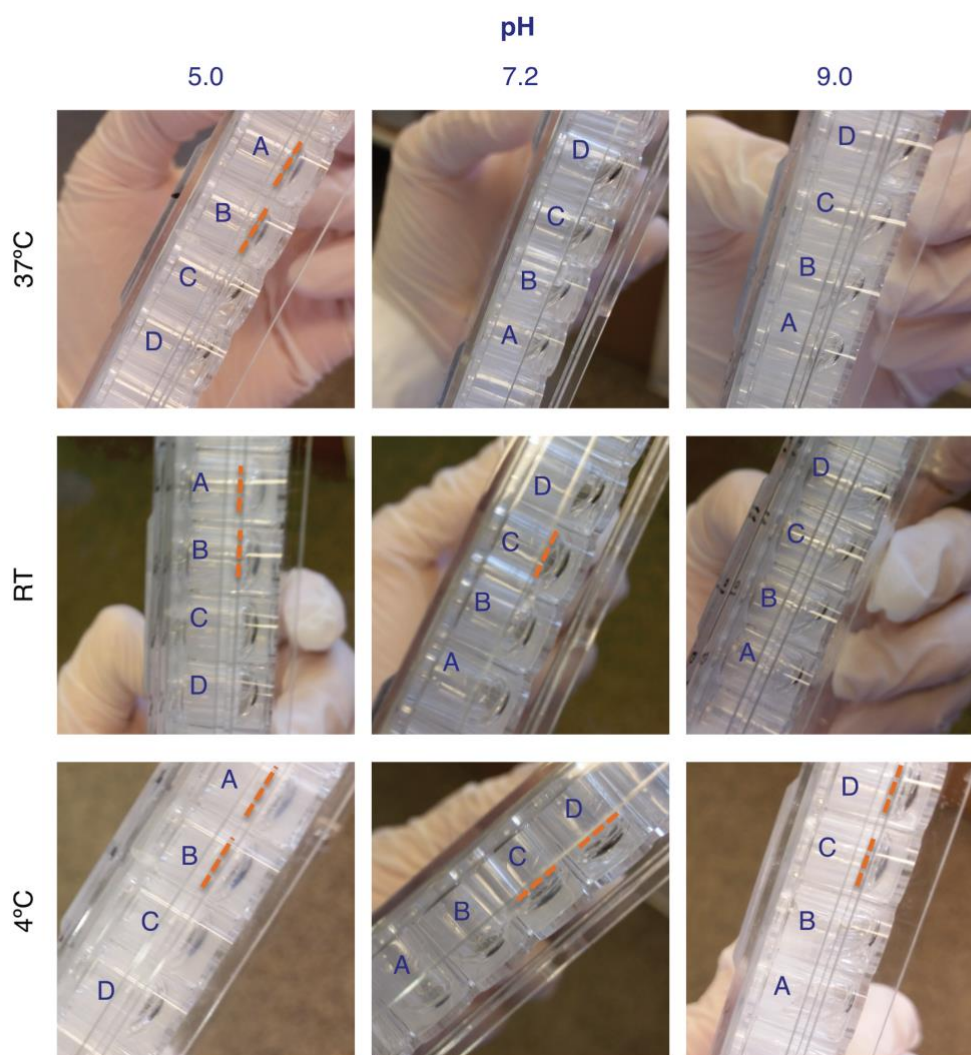


Fig. 17. Macroscopic observations of collagen and gelatin scaffolds fabrication. Scaffold manufacture from collagen, gelatin or a combination of these solutions was evaluated at 4°C, RT or 37°C, and pH 5.0, 7.2, or 9.0. BDDGE was used as cross-linker. Groups A and B polymerized at pH 5.0 independently of the temperature, whereas C and D polymerized at 4°C regardless the pH. The dashed lines denote the wells where the solution polymerized and remained solid, i. e., the liquid did not leak by inclination. *BDDGE: 1,4-Butanediol diglycidyl ether, A: Collagen with 10 % BDDGE, B: Collagen with 10 % BDDGE, C: Collagen and gelatin, 10 % BDDGE, D: Gelatin with 10 % BDDGE.*

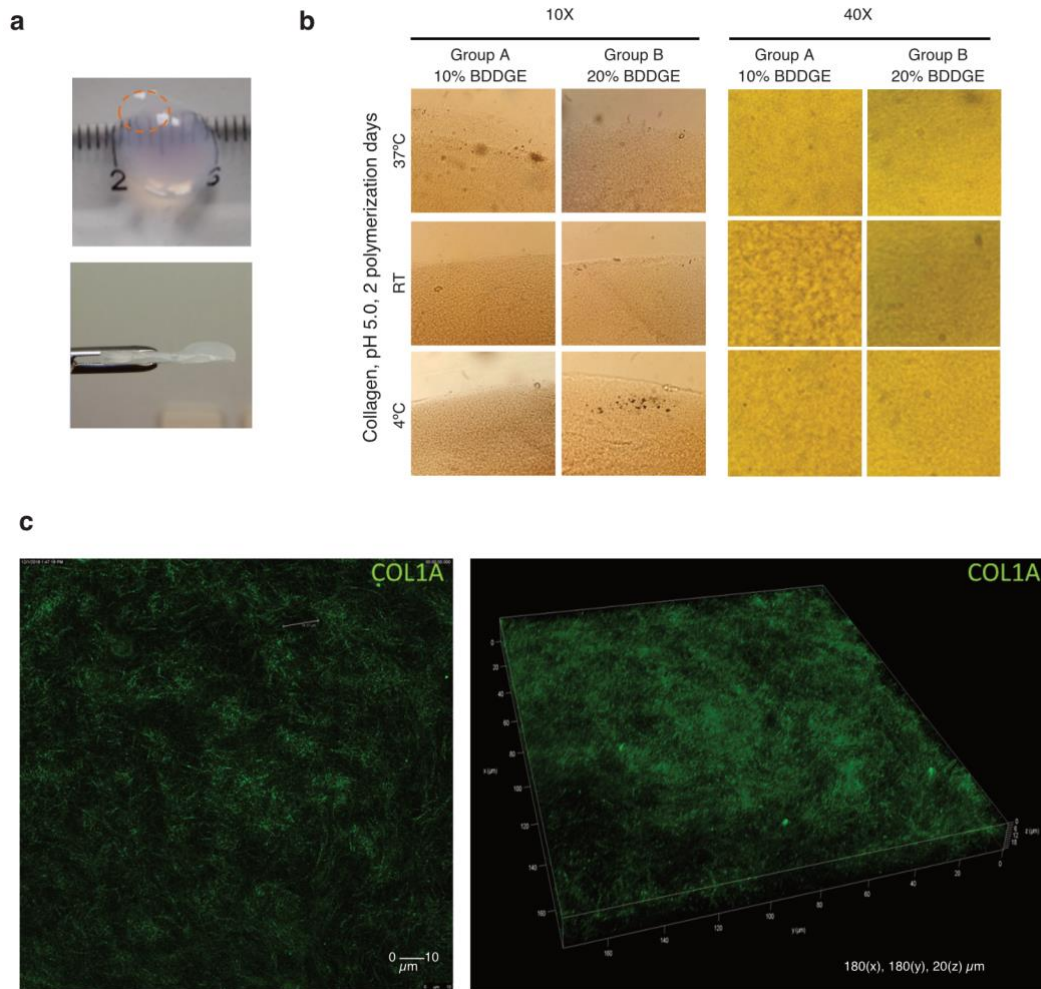


Fig. 18. Microscopic observations of the collagen scaffolds. (a) Picture of a scaffold made from collagen at pH 5.0 with 10 % BDDGE. The dashed orange circle denotes the regions of images taken in a higher magnification that are seen in (b). (b) Optical microscopic view of the collagen scaffolds with 10 % or 20 % BDDGE at 10X (left) or 40X (right) magnification. (c) Confocal microscopy image with specific staining of the collagen network. Scale bar of the 2D image: 10 μm , dimension of the 3D image: 180 (x), 180 (y), 20 (z) μm . *BDDGE*: 1,4-Butanediol diglycidyl ether, *COL1A*: monoclonal antibody against collagen-1A, **A**: Collagen with 10 % BDDGE, **B**: Collagen with 10 % BDDGE, **C**: Collagen and gelatin, 10 % BDDGE, **D**: Gelatin with 10 % BDDGE.

4.10. Mobilization of hBM-MSCs into collagen scaffolds

Intermittent mechanical stimulation was applied to collagen scaffolds with 1×10^5 hBM-MSCs seeded in the cell reservoir (Fig. 19). Mechanical stimulation significantly induced the mobilization of hBM-MSCs into the collagen scaffolds as 245 ± 42 viable cells/ mm^3 were found in the loaded scaffolds compared to 22 ± 6 viable cells/ mm^3 in the unloaded control (p-value < 0.0001 , Appendix B). In addition, the mechanical stimulation seemed not to be harmful for the cells as 93.5 % of cells were viable in loaded scaffolds and 89.4 % (Table 6) in the unloaded counterpart.

Table 6. Descriptive statistics of hBM-MSCs in collagen scaffolds. Human cells that mobilized into functionalized collagen after intermittent mechanical stimulation (+ Loading) or no stimulation (-Loading) for the controls were quantified and the descriptive statistics was calculated. More viable cells were seen in collagen scaffolds. The cell viability was not affected in any condition and was higher after loading. N= number of donors. It is the mean of the technical replicates within every donor.

Group	Viability	N (cells/mm ³)	Mean	Std Dev	Min	Median	Max	% viability
-Loading	Non-viable	4	3	2	1	3	5	89.37
-Loading	Viable	4	22	6	17	21	32	
+Loading	Non-viable	4	17	12	3	17	32	93.50
+Loading	Viable	4	245	42	205	237	300	

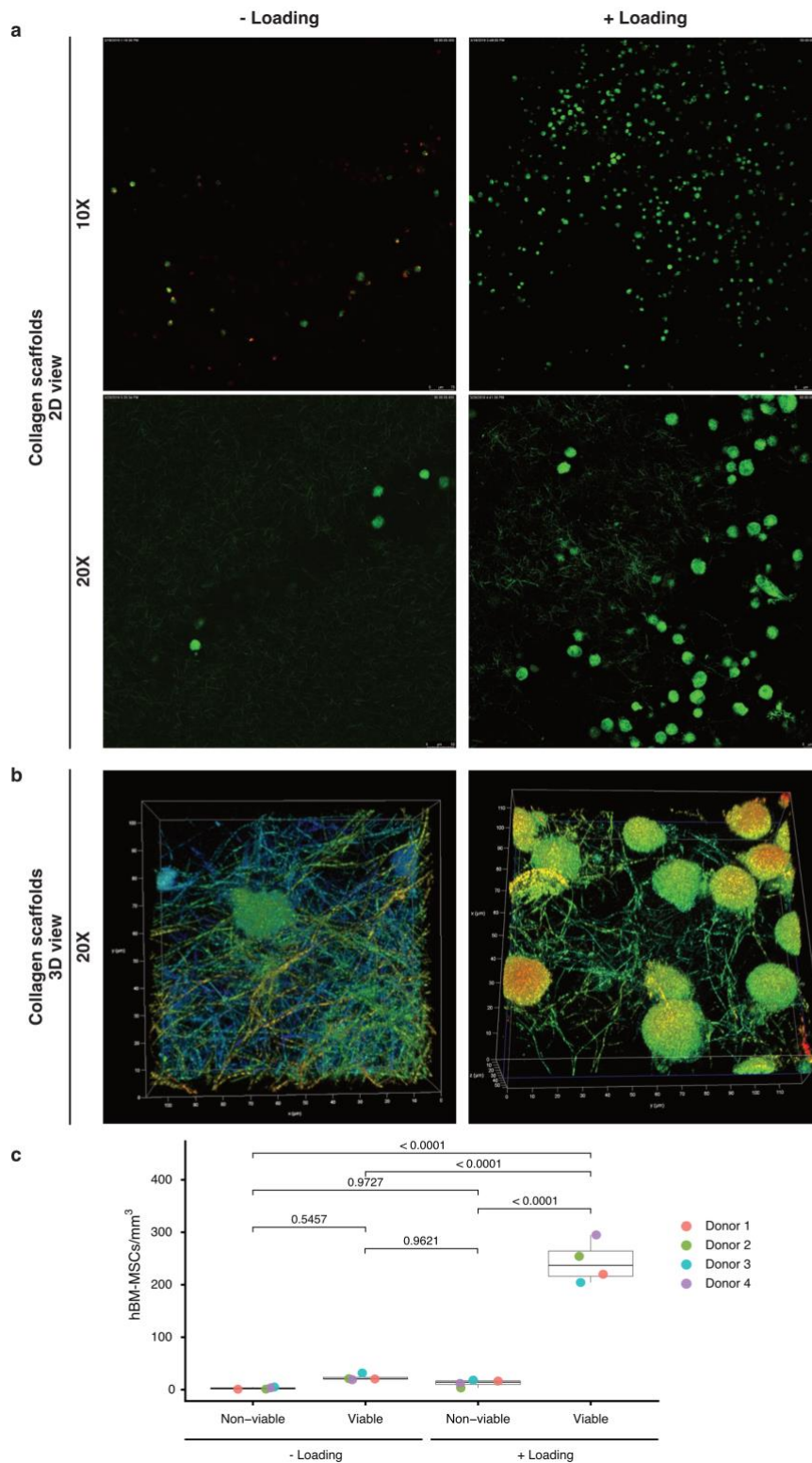


Fig. 19. hBM-MSCs mobilized into collagen scaffolds. (a) The cells in the scaffolds were visualized by confocal microscopy after 24 hours of intermittent mechanical stimulation or no loading (- Loading) application for the controls. Viable cells were seen in green after staining with C-AM, non-viable were stained with EthD-1 and are seen in red. (b) 3D images of the cells with or without loading. Pseudo-colors were used as a tool for a better visualization of interconnections of cells and collagen fibers. 20X magnification plus 5X of digital zoom. Scale bars: 150 μm (top), 50 μm (bottom). (c) A statistically significant higher number of viable cells are found in the scaffolds after mechanical loading. Examinations were done using cells from four different donors; every dot represents the mean of a technical triplicate. ANOVA test was done adjusting multiple comparisons by Sidak. *C-AM*: Calcein-AM, *EthD-1*: Ethidium homodimer-1.

4.11. Morphometry of mobilized cells

As we found cells in the scaffolds after mechanical stimulation, changes in the cell morphology would provide hints of active or passive cell mobilization. The image analysis pipeline using LAS X allowed us to extract a variety of features (Fig. 5), obtained after the cells were quantified using LAS X as previously explained in Fig. 6. Morphometric parameters as volume, surface area, sphericity and diameter were evaluated to analyze possible changes in the shape of hBM-MSCs after mechanical stimulation. Loading seemed not to change the cells shape as no significant changes were seen in any of the morphometric features ($p > 0.05$) (Fig. 20).

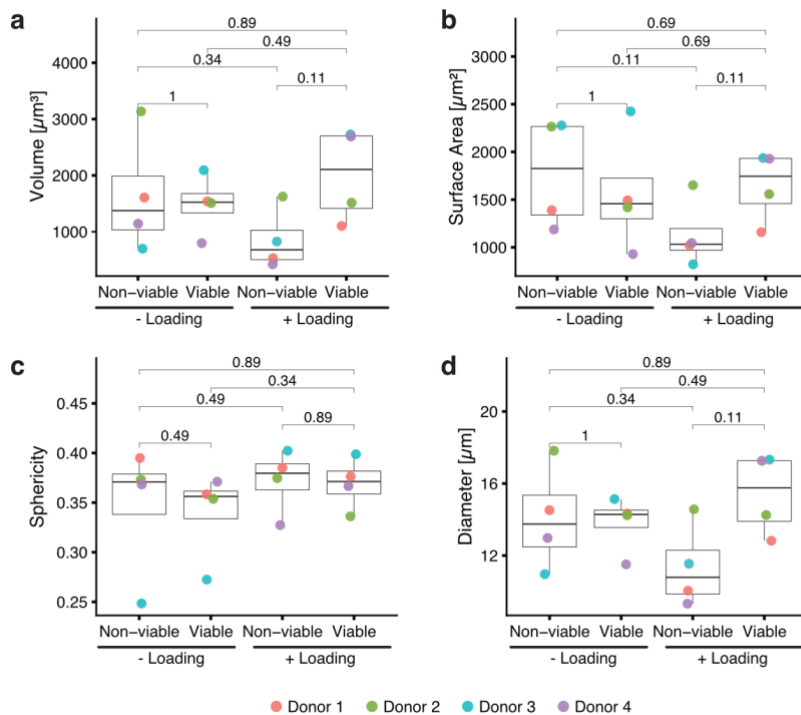


Fig. 20. Morphometric of hBM-MSCs in the scaffolds. The morphology of viable and non-viable pBM-MSCs found in collagen scaffolds was analyzed by comparing volume (a), surface area (b) sphericity (c) and diameter (d). No statistically significant changes were seen in any of the conditions, this is important to consider if the cell could have changed its morphology to actively migrate. Examinations were done using cells from four different donors, every dot represents the mean of a technical triplicate.

4.12. Comparison of mechanical stimulation of hBM-MSCs mobilized on different sort of scaffolds

As previously seen in Figs. 16 and 19, intermittent mechanical loading increased the number of hBM-MSCs per mm³ in scaffolds. Thus, further analyses comparing the counts of alginate-Ln and collagen scaffolds were performed as shown in Fig. 21a and Appendix C.

A significant difference between alginate-Ln and collagen scaffolds regarding their count of cells was found (p-value <0.0001, t-test in appendix C, Table C1). 10-fold more cells were seen when using mechanical stimulation on collagen scaffolds as 245 viable cells were detected in loaded collagen scaffolds and 22 cells the unloaded controls (Fig. 21a).

ANOVA test was applied for variables “loading”, “viability” and “biomaterial”, revealing a difference for the tested model (p-value < 0.0001, appendix C, Table C2). Therefore, the interaction between the variables was further evaluated by pairwise comparisons (p-value < 0.0001, appendix C, Table C3). The results indicate that intermittent mechanical loading induced mobilization of viable cells in both types of scaffolds but it was significantly higher in collagen scaffolds (p-value < 0.0001), cell viability was not affected (p value = 0.9993).

No significant difference was seen for unloaded conditions for viable (p-value = 0.553) or not viable cells (p-value = 1.0000). In addition, more viable cells were seen in collagen scaffolds than non-viable cells when loading was applied (p-value < 0.0001, Fig. 21a). Indicating that mechanical stimulation does not affect the cell viability.

The counts of porcine and human cells were compared to the sort of scaffold used during mechanical stimulation or not stimulation for the controls (Fig. 21 b). Mechanical stimulation increased mobilization of pBM-MSCs and hBM-MSCs with alginate-Ln and collagen scaffolds, respectively. Surprisingly, only minor mobilization of hBM-MSC into alginate-Ln scaffolds was observed.

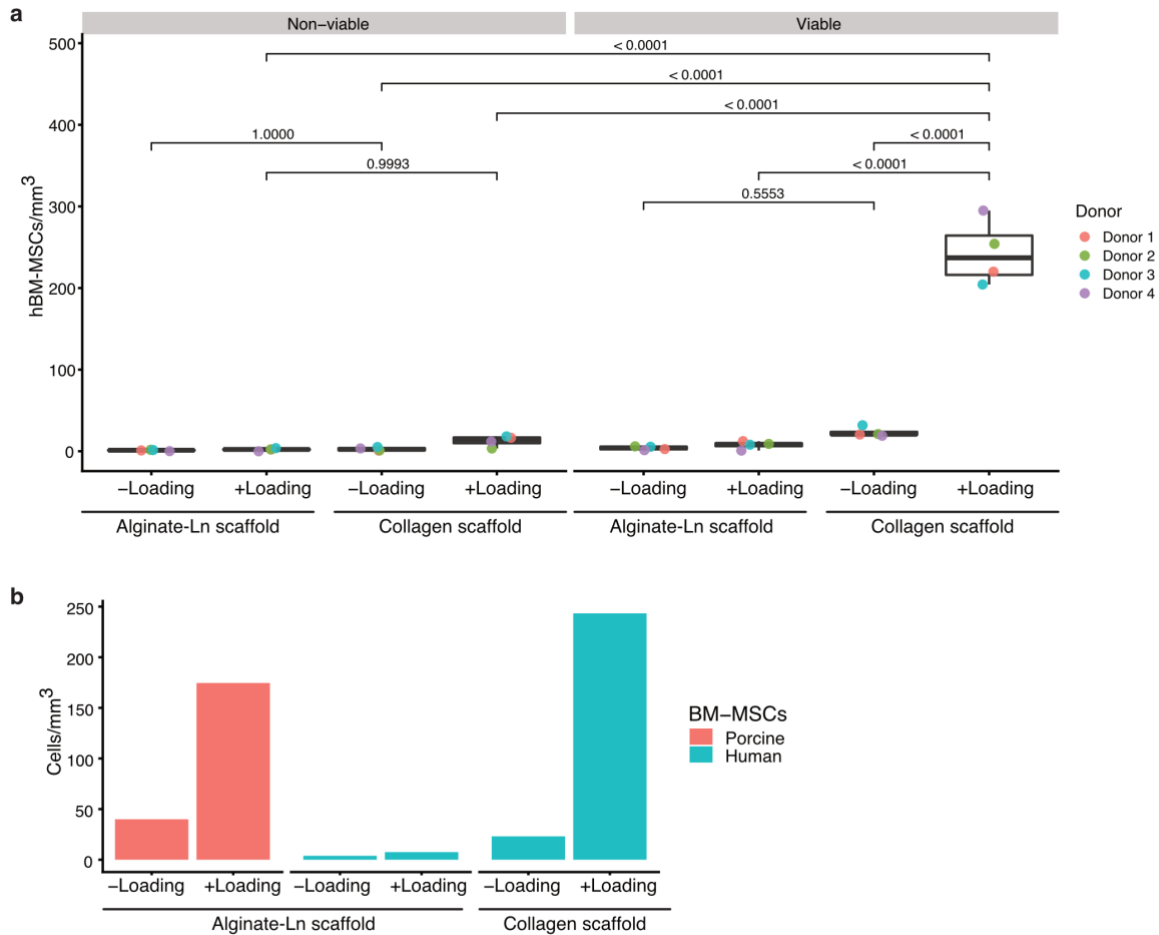


Fig. 21. Comparison of counts of cells in alginate-Ln and collagen scaffolds. (a) Mechanical loading, viability and type of the scaffold were statistically compared with respect to the number of cells found in the scaffolds. Collagen scaffolds contained greater counts of viable cells than alginate-Ln scaffolds. Unloaded conditions did not show differences in the amount of cells, independently of the viability or biomaterial of the scaffold. Examinations were done using cells from four different donors; every dot represents the mean of a technical triplicate. ANOVA test was done adjusting multiple comparisons by Sidak. **(b)** Comparison between the cell density of porcine or human BM-MSCs obtained after mechanical stimulation with respect to the type of the scaffold used; n ($pBM-MSCs$) = 1 from a technical triplicate, n ($hBM-MSCs$) = 4 from technical triplicates.

4.13. Analysis of the biomechanical data

To confirm that the bioreactor worked well and ran the requested mechanical setup (see section 3.3.8), the mechanical data of every examination was analyzed. We found that the bioreactor stimulated the scaffolds over 24.13 ± 0.08 hours for alginate-Ln scaffolds and 23.64 ± 0.86 hours for collagen scaffolds, using an intermittent periodic regime with 0.3 Hz and resting time of 10 seconds every 180 cycles (Fig. 22, appendix D). No contamination was observed when the examinations were concluded.

For the calculations, the first and the last periods of every run were removed since these contained outliers caused by the piston moving down and up to start and finish the experiment, respectively; thus, those values were not part of the examination. To calculate the displacement values during the dynamic mechanical stimulation, the values between the lift maneuvers ± 2 cycles were removed as explained in (Fig. 5) for descriptive statistics calculation of force and piston displacement.

The piston loaded the specimen for 10 min, displacing dynamically to strain 10 % the scaffold with respect to its original height. Then, the piston lifted and released the scaffold for 10 seconds as seen in Fig. 22b. The measured displacements were $277.90 \pm 53.01 \mu\text{m}$ for alginate-Ln scaffolds and $202.20 \pm 11.10 \mu\text{m}$ for collagen scaffolds examinations. In addition, the calculated mean of the force-amplitude for alginate-Ln scaffold was $1.16 \pm 0.42 \text{ N}$, while the force for collagen examinations was $1.08 \pm 0.13 \text{ N}$ (Table 7).

Furthermore, a single peak of force was observed in every period at the end of the lift maneuver (Fig. 22b).

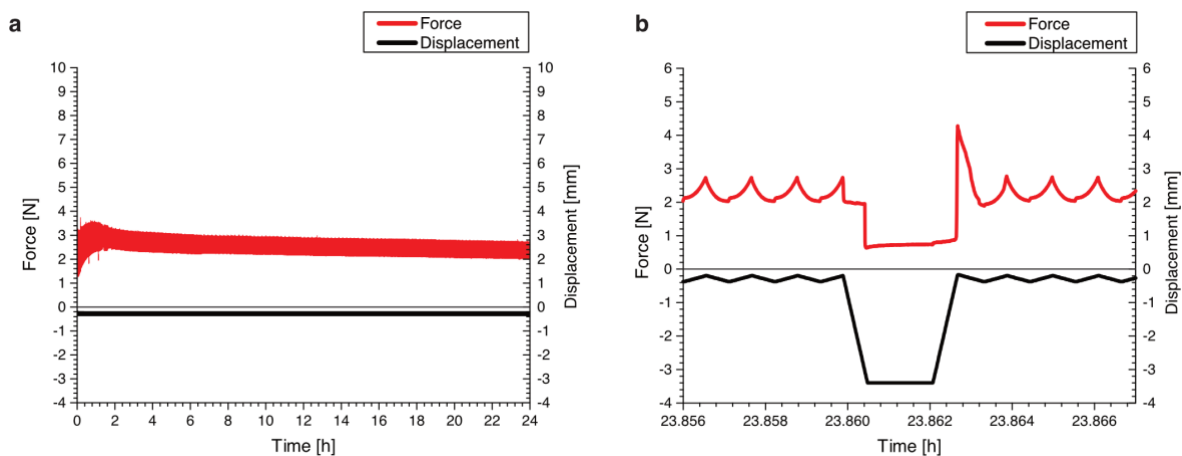


Fig. 22. Biomechanical data. (a) Overview of a complete examination. The force exerted over the specimen and detected by the force sensor is seen in red. The displacements of the piston detected by the gauge are seen in black. (b) Lift maneuver. An unloaded phase of the intermittent dynamic mechanical loading is shown in detail. The piston dynamically moves for 10 minutes and compresses the scaffolds until an unloaded phase is reached, in which it moves upward (downward in the depicted record as a black line) and releases the scaffold for 10 seconds. A force peak was seen when the piston compresses the scaffold again after the lift maneuver. Adapted image from Ref⁴ with the permission of PLoS One, license CC-BY.

Table 7. Descriptive statistics of the mechanical stimulation parameters for the examinations with alginate-Ln and collagen scaffolds. Parameters as piston displacement, force, time and number of periods were calculated for all mechanical examinations for hBM-MSCs and pBM-MSCs. Force values in examinations with pBM-MSCs are given as amplitudes since the offset force of the bioreactor was unknown for this samples. For the force values of hBM-MSCs examinations the offset was subtracted. N= number of examinations executed in the bioreactor.

Cell	Scaffold	Data	N	Mean	Std			
					Dev	Min	Median	Max
hBM-MSCs	Alginate-Ln	Force (N)	12	1.16	0.42	0.69	1.15	2.23
		Displacement (μm)	12	277.90	53.01	174.05	287.93	359.01
		# periods	12	142.58	16.42	108.00	151.50	156.00
		Time (h)	12	24.13	0.08	23.95	24.16	24.21
	Collagen	Force (N)	11	1.08	0.13	0.88	1.09	1.25
		Displacement (μm)	11	202.20	11.10	193.18	199.68	225.73
		# periods	11	133.27	10.73	118.00	141.00	143.00
		Time (h)	11	23.64	0.86	22.52	23.40	24.95
pBM-MSCs	Alginate	Force amplitude (N)	3	1.88	1.91	0.72	0.84	4.09
		Time (h)	3	24.87	1.03	23.71	25.25	25.67
		Displacement (μm)	3	183.60	22.47	160.11	185.81	204.89
		# periods	3	135.67	9.45	125.00	139.00	143.00
	Alginate-Ln	Force amplitude (N)	3	1.84	1.30	0.38	2.27	2.88
		Time (h)	3	23.87	2.38	21.24	24.49	25.89
		Displacement (μm)	3	187.49	19.81	165.04	194.88	202.54
		# periods	3	136.67	6.03	131.00	136.00	143.00
	Alginate + alginate-Ln	Force amplitude (N)	6	1.86	1.46	0.38	1.55	4.09
		Displacement (μm)	6	185.54	19.07	160.11	190.35	204.89
		# periods	6	136.17	7.11	125.00	137.50	143.00
		Time (h)	6	24.37	1.73	21.24	24.87	25.89
Summary of all examinatio	All	Displacement all	29	230.08	54.07	160.109	202.535	359.013
		Time all	29	23.99	0.94	21.2387	24.136	25.8861
		# periods	29	137.72	13.21	108	142	156
	hBM-MSCs	Force (N)	11	1.08	0.13	0.87634	1.09299	1.25074
		pBM-MSCs	Force amplitude (N)	6	1.86	1.46	0.38395	1.55157

The scaffolds revealed no indications of heavy damage after the mechanical stress produced by the dynamic compression. A trace of stress was visible at the scaffolds after loading (Fig. 23, appendix E).

5. Discussion

This work was focused on evaluating whether dynamic mechanical stimulation had an effect on mobilizing mesenchymal stromal cells toward scaffolds in a bioreactor system. There is an unmet need in AC treatments: Microfracture, ACI and mosaicplasty are the preferred treatments for AC defects, but those still fail to obtain a complete long lasting regeneration of AC³. One of the possible drawbacks to obtain a complete in situ regeneration of AC after microfracturing is if too few progenitor cells mobilize and migrate, resulting in fibrocartilage³¹. Therefore, this work provides a series of tools and methods *in vitro* where controlled variables can be used to evaluate cell mobilization under mechanical stimulation. We were focused on imitating an *in vitro* situation comparable when there is a defect in the cartilage layer of the tibia plateau of a knee joint by a modified bioreactor^{4,93}. Our aim was to evaluate whether mechanical stimulation had an effect on mobilizing BM-MSCs toward scaffolds in a bioreactor system and we found that intermittent mechanical stimulation induced the mobilization of pBM-MSCs into functionalized alginate-Ln scaffolds and hBM-MSCs into collagen scaffolds (Figs. 15 and 19).

This study is a novel hypothesis with little evidence in the literature. Therefore, it was challenging all the parameters that have to be proposed, evaluated, established and optimized. Parameters for the bioreactor setup as frequency, amplitude, time, and strain were identified and evaluated to obtain a suitable mechanical program in which the cells mobilized. This is, the ideal amplitude of the scaffold was 2 mm that was compressed with 10 % strain by piston displacements of 200 μm at 0.3 Hz for 24 hours but in an intermittent loading mode.

Additionally, a proper technique to proof or discard cell mobilization in the self-made scaffolds had to be established. Thus, confocal microscopy was selected because the imaging was possible for fresh scaffolds, which means that the hydrogels would not dehydrated, preserving their morphology and cell viability was detected right after the end of the mechanical stimulation. Furthermore, a pipeline based on LAS X was established for quantifying the cells in 3D. This allowed to quantify viable and non-viable cells and also several features regarding their morphology.

Having achieved and optimized the production of scaffolds and elastic rings right in shape to fit in the scaffolds, established the method to visualize and quantify the cells in the scaffolds,

analyzed mechanical loading protocols, we found that mechanical stimulation induced mobilization of BM-MSCs into scaffolds, but it happened when mechanical stimulation was applied intermittently and also depended of the sort of cell and scaffold used.

The study provided herein suggests that intermittent biomechanical loading induces the mobilization of cells from a lower compartment into scaffolds against gravity, supporting the hypothesis that endogenous cells could be mobilized and recruited by biomechanical loading when the subchondral bone is opened ⁴.

As many points are to be discussed as a result of this work, this section will 1) include the analysis and considerations that took place before placing the bioreactor into operation with MSCs; this comprises the analysis of the establishment, standardization and optimization methods that were necessary to operate the bioreactor in optimal conditions, 2) analyze the findings of BM-MSCs mobilization into scaffolds after mechanical stimulation, 3) consider the limitations of the study, 4) point out the conclusions and 5) suggest the outlook.

5.1. Considerations for the established and optimized protocols: Prequel to the mechanical stimulation application on MSCs

To resemble *in vitro* a realistic biomechanical situation of the joints occurring *in vivo* is challenging, since all the relevant forces and amplitudes on the knee joint acting simultaneously are hard to identify. These mainly depend on the physical activity and particular conditions of the individuals. Strain is a standard biomechanical parameter used in this field. It is known as the percentage of reduction in the thickness of cartilage when it is compressed or mechanically loaded ³⁸.

5.1.1. Bioreactor

Parameters as frequency and strain used in this study were applied as previously reported ⁹⁷; total time ¹⁰² and duration of the unload phase ⁵⁷ were within the ranges of previous studies. Several specifications needed to be established before, such as elastic ring and scaffold fabrication (Figs. 3 and 7), cell isolation (Figs. 4, 9-11), mechanical program setup and optimization (Fig. 5) and cell visualization and quantification (Figs. 6 and 12).

5.1.2. Alginate scaffolds

A mold for casting the scaffolds was built (Fig. 3). Its design and metal composition made possible to easily handle scaffolds and to keep sterility. One of the common problems when making hydrogels is bubble formation and undesired shapes of the scaffolds. As in this work, the dimensions and shape of the scaffold were important for fitting it along the other components of the cartridge. Hence, the mold was assembled in between with paper filter moistened with CaCl_2^{2+} , which was essential for preserving the desired shape of scaffold and to allow a proper ionic polymerization of the gel. On the other hand, 0.9 % NaCl was the optimal solvent for the alginate since the scaffolds were easily dissolved in PBS.

5.1.3. Elastic rings

As mechanical loading was simultaneously applied to the elastic ring and scaffold through the piston (Fig. 1), the elastic ring had an essential role besides holding the scaffold in place. It created the environment for lateral semi-confined compression because it was compressible, allowing the scaffold laterally displace during loading application.

For every mechanical examination in the bioreactor, the configuration of the experiment was set in EasyMotion program by the user. Then, the load was measured through the force sensor and recorded in Bioreactor GUI at 50 Hz (Fig. 5a). Therefore, more than 4.3×10^6 values were obtained for an examination of 24 hours, providing high accuracy of the recorded mechanical data. Nevertheless, such amount of data made difficult to use traditional analysis software. Thus, the data were exported as TDMS files and analyzed using the Origin software. To calculate the displacement and force values of a whole examination, the lifts maneuvers between the periods were removed because the displacement of the piston abruptly changed for the unload phase (Fig. 5c). This allowed us to have a better estimation of the real displacement and force values during the dynamic mechanical examination.

The elastic rings were stiffer after sterilization by heating and the measurements seemed to be homogeneous between them after sterilization (Fig. 7a), probably because the heat released some air bubbles that may have left inside of the silicone. Though, no changes in the height of composition were evident macroscopically.

When comparing the rings based on the stiffness after sterilization, three main clusters were obtained (Fig. 7b), meaning that the most similar rings were grouped. The members of the

cluster A showed high similarity between each other, but also shared more similarity to the members of clusters B and C. Therefore, three rings from cluster A were selected for further stiffness analysis with scaffolds (Fig. 7c). The displacement was compared to force but the data did not fit a linear regression (Fig. 7c). Thus, a polynomial regression was performed, obtaining a third order polynomial regression as the best model for fitting the data. The stiffness analysis of the elastic rings together with scaffolds suggests that scaffolds did not alter the stiffness shown by the elastic rings alone (Fig. 7c).

Some of the measurements while compressing laid or reached the upper limit allowed for the force sensor (10.9 N), which are represented as missing values in Table 3. Hence, to keep the strain as 10 %, the height of the scaffold had to be reduced to 2 mm. Thus, the stiffness of 2 mm scaffolds was tested, showing that the influence of the force was minimal (Fig. 7d). This suggested that it was better to change the height of the elastic rings from 3 to 2 mm. Consequently, 10 % strain was applied for all the examinations in the bioreactor seen as 200 μm . Every examination had a new sterilized silicone ring of 2 mm height as all the stiffness values at 10 % strain (200 μm of ring compression) were similar and also this height did not pose a danger to the sensor.

5.1.4. pBM-MSCs isolation and characterization

The next task in the series of pretests was to establish a protocol for pBM-MSCs isolation and characterization. One of the open questions was to determine how to properly isolate the cells from femoral bones. pBM-MSCs have been widely used in the past, however, most of the protocols are based on cell aspiration from the iliac crest^{103, 104}.

pBM-MSCs from juvenile pigs were isolated from femora at the intertrochanteric or intercondylar regions. The cells from piglets were preferentially isolated from the intercondylar region because sometimes the tissues nearby the hip were already exposed. To determine any difference on isolating the cells from different locations of femoral bones, a correlation was performed between the cell density harvested at 70 – 80 % confluency and with the amount of bone marrow collected when isolated (Fig. 8a) or with the time until subconfluence at passage 0 (Fig. 8b) with respect to the isolation location, we did not observe correlation. Previously published reports with experiments performed at higher passages show correlation between cell density and time¹⁰⁵⁻¹⁰⁷.

Likewise there was no difference with respect to intertrochanteric or intercondylar location (p-value = 0.4363) and the amount of BM (Fig. 8a). The negative slope seen in Fig. 8a would indicate that the more BM tissue isolated, the less cell density is obtained. However, since our cell isolation method consisted of opening the bone and taking the BM out with a surgical spoon, it is possible that as much the BM was scrapped, spongy bone was taken out, which is heavy (Fig. 8a). The extraction of bone marrow in mice is usually done by using a syringe and several intermediate washing steps ¹⁰⁸. Therefore, it would be useful to apply a similar protocol to find out if the negative slope was caused by the isolation method.

MSCs isolated from piglets seemed to grow faster than from juvenile pigs (Fig. 8b). Although the amount of bone marrow was smaller when isolated from piglets, these cells took shorter time to reach subconfluence. This is as expected since younger MSCs proliferate faster ¹⁰⁹. Despite that the amount of bone marrow was smaller when isolated from piglets, these cells took shorter time to reach subconfluence. Therefore, further experiments were done using BM-MSCs from piglets.

pBM-MSC fulfilled MSCs criteria, they were plastic-adherent and displayed a fibroblastoid morphology ^{110, 111}. The expression of surface markers was as expected for MSC. We showed that human antibodies were grossly cross-reactive, except for HLA/SLA, which are species-specific. As expected, HLA-ABC and HLA-DR did not reacted with porcine cells but SLA-1 and SLA-DR did, as these markers are specie specific. Thus, human antibodies can also be used for immunophenotyping pBM-MSCs that were particularly isolated.

5.1.5. Image analysis pipeline

Validating the established image analysis pipeline by comparing expected to counted cells, we verified that the number of cells in the scaffolds was correctly counted. We cannot exclude that some cells could have proliferated and others died over the time period of the experiment. However, MSCs have a typical doubling time of 30 hours (AG Bieback, personal communication). Further, there are different quantification pipelines and algorithms that use machine learning to perform segmentation, quantification, and classification. Such as ilastik ¹¹², Weka ¹¹³, CellCognition ¹¹⁴, and SuRVoS ¹¹⁴. In the particular case of the work presented here, the main goal of the quantification pipeline was to perform segmentation of cells from 3D images and quantify the total number of cells in a particular volume, a task for which a high accuracy rate was obtained. In future work, it would be worth to complement the

obtained information by LAS X with the classification utilities from the software mentioned above, i.e., to evaluate if different sub-populations of cells were present inside a scaffold.

5.2. Mobilization of MSCs into the scaffolds

We showed that functionalization of the scaffold as well as intermittent loading induced a significant number of cells to migrate into the scaffolds. Therefore, it was important to contrast the findings with the literature.

5.2.1. Contrasting our bioreactor system with other studies

Based on a systematic literature search, this are the first results suggesting mobilization of MSCs from a lower compartment to another at the top against gravity, induced by biomechanical stimulation *in vitro*⁴. Migration of chondrocytes under mechanical stimulation has been previously stated^{115, 116} but here the system was applied intermittently for MSCs after have seen high death cell rate with continuos stimulation.

Ode and collaborators, using a bioreactor system previously described¹¹⁷, addressed migration of MSCs under mechanical stimulation, demonstrating that loading hampered the mobilization of MSCs in bone healing context¹¹⁸. However, whereas Ode at al. used a pneumatic force application system¹¹⁷, we applied the force transmission was performed mechanically from a step motor over the stiff piston to the surfaces of the scaffold and silicone ring. The loading protocols also differed since Ode and collaborators applied 20 % strain at 1 Hz for 72 hours, while in our study the parameters were 10 % strain at 0.3 Hz frequency as previously reported in⁹⁷, intermittently for 24 hours. The comparison of both approaches supports the assumption that mobilization of MSCs was not induced when applying mechanical loading alone (Fig. 15). We observed that the pBM-MSCs were found in the hydrogel only when mechanical loading was applied intermittently and the scaffolds were functionalized with LN521 (or when collagen scaffolds where used for hBM-MSCs). Furthermore, higher levels of cell viability in pBM-MSCs were found in the experiments performed using alginate-Ln, which indicates that LN521 may contribute to the wellness of cells during the test. This may explain why lower cell viability was found under loading in alginate scaffolds (Fig. 15). To have found that funcionalizing the scaffolds resulted in an

improvement of the experimental setup supports the rationale of building a bioreactor like this, since it would allow to understand which substances could be attractive for cell recruitment for *in situ* regeneration.

5.2.2. Culture conditions and continuous vs. intermittent loading

When the subchondral bone is perforated in a microfracture surgery, blood clots are formed and a suitable environment for tissue healing is created, promoting migration of MSCs and releasing growth factors and cytokines ¹¹⁹. Unlike the BM, where cells can adhere in the stroma, the cell reservoir in our bioreactor was a cylindrical container with a flat bottom, where a suspension of cells would sediment. Therefore, it was important to increase the viscosity of the cell suspension by adding alginate or collagen, i. e., the cells were seeded in the bioreactor reservoir as a viscous solution. This cultivation conditions might have avoided cell sedimentation during the mechanical stimulation and helped mobilizing the cells.

Continuous loading seemed to harm the cells, probably due to the lack of nutrients and gases exchange when a continuous regime was used for 24 hours. The cell reservoir had a limited size and thus, medium supply could affect viability within 24 hours. Hence, it is possible that the conditions in the cell reservoir were not optimal for 1×10^5 cells as a volume of 80 μL of medium and alginate solution was limited, and the lack of nutrients and waste disposal may have harmed some cells for the observation time.

Accordingly, we adapted an intermittent regime, which in fact increased the viability of the cells (Fig. 14). Because of the high cell death observed under continuous stimulation, we applied important changes in the software and hardware of the bioreactor had to be applied to provide nutrients to the cells by loading intermittently (Fig. 14 a), which solved the problem. The apparent increase of cell viability observed once the load was applied intermittently, suggests that nutrients and gas exchange may have occurred during the lifts of the piston. Moreover, the unloaded and intermittently loaded scaffolds acquired a reddish color, indicating that penetration and even distribution of cell culture medium in the scaffolds was allowed by the lift maneuver of the piston and it was independent of the exerted compression (observation not shown). Therefore, the culture medium passed through the scaffold and reached the cells located at the cell reservoir, and the elastic ring prevented bypasses by a sealing effect under pressure. The applied intermittent dynamic mechanical stimulation seemed not to harm the cells when using functionalized scaffolds; in contrast, more viable

cells were observed even after finding one value of the replicates close to the non-stimulated control (Fig. 14).

5.2.3. Scaffold functionalization

The results indicate the necessity of functionalizing the scaffolds with LN521 to get more MSCs in since the cells were not notably found in the scaffold made of only alginate (Fig. 15). LN521 is a basement membrane protein present in stem cells niches, involved in cell adhesion, migration, and differentiation¹²⁰. Therefore, structural proteins like LN521 may serve as adhesion factors for pBM-MSCs in the scaffolds. The functionalized scaffolds allowed holding a higher number of cells after intermittent loading, supporting the hypothesis regarding mechanical stimulation helping to transfer cells.

Laminin cannot form hydrogels by its own due to the absence of electrostatic interactions or hydrogen bonding. However, it can be combined within other hydrogels where functional groups conjugate¹²¹. One of the limitations of this experimental setup is that it is not possible to be entirely certain about the complete integration of LN521 into the alginate structure at molecular level, but probably some of the LN521 molecules were just trapped in the internal network of the scaffold. The use of oxidizing agents as IO_4^- when preparing the scaffolds can be addressed for future approaches, allowing interaction between aldehyde groups of the oxidized alginate and amine residues of the laminin, as previously reported¹²².

It is known that laminin increases adhesion of stem cells on matrices and participates on signaling⁷¹. For instance, embryonic stem cells and induced pluripotent stem cells anchor to LN511/521 via integrin α_6 , β_1 ⁷⁰. Therefore, it is possible that more pBM-MSCs were mobilized on the functionalized scaffolds via integrin-LN interactions. It is a matter of future studies to unravel details of the possible biochemical mechanism.

As to have functionalized the alginate scaffolds with LN521 contributed to find more pBM-MSCs after intermittent mechanical stimulation, the same experimental conditions were tested on hBM-MSCs (Fig. 16a). Despite of the statistical significance (if p-value < 0.05) when comparing mechanical stimulation on viable cells, the counts of hBM-MSCs were low (Table A1, Fig. 16a); in particular, compared to the counts of porcine cells that were mobilized under the same conditions (Fig. 15). Therefore, the whole scaffold was imaged and the cells were mainly seen on the surface of the scaffolds and interestingly, more cells in the loaded

scaffolds. The scaffold is an interconnected meshwork in a 3D shape; hence, mechanical stimulation probably modified slightly the scaffold structure by physical means, allowing more cells in.

It is still to be investigated why the cells were located mostly on the surface of the scaffold. However, despite that alginate has been widely used for hydrogels preparation, there is not a real consensus regarding its microstructure since it depends on its particular chemical composition, polymerization approach and analytical method used to visualize it. It is reported that alginate scaffolds have pore size from nm to a few μm ^{123, 124}. Therefore, it can be speculated hBM-MSCs were mostly trapped. On the other hand, the LN521 used in this study corresponds to human-specific full length molecule (information from the manufacturer), which might have caused a strong adhesion to hBM-MSCs but weaker to pBM-MSCs. Future experiments with alginate scaffolds made with different concentrations of LN521 may provide better cues in this regard.

A slight mark on the surface of the lower side of the loaded scaffolds was observed, which corresponded to the circumference of the cell reservoir without apparent significant damage of the gel at microscopic level (Fig. 23, appendix E). This indicates that this side of the gel probably stretched toward the cell reservoir during loading. It may be speculated that a modest change in shape of the loaded gels might cause an increase of the superficial area, promoting the adsorption/adhesion of cells on the scaffolds. However, it was the combination of LN521 and loading that resulted in more cells in the scaffolds.

Polymerization of collagen to form a scaffold for the required dimensions was challenging since it is a softer biomaterial compared to alginate. The architecture of collagen scaffold meshwork mainly depends on the temperature and pH⁶⁷. Usual parameters for polymerization are temperatures ranging from 4.0 to 37°C and pH from 5.0 to 10.0¹²⁵. Changes in the pH for polymerization have been described to produce different crosslinking efficacies and variation in the reaction time⁶⁸. In addition, crosslinker as BDDGE may be used for the preparation of hyaluronic acid and collagen composites^{68, 69}. Therefore, the collagen-I solution used in this study was tested for different polymerization conditions, as described in Methods section. The collagen scaffolds at pH 5.0 seemed to be more solid regardless the temperature or crosslinker concentration, compared to the other conditions. Therefore, the preferred condition for

collagen-I scaffold polymerization was RT, pH 5.0 with 10 % BDGGE (Figs. 17 and 18). The scaffold edges corroborate a successful polymerization of the collagen solution.

Commercial collagen-I solutions as the used here may be enhanced using BDDGE to form composites, since the epoxy groups from the crosslinker agent react with the amine residues of the collagen⁶⁸, probably enhancing the meshwork of the scaffold (Fig. 18). The collagen-I scaffolds made here seem not to be harmful for the cells, as the cell viability was not affected. Besides, the reported toxicity of BDDGE is low (< 2 ppm) when used in cosmetic products⁶⁹.

Intermittent mechanical stimulation applied on hBM-MSCs using collagen scaffolds showed a statistically significant difference between viable loaded and unloaded cells. Mechanical stimulation may have loosened up the scaffold structure, and consequently, the cells could penetrate or be mobilized easier. The meshwork of unloaded collagen scaffolds looked more condensed than the loaded counterpart (Fig. 19 a and b). Anyhow data suggest that additional factors, besides the mechanical loading, can be involved in enriching the loaded scaffolds with viable cells.

The bioreactor exerted similar mechanical stimulation for hBM-MSCs loaded with alginate or collagen scaffolds regarding the duration and applied force (Table 7). Noteworthy, the actual displacement exerted on the alginate-Ln examinations was higher than for collagen scaffolds, but without providing a higher force. It was also observed that collagen scaffolds seemed to be softer compared to the alginate composites. Therefore, it would be possible that collagen scaffolds exert less resistance to the piston when it is displacing to apply load.

On the other hand, the force for the examinations with pBM-MSCs refers to the amplitude of this value, since the actual offset was unknown (Table 7). The values for hBM-MSCs were the actual force, since the offset was known and was subtracted.

From the mechanical point of view, the load pattern applied in this study showed a single higher peak of the force in every period induced after the lift maneuver (Fig. 22b), probably due to the piston moved downwards with a higher velocity after the released period.

This study was a high risk study based on the hypothesis that biomechanical loading may induce endogenous mobilization of MSCs. To address this, we first built a bioreactor,

optimized its setup, optimized scaffolds and then addressed recruitment of MSCs (both porcine and human) into different types of scaffold using intermittent loading. The experimental approach that is presented here has a unique hardware and software architecture, composed of separated devices for cell cultivation, mechanical application, and software (Fig 1, 2 and 14b). To the best of our knowledge this is the first study to have generated an *in vitro* platform to study this. Previous data have analyzed endogenous mobilization by microfracture *in vivo* or *in vitro* by using chemotactic migration, e.g. in boyden chambers ^{25, 126-128}.. Whereas the first allow to address biomechanical aspects –albeit without any chance of standardization and parameter permutation, the latter does not allow for biomechanical aspects.

It is not yet clear how the cells shifted upward from the reservoir to the scaffold when were loaded. On one side, if the cells were mobilized toward the scaffolds only by external mechanical reasons rather than by the cells themselves, we would expect the same ration of viable to non-viable cells in the scaffolds (Fig. 21). On the other side, if the cells used any biological active process as migration, one may expect a change in the morphology when loading. But no significant differences were found regarding the shape (Fig. 20).

The cells mainly move by lamellipodial or amoeboid mode ⁷⁹. It is reported that collagen fibers are ideal for integrin mediated migration ⁹⁰. Specific tests for cell migration should be part of future studies. For instance, assays evaluating disruption of focal adhesions of integrins, knockdown assays or inhibitors for molecules of the RhoA-ROCK-Myosin II pathway can elucidate whether actomyosin contractility is modified when mechanical stimulation is applied. Other possibility may be addressed to evaluate if loading modifies the gene activation and proteolytic activity of metalloproteinases, which would indicate migration or a change of the migration mode. Staining of microtubules and nuclei would also elucidate whether the microtubule organize centre is reorientated under loading and cell motility is activated to migrate.

Evidence in line with our findings of cells mobilizing against gravity are cancer cells that activate their migration machinery under microgravity environments, in particular, lamellipodial migration as suggested by activation of MMP-2, MMP-9 ¹²⁹ and polymerized actin protrusions ¹³⁰.

To explain the mechanisms of how the cells were transferred into the scaffolds is still challenging and opens new perspectives to be explored in detail in forthcoming research. To explore whether loading induces fluid movement from the lower compartment toward the scaffold, dark ink was placed at the cell reservoir in an early stage feasibility examination of the bioreactor. The ink diffused in the unloaded scaffolds showing a visible gradient, while fully stained the loaded scaffolds (Fig. 24, appendix F). This result suggests that mechanical loading induces fluid to move through the scaffold. It is a matter of future studies to explain whether the cells were sucked-up or activated by other mechanisms to displace themselves. LN521 functionalization was important either to attract porcine cells or to allow adherence of dispersed cells within the scaffold or both, as collagen for human cells.

Bone marrow is currently the most common MSCs source for cartilage regeneration research either alone or with biological scaffolds as so called matrix-augmented bone marrow stimulation¹³¹. The present experimental approach might be comparable to the *in vivo* situation when the subchondral lamella has been opened i.e., after microfracturing. As previously mentioned, current strategies for AC repair fail to produce hyaline cartilage. The presented bioreactor regime could provide new insights suggesting that endogenous progenitor cell mobilization to the defect site could be targeted by intermittent mechanical loading and functionalized-scaffolds. Moreover, mechanical loading is important in AC for distribution of nutrients, reinforce ECM content, fiber organization, and waste disposal^{32, 33, 35}. The bioreactor system provides a first insight of loading probably involved in MSCs recruitment. An approach that achieves MSCs endogenous recruitment of MSCs, a proper combination of factors for chondrogenic differentiation, and phenotype maintenance would be beneficial for a fully functional regenerated AC.

5.2.4. Image-based analyses

We were able to image the cells in the scaffolds with fresh stainings since the refractive index of the scaffold, medium and immersion objective matched. Thus, the shape of the scaffolds was preserved as no fixation was needed. This was important because shrinkage, which is a consequence of fixation, changes the shape of the cells and the nature of the scaffold meshwork. In this work, we obtained images with the original morphology and distribution within the scaffolds.

One of the most important features of the optimized protocol was the possibility to quantify cell viability in the scaffolds, staining with dyes only usable with non-fixed cells. Hence, this would also bring the possibility of analyzing the spatial distribution of viable and non-viable cells in 3D in future analyses.

Besides the qualitative information obtained from the images, we were able to establish an image analysis pipeline which allowed to locate, quantify and determine viability of cells within the 3D scaffold. Furthermore, to exploit the fact that we have all the cells in their original shape, we were able to recover all the measurements obtained from the morphology of cells. Thus, from the features obtained when the cells were quantified, diameter, volume, surface area, and sphericity were analyzed according to the experimental conditions (Fig. 20), showing no significant differences, which suggest that the cells did not change in shape when loading was applied. In addition, it indicates that an active movement from the cells probably did not take place, as it requires rearrangement of the morphology⁸⁴.

Previous attempts to quantify and retrieve morphological measurements from cells enclosed in a three dimensional space have been done by ilastik¹¹², Weka¹¹³, CellCognition¹¹⁴, and SuRVoS¹¹⁴ among others. In this study, the customized pipeline in LAS X was validated and provided a huge advantage because its ease of use, providing a user friendly interface and results files.

5.3. Limitations of the study

This is a proof-of-concept study. The approach was highly risky, as we had not only very little indications that the approach may work to help assessing our hypothesis experimentally. A number of challenges had to be achieved as 1) reproducible fabrication of scaffolds good in shape and consistency, 2) finding proper biomaterials for making better scaffolds, 3) optimizing cell visualization protocol that allowed to evaluate not only if more cells were present in the scaffolds but also if they were alive after loading application, 4) optimizing quantification of cells in the scaffolds, 5) finding the mechanical program to be applied in the bioreactor (continuous vs. intermittent loading) and 6) understanding the mechanical data of the bioreactor without literature support (the bioreactor is a unique setup). Thus, of course, this study has its limitations. For instance, small fluctuation between in the force and displacement values between the examinations was observed (Table 7), but they showed

similar behavior between them (Fig. 25 in Appendix G). On the one hand, sample numbers are low and need to be reproduced in larger scale to assess potential donor-specific differences. Still, for technical replicates the increase in cell numbers was highly reproducible and also found in hBM-MSCs. Here testing, cells from four different donors how comparable results of increased mobilization into collagen scaffolds are. The effect on the number of cells found in the scaffolds was 10-fold higher after we applied intermittent mechanical stimulation on collagen scaffolds. Nevertheless, the effect on the number of cells found in the scaffolds was 4-5-fold higher after intermittent mechanical stimulation, functionalized the alginate scaffold with the structural protein LN521, and dispersed the MSCs in the lower reservoir preventing cell sedimentation by adding alginate or collagen in solution.

With this bioreactor being a prototype to test the hypothesis of load inducing the mobilization of MSCs, the design is subject to improvements, e.g., self-replenishment of culture medium, scaffold composition, addition of supplementary factors in the culture medium for growth or differentiation.

The findings of this study allowed us to apply for a Model Utility Protection Patent, to publish an original paper and to communicate the developed methods and results in oral and poster presentations.

5.4. Conclusions

In this study, the role of mechanical loading on mobilizing mesenchymal stromal cells toward scaffolds in a bioreactor system *in vitro* was evaluated. The results suggest that intermittent mechanical stimulation promotes the mobilization of pBM-MSCs into alginate-Ln scaffolds and hBM-MSCs into collagen scaffolds. The cells are mobilized from a lower compartment of the bioreactor toward the scaffolds in another compartment above, against gravity.

We were able to identify and optimize parameters as frequency, amplitude, time, strain to put the bioreactor into operation. In particular, the amplitude was optimized as it was proven to be better to use scaffolds and elastic rings of 2 mm rather than 3 mm height because then, it was possible to obtain correct displacements from the piston able to compress the scaffolds 10 % strain.

Remarkably, as continuous mechanical stimulation showed to be harmful for the cells, we optimized the mechanical loading program to an intermittent stimulation, which showed to be better mobilizing cells in the scaffolds and also increasing cell viability.

Additionally, the production of scaffolds that fitted in the cartridge of the bioreactor was established. Optimization of such scaffolds was done by functionalizing alginate scaffolds with LN521 and producing stable collagen-I scaffolds.

From this work, an imaged based pipeline was established to quantify cells in 3D according to their viability. Thus, it was possible to 1) visualize the cells within the scaffolds, 2) quantify the total number of cells and 3) discriminate between viable and non-viable cells.

Finally, our results suggest that mechanical stimulation induces mobilization of mesenchymal stromal cells into scaffolds, happening when mechanical stimulation is applied intermittently and depends on the sort of cell and scaffold used. In particular, the optimal condition for mobilization of porcine derived BM-MSCs was obtained with an alginate scaffold functionalized with laminin, obtaining a 4-5-fold increase in the number of mobilized cells compared to the non-loaded scaffolds. Likewise, 10-fold increase of the counted human derived BM-MSCs were seen in collagen scaffolds.

Thus, the bioreactor presented here has unique hardware and software architecture, composed of separated devices for cell cultivation and mechanical application. For future studies, we provide tested protocols based on human and porcine models and an optimized tool to evaluate mobilization of cells against gravity under mechanical stimulation.

5.5. Outlook

Future studies are necessary to find out whether the phenomenon suggested with these results will also be observed using different scaffolds, human adult MSCs from different sources, different incubation times, cytokines and growth factors and what other mechanical parameters or protocols may enrich the scaffolds with viable and functional cells.

Thus, the relevance of these findings for the orthopedic experimental research field is to establish a biomechanical system *in vitro* that provides the chance to evaluate mechanical

stimulation for cells moving from a compartment beneath, simulating MSCs moving from bone marrow *in vivo*. Our proof-of-concept study demonstrates that in fact it is possible to mobilize cells into scaffolds against gravity by intermittent biomechanical loading. Extended to future studies, it may help now to study molecular cues of mobilized versus non-mobilized cells and identify additional mechanical and chemical factors for inducing cells to be recruited by a given condition. Further steps will assess whether mechanical loading can induce MCSs for bone or cartilage differentiation. Nonetheless, the first results of the presented study suggest that mechanical stimulation may have an important impact on the mobilization of stem/stromal cells. Thus, a combination of the current strategies applied for AC-regeneration as microfracture, biomechanical protocols and functionalized scaffolds might enhance the outcomes of the current treatments applied in osteoarthritis or AC-trauma.

6. Summary

Articular cartilage (AC) is a viscoelastic avascular tissue mainly composed of chondrocytes embedded in a rich extracellular matrix that bears and distributes loads occurring in the joints. The absence of vessels restricts its regenerative capability. Hence, joint motion facilitates nutrient deposition and cell waste disposal. Mechanical stimulation contributes to the homeostasis of functional AC by supporting delivery of nutrients, cytokines and growth factors between the distant chondrocytes. Current techniques to treat AC defects still fail to entirely heal and to achieve a native-like AC. Instead, a fibrous tissue with poor mechanical and biochemical properties is obtained. Since the knee joint has neighboring niches of stem cells, we hypothesized that mechanical stimulation might enhance the mobilization of endogenous mesenchymal stem/stromal cells (MSCs) from nearby niches as the bone marrow (BM).

This study aimed to introduce a novel bioreactor system *in vitro*, capable of inducing dynamic mechanical loading on a scaffold; and evaluate whether MSCs could be mobilized from a compartment beneath to a scaffold after the mechanical stimulation, as cells might move when the subchondral bone is opened. This was a risky approach, as there are little evidences existing to base our assumption on; and both, the bioreactor as well as the experimental setup (including efficient cell characterization in 3D) had to be developed, optimized and then finally evaluated.

A novel mechanical system for evaluating mobilization of cells in a 3D context *in vitro* is presented. The system consists of a) a compression bioreactor able to induce loading on scaffolds, b) custom-made software for settings for management and data recording, c) cell loading experiments and d) 3D image-based biological evaluation.

The mechanical stimulation acted on an acellular scaffold made of alginate, functionalized-alginate or collagen, and a cell reservoir containing porcine or human BM-MSCs (pBM-MSCs and hBM-MSCs, respectively) below it. The mechanical loading program was set up as 10 % strain regarding the original height of the scaffold, 24 hours at 0.3 Hz, under dynamic continuous or intermittent regime, with unload phases of 10 seconds each 180 cycles when intermittent loading was used.

Supporting our hypothesis, intermittent mechanical stimulation induced the mobilization of hBM-MSCs in collagen scaffolds 10-fold compared to the unloaded control, as well as pBM-MSCs mobilized 4-fold in functionalized-alginate scaffold, when intermittently loaded. Remarkably, the viability of mobilized cells was not compromised by intermittent mechanical loading application as evaluated under an optimized and validated protocol for counting and viability cell detection in 3D. In addition, we found that the bioreactor was able to stimulate the scaffolds and the cells for 23.09 ± 0.94 hours in 137.72 ± 13.21 periods, exerting compression with vertical piston displacements of $230.08 \pm 54.07 \mu\text{m}$, force of $1.08 \pm 0.13 \text{ N}$ for hBM-MSCs and force-amplitude of $1.86 \pm 1.46 \text{ N}$ for pBM-MSCs.

In this study, a bioreactor system comprising unique hardware and software architecture, separated devices for cell cultivation, mechanical application, and software was optimized to evaluate the role of mechanical stimulation on mobilizing MSCs toward scaffolds *in vitro*. The bioreactor system worked well as it was able to provide mechanical stimulation over the scaffolds. Remarkably, intermittent mechanical stimulation induced the mobilization of viable pBM-MSCs into functionalized-alginate and hBM-MSCs collagen scaffolds. The cells were mobilized from a lower compartment of the bioreactor toward the scaffolds in another compartment above, against gravity.

As a first step to induce cartilage regeneration *in situ*, this study provides a tool to enrich acellular scaffolds with viable MSCs after mechanical stimulation. Thus, the applicability of these findings for the orthopedic research field is to establish a biomechanical system *in vitro* with the possibility to use mechanical stimulation on cells moving from a compartment beneath, simulating MSCs moving *in vivo* from bone marrow into the cartilage defect in a knee joint. This experimental approach might be used in the future to study molecular factors of mobilized and non-mobilized cells that help to identify further biochemical or mechanical agents for recruiting cells *in vitro*. Further studies need to be done to address whether cartilage regeneration can be done using the mobilized MSCs. A strategy that combines biomechanical protocols and functionalized scaffolds, as the presented here, with current strategies already used for AC-regeneration as microfracture might contribute to a better outcome of the current treatments applied in osteoarthritis or AC-trauma.

Derived from this study, we were able to apply for a Model Utility Protection Patent, we published an original paper and we also had the opportunity to communicate the developed methods and interesting findings in oral and poster presentations.

This doctoral research thesis was developed under the doctoral program of the Cooperative Research Training Group: Tissue Analytics for Stem Cell based Diagnostics and Therapy (TASCDT).

7. References

1. Cole, BJ: Surgical Management of Articular Cartilage Defects in the Knee. *J Bone Joint Surg Am*, 91: 1778-1790, 2009.
2. Jacobi, M, Villa, V, Magnussen, RA, Neyret, P: MACI - a new era? *Sports Med Arthrosc Rehabil Ther Technol*, 3: 10, 2011.
3. Choi, JR, Yong, KW, Choi, JY: Effects of mechanical loading on human mesenchymal stem cells for cartilage tissue engineering. *J Cell Physiol*, 233: 1913-1928, 2018.
4. Gamez, C, Schneider-Wald, B, Schuette, A, Mack, M, Hauk, L, Khan, AUM, Gretz, N, Stoffel, M, Bieback, K, Schwarz, ML: Bioreactor for mobilization of mesenchymal stem/stromal cells into scaffolds under mechanical stimulation: Preliminary results. *PLoS One*, 15: e0227553, 2020.
5. Makris, EA, Gomoll, AH, Malizos, KN, Hu, JC, Athanasiou, KA: Repair and tissue engineering techniques for articular cartilage. *Nat Rev Rheumatol*, 11: 21-34, 2015.
6. Ashraf, S, Cha, BH, Kim, JS, Ahn, J, Han, I, Park, H, Lee, SH: Regulation of senescence associated signaling mechanisms in chondrocytes for cartilage tissue regeneration. *Osteoarthritis Cartilage*, 24: 196-205, 2016.
7. Rosa, D, Di Donato, SL, Balato, G, D'Addona, A, Smeraglia, F, Correra, G, Di Vico, G: How to Manage a Failed Cartilage Repair: A Systematic Literature Review. *Joints*, 5: 93-106, 2017.
8. Akkiraju, H, Nohe, A: Role of Chondrocytes in Cartilage Formation, Progression of Osteoarthritis and Cartilage Regeneration. *J Dev Biol*, 3: 177-192, 2015.
9. Armiento, AR, Stoddart, MJ, Alini, M, Eglin, D: Biomaterials for articular cartilage tissue engineering: Learning from biology. *Acta Biomater*, 65: 1-20, 2018.
10. Pouran, B, Arbabi, V, Bajpayee, AG, van Tiel, J, Toyras, J, Jurvelin, JS, Malda, J, Zadpoor, AA, Weinans, H: Multi-scale imaging techniques to investigate solute transport across articular cartilage. *J Biomech*, 78: 10-20, 2018.

11. Mabvuure, NH, S.; Khan, W.:: The Role of Bioreactors in Cartilage Tissue Engineering. *Current Stem Cell Research & Therapy*, 7, 2012.
12. Knudson, CB, Knudson, W: Cartilage proteoglycans. *Semin Cell Dev Biol*, 12: 69-78, 2001.
13. Lories, RJL, F.P.:: Chapter 3 - Overview of Joint and Cartilage Biology. In: *Genetics of Bone Biology and Skeletal Disease*. Elsevier, 2013, pp 35-51.
14. Usami, Y, Gunawardena, AT, Iwamoto, M, Enomoto-Iwamoto, M: Wnt signaling in cartilage development and diseases: lessons from animal studies. *Lab Invest*, 96: 186-196, 2016.
15. Watkins, JM, I.:: Chapter 4: Connective tissues. In: *The Pocket Podiatry Guide: Functional Anatomy*. Elsevier, 2009.
16. Pollard, TDE, W.C.; Lippincott-Schwartz, J.; Johnson, G.T.:: *Cell Biology*, Philadelphia, PA : Elsevier, 2017.
17. Aspberg, A: Cartilage Proteoglycans. In: *Cartilage Volume 1: Physiology and Development*. edited by GRÄSSEL, S., ASZÓDI, A., Springer, 2016.
18. Lowe, J, Almarza, AJ: A review of in-vitro fibrocartilage tissue engineered therapies with a focus on the temporomandibular joint. *Arch Oral Biol*, 83: 193-201, 2017.
19. Robinson, DL, Kersh, ME, Walsh, NC, Ackland, DC, de Steiger, RN, Pandya, MG: Mechanical properties of normal and osteoarthritic human articular cartilage. *J Mech Behav Biomed Mater*, 61: 96-109, 2016.
20. Jung, CK: Articular Cartilage: Histology and Physiology. In: *Techniques in Cartilage Repair Surgery*. Springer, 2014.
21. Hunziker, EB, Kapfinger, E, Geiss, J: The structural architecture of adult mammalian articular cartilage evolves by a synchronized process of tissue resorption and neoformation during postnatal development. *Osteoarthritis Cartilage*, 15: 403-413, 2007.
22. Gadjanski, I, Spiller, K, Vunjak-Novakovic, G: Time-dependent processes in stem cell-based tissue engineering of articular cartilage. *Stem Cell Rev Rep*, 8: 863-881, 2012.

23. Fisher, M, Ackley, T, Richard, K, Oei, B, Dealy, CN: Osteoarthritis at the Cellular Level: Mechanisms, Clinical Perspectives, and Insights From Development. In: *Encyclopedia of Biomedical Engineering*. 2019, pp 660-676.
24. Fox, AJS, Bedi, A, Rodeo, SA: The basic science of articular cartilage: structure, composition, and function. *Sports Health*, 1: 461-468, 2009.
25. De Bari, C, Roelofs, AJ: Stem cell-based therapeutic strategies for cartilage defects and osteoarthritis. *Curr Opin Pharmacol*, 40: 74-80, 2018.
26. Loeser, RF: Aging and osteoarthritis. *Curr Opin Rheumatol*, 23: 492-496, 2011.
27. Lepage, SIM, Robson, N, Gilmore, H, Davis, O, Hooper, A, St John, S, Kamesan, V, Gelis, P, Carvajal, D, Hurtig, M, Koch, TG: Beyond Cartilage Repair: The Role of the Osteochondral Unit in Joint Health and Disease. *Tissue Eng Part B Rev*, 25: 114-125, 2019.
28. Medvedeva, EV, Grebenik, EA, Gornostaeva, SN, Telpuhov, VI, Lychagin, AV, Timashev, PS, Chagin, AS: Repair of Damaged Articular Cartilage: Current Approaches and Future Directions. *Int J Mol Sci*, 19, 2018.
29. Nam, Y, Rim, YA, Lee, J, Ju, JH: Current Therapeutic Strategies for Stem Cell-Based Cartilage Regeneration. *Stem Cells Int*, 2018: 8490489, 2018.
30. Madeira, C, Santhagunam, A, Salgueiro, JB, Cabral, JM: Advanced cell therapies for articular cartilage regeneration. *Trends Biotechnol*, 33: 35-42, 2015.
31. Im, GI: Endogenous Cartilage Repair by Recruitment of Stem Cells. *Tissue Eng Part B Rev*, 22: 160-171, 2016.
32. Mouw, JK, Connelly, JT, Wilson, CG, Michael, KE, Levenston, ME: Dynamic compression regulates the expression and synthesis of chondrocyte-specific matrix molecules in bone marrow stromal cells. *Stem Cells*, 25: 655-663, 2007.
33. Salinas, EY, Hu, JC, Athanasiou, K: A Guide for Using Mechanical Stimulation to Enhance Tissue-Engineered Articular Cartilage Properties. *Tissue Eng Part B Rev*, 24: 345-358, 2018.

34. Jeon, JE, Schrobback, K, Hutmacher, DW, Klein, TJ: Dynamic compression improves biosynthesis of human zonal chondrocytes from osteoarthritis patients. *Osteoarthritis Cartilage*, 20: 906-915, 2012.
35. Li, K, Zhang, C, Qiu, L, Gao, L, Zhang, X: Advances in Application of Mechanical Stimuli in Bioreactors for Cartilage Tissue Engineering. *Tissue Eng Part B Rev*, 23: 399-411, 2017.
36. DiDomenico, CD, Goodearl, A, Yarilina, A, Sun, V, Mitra, S, Sterman, AS, Bonassar, LJ: The Effect of Antibody Size and Mechanical Loading on Solute Diffusion Through the Articular Surface of Cartilage. *J Biomech Eng*, 139, 2017.
37. DiDomenico, CD, Lintz, M, Bonassar, LJ: Molecular transport in articular cartilage - what have we learned from the past 50 years? *Nat Rev Rheumatol*, 14: 393-403, 2018.
38. Coleman, JL, Widmyer, MR, Leddy, HA, Utturkar, GM, Spritzer, CE, Moorman, CT, 3rd, Guilak, F, DeFrate, LE: Diurnal variations in articular cartilage thickness and strain in the human knee. *J Biomech*, 46: 541-547, 2013.
39. Sanchez-Adams, J, Leddy, HA, McNulty, AL, O'Connor, CJ, Guilak, F: The mechanobiology of articular cartilage: bearing the burden of osteoarthritis. *Curr Rheumatol Rep*, 16: 451, 2014.
40. Elder, BD, Athanasiou, K.A.: Hydrostatic Pressure in Articular Cartilage Tissue Engineering: From Chondrocytes to Tissue Regeneration. *Tissue Eng Part B*, 15, 2009.
41. Lee, JK, Huwe, LW, Paschos, N, Aryaei, A, Gegg, CA, Hu, JC, Athanasiou, KA: Tension stimulation drives tissue formation in scaffold-free systems. *Nat Mater*, 16: 864-873, 2017.
42. Shahin, K, Doran, PM: Shear and Compression Bioreactor for Cartilage Synthesis. *Methods in molecular biology (Clifton, NJ)*, 1340: 221-233, 2015.
43. Weber, JF, Perez, R, Waldman, SD: Mechanobioreactors for Cartilage Tissue Engineering. *Methods in molecular biology (Clifton, NJ)*, 1340: 203-219, 2015.
44. Darling, EMAKA: Articular Cartilage Bioreactors and Bioprocesses. *Tissue Eng*, 9, 2003.

45. Concaro, S, Gustavson, F, Gatenholm, P: Bioreactors for Tissue Engineering of Cartilage. In, 2008.
46. Anderson, DE, Johnstone, B: Dynamic Mechanical Compression of Chondrocytes for Tissue Engineering: A Critical Review. *Front Bioeng Biotechnol*, 5: 76, 2017.
47. Wong, M, Carter, DR: Articular cartilage functional histomorphology and mechanobiology: a research perspective. *Bone*, 33: 1-13, 2003.
48. O'Hara, BPU, J.P.; Maroudas, A.: Influence of cyclic loading on the nutrition of articular cartilage. *Ann Rheum Dis*, 49: 536-539, 1990.
49. Grodzinsky, AJL, M.E.; , Jin, M, Frank, E: Cartilage tissue remodeling in response to mechanical forces. *Annu Rev Biomed*, 02: 691–713, 2000.
50. Lucchinetti, E, Adams, CS, Horton, WE, Jr., Torzilli, PA: Cartilage viability after repetitive loading: a preliminary report. *Osteoarthritis Cartilage*, 10: 71-81, 2002.
51. Torzilli P.A.; Grigiene, R: Continuous cyclic load reduces proteoglycan release from articular cartilage. *Osteoarthritis and Cartilage* 6: 260-268, 1998.
52. Fitzgerald, JB, Jin, M, Grodzinsky, AJ: Shear and compression differentially regulate clusters of functionally related temporal transcription patterns in cartilage tissue. *J Biol Chem*, 281: 24095-24103, 2006.
53. Darling E.M., Athanasiou, KA: Articular Cartilage Bioreactors and Bioprocesses. *Tissue Eng* 9, 2003.
54. Bonzani, IC, Campbell, JJ, Knight, MM, Williams, A, Lee, DA, Bader, DL, Stevens, MM: Dynamic compressive strain influences chondrogenic gene expression in human periosteal cells: a case study. *J Mech Behav Biomed Mater*, 11: 72-81, 2012.
55. Sauerland, K, Steinmeyer, J: Intermittent mechanical loading of articular cartilage explants modulates chondroitin sulfate fine structure. *Osteoarthritis Cartilage*, 15: 1403-1409, 2007.
56. Steinmeyer, J, Knue, S., Raiss, R.H., Pelzer, I.: Effects of intermittently applied cyclic loading on proteoglycan metabolism and swelling behaviour of articular cartilage explants. *Osteoarthritis and Cartilage*, 7: 155-164, 1999.

57. Sauerland, K, Raiss, RX, Steinmeyer, J: Proteoglycan metabolism and viability of articular cartilage explants as modulated by the frequency of intermittent loading. *Osteoarthritis and Cartilage*, 11: 343-350, 2003.
58. Caron, MM, Emans, PJ, Coolson, MM, Voss, L, Surtel, DA, Cremers, A, van Rhijn, LW, Welting, TJ: Redifferentiation of dedifferentiated human articular chondrocytes: comparison of 2D and 3D cultures. *Osteoarthritis Cartilage*, 20: 1170-1178, 2012.
59. Chen, JLD, L.; Zhu, W.; Xiong, J.; Wang, D.: Extracellular matrix production in vitro in cartilage tissue engineering. *Journal of Translational Medicine*, 12, 2014.
60. Andersen, T, Auk-Emblem, P, Dornish, M: 3D Cell Culture in Alginate Hydrogels. *Microarrays (Basel)*, 4: 133-161, 2015.
61. Häuselmann, HJF, R.J.; Mok, S.S.; Schmid, T.M.; Block, J.A.; Aydelotte, M.B.; Kuettner, K.E.; Thonar, E.; Phenotypic stability of bovine articular chondrocytes after long-term culture in alginate beads. *Journal of Cell Science* 107: 17-27, 1994.
62. Kuo, CKM, P.X.;; Ionically crosslinked alginate hydrogels as scaffolds for tissue engineering: Part 1. Structure, gelation rate and mechanical properties. *Biomaterials*, 22: 511- 521, 2001.
63. Lee, KY, Mooney, DJ: Alginate: properties and biomedical applications. *Prog Polym Sci*, 37: 106-126, 2012.
64. Takeshita, S, Oda, T: Usefulness of Alginate Lyases Derived from Marine Organisms for the Preparation of Alginate Oligomers with Various Bioactivities. *Adv Food Nutr Res*, 79: 137-160, 2016.
65. Alba, KK, V.;; Seaweed Polysaccharides (Agar, Alginate Carrageenan). In: *Reference Module in Food Science*. edited by SMITHERS, G. W., Elsevier, 2018.
66. Grässel, S: Collagens in Hyaline Cartilage. In: *Cartilage: Volume 1: Physiology and Development*. edited by GRÄSSEL, S. A., A., Susanne Grässel, Attila Aszódi, 2016, pp 267.
67. Doyle, AD: Generation of 3D Collagen Gels with Controlled Diverse Architectures. *Curr Protoc Cell Biol*, 72: 10 20 11-10 20 16, 2016.

68. Zeeman, R, ; Dijkstra, PJ.,; van Wachem, PB.,; van Luyn, MJA.,; Hendriks, M.,; Cahalan, PT.,; Feijen, J.,: The kinetics of 1,4-butanediol diglycidyl ether crosslinking of dermal sheep collagen. *Journal of Biomedical Materials Research*, 5: 541-548, 1999.
69. De Boulle, K, Glogau, R, Kono, T, Nathan, M, Tezel, A, Roca-Martinez, JX, Paliwal, S, Stroumpoulis, D: A review of the metabolism of 1,4-butanediol diglycidyl ether-crosslinked hyaluronic acid dermal fillers. *Dermatol Surg*, 39: 1758-1766, 2013.
70. Yamada, M, Sekiguchi, K: Molecular Basis of Laminin-Integrin Interactions. *Curr Top Membr*, 76: 197-229, 2015.
71. Rodin, S, Antonsson, L, Hovatta, O, Tryggvason, K: Monolayer culturing and cloning of human pluripotent stem cells on laminin-521-based matrices under xeno-free and chemically defined conditions. *Nat Protoc*, 9: 2354-2368, 2014.
72. Rennert, RC, Sorkin, M, Garg, RK, Gurtner, GC: Stem cell recruitment after injury: lessons for regenerative medicine. *Regenerative Medicine*, 7: 833-850, 2012.
73. Karagianni, MS, T.J.; Bieback, K.: Towards Clinical Application of Mesenchymal Stromal Cells: Perspectives and Requirements for Orthopaedic Applications. In: *Tissue Regeneration From Basic Biology to Clinical Application*. edited by DAVIES, J., London, UK IntechOpen, 2012.
74. Richter, W: Mesenchymal stem cells and cartilage in situ regeneration. *J Intern Med*, 266: 390-405, 2009.
75. Solchaga, LA, Penick, KJ, Welter, JF: Chondrogenic differentiation of bone marrow-derived mesenchymal stem cells: tips and tricks. *Methods in molecular biology (Clifton, NJ)*, 698: 253-278, 2011.
76. Fellows, CR, Matta, C, Zakany, R, Khan, IM, Mobasheri, A: Adipose, Bone Marrow and Synovial Joint-Derived Mesenchymal Stem Cells for Cartilage Repair. *Front Genet*, 7: 213, 2016.
77. Toh, WS, Foldager, CB, Pei, M, Hui, JH: Advances in mesenchymal stem cell-based strategies for cartilage repair and regeneration. *Stem Cell Rev Rep*, 10: 686-696, 2014.
78. Friedl, P, Wolf, K: Plasticity of cell migration: a multiscale tuning model. *J Cell Biol*, 188: 11-19, 2010.

79. Yamada, KM, Sixt, M: Mechanisms of 3D cell migration. *Nat Rev Mol Cell Biol*, 20: 738-752, 2019.
80. Doyle, AD, Wang, FW, Matsumoto, K, Yamada, KM: One-dimensional topography underlies three-dimensional fibrillar cell migration. *J Cell Biol*, 184: 481-490, 2009.
81. Petrie, RJ, Gavara, N, Chadwick, RS, Yamada, KM: Nonpolarized signaling reveals two distinct modes of 3D cell migration. *J Cell Biol*, 197: 439-455, 2012.
82. Parsons, JT, Horwitz, AR, Schwartz, MA: Cell adhesion: integrating cytoskeletal dynamics and cellular tension. *Nat Rev Mol Cell Biol*, 11: 633-643, 2010.
83. Caswell, PT, Zech, T: Actin-Based Cell Protrusion in a 3D Matrix. *Trends Cell Biol*, 28: 823-834, 2018.
84. Qu, F, Guilak, F, Mauck, RL: Cell migration: implications for repair and regeneration in joint disease. *Nat Rev Rheumatol*, 15: 167-179, 2019.
85. Ridley, AJS, M.A; Burridge, K.; Firtel, R.A.; Ginsberg, M.H.; Borisy, G.; Parsons, J.T.; Horwitz, A.R.:: Cell Migration: Integrating Signals from Front to Back. *Science*, 302: 1704-1709, 2003.
86. Petrie, RJ, Yamada, KM: At the leading edge of three-dimensional cell migration. *J Cell Sci*, 125: 5917-5926, 2012.
87. Mierke, CT: Physical view on migration modes. *Cell Adh Migr*, 9: 367-379, 2015.
88. Bergert, M, Erzberger, A, Desai, RA, Aspalter, IM, Oates, AC, Charras, G, Salbreux, G, Paluch, EK: Force transmission during adhesion-independent migration. *Nat Cell Biol*, 17: 524-529, 2015.
89. de Lucas, B, Bernal, A, Perez, LM, San Martin, N, Galvez, BG: Membrane Blebbing Is Required for Mesenchymal Precursor Migration. *PLoS One*, 11: e0150004, 2016.
90. Charras, G, Sahai, E: Physical influences of the extracellular environment on cell migration. *Nat Rev Mol Cell Biol*, 15: 813-824, 2014.
91. Doyle, AD, Petrie, RJ, Kutys, ML, Yamada, KM: Dimensions in cell migration. *Curr Opin Cell Biol*, 25: 642-649, 2013.

92. Welch, MD: Cell migration, freshly squeezed. *Cell*, 160: 581-582, 2015.
93. Stoffel, M, Willenberg, W, Azarnoosh, M, Fuhrmann-Nelles, N, Zhou, B, Markert, B: Towards bioreactor development with physiological motion control and its applications. *Med Eng Phys*, 39: 106-112, 2017.
94. Shankar, KG, Gostynska, N, Montesi, M, Panseri, S, Sprio, S, Kon, E, Marcacci, M, Tampieri, A, Sandri, M: Investigation of different cross-linking approaches on 3D gelatin scaffolds for tissue engineering application: A comparative analysis. *Int J Biol Macromol*, 95: 1199-1209, 2017.
95. Schwarz, ML, Schneider-Wald, B, Brade, J, Schleich, D, Schutte, A, Reising, G: Instruments for reproducible setting of defects in cartilage and harvesting of osteochondral plugs for standardisation of preclinical tests for articular cartilage regeneration. *J Orthop Surg Res*, 10: 117, 2015.
96. Bieback, K, Hecker, A, Kocaomer, A, Lannert, H, Schallmoser, K, Strunk, D, Kluter, H: Human alternatives to fetal bovine serum for the expansion of mesenchymal stromal cells from bone marrow. *Stem Cells*, 27: 2331-2341, 2009.
97. Nebelung, S, Gavenis, K, Luring, C, Zhou, B, Mueller-Rath, R, Stoffel, M, Tingart, M, Rath, B: Simultaneous anabolic and catabolic responses of human chondrocytes seeded in collagen hydrogels to long-term continuous dynamic compression. *Ann Anat*, 194: 351-358, 2012.
98. Gamez, C, Khan, A.M., Torelli, A., Schneider-Wald, B., Gretz, N., Wolf, I., Bieback, K., Schwarz, ML.: Image processing workflow to visualize and quantify MSCs in 3D. *German Congress of Orthopedic and Trauma Surgery (DKOU 2018)*. Berlin, German Medical Science, 2018.
99. Dorland, YL, Cornelissen, AS, Kuijk, C, Tol, S, Hoogenboezem, M, van Buul, JD, Nolte, MA, Voermans, C, Huveneers, S: Nuclear shape, protrusive behaviour and in vivo retention of human bone marrow mesenchymal stromal cells is controlled by Lamin-A/C expression. *Sci Rep*, 9: 14401, 2019.
100. Yin, L, Wu, Y, Yang, Z, Tee, CA, Denslin, V, Lai, Z, Lim, CT, Lee, EH, Han, J: Microfluidic label-free selection of mesenchymal stem cell subpopulation during

- culture expansion extends the chondrogenic potential in vitro. *Lab Chip*, 18: 878-889, 2018.
101. Guo, KT, SchAfer, R, Paul, A, Gerber, A, Ziemer, G, Wendel, HP: A new technique for the isolation and surface immobilization of mesenchymal stem cells from whole bone marrow using high-specific DNA aptamers. *Stem Cells*, 24: 2220-2231, 2006.
102. Steinmeyer, J, Knue, S.: The Proteoglycan Metabolism of Mature Bovine Articular Cartilage Explants Superimposed to Continuously Applied Cyclic Mechanical Loading. *Biochem Biophys Res Commun*, 240: 216–221, 1997.
103. Branco, E, Cabral, R, Gomes, BD, Kfoury, JR, Jr., Miglino, MA: Bone marrow cells of swine: collection and separation. *Microsc Res Tech*, 75: 917-920, 2012.
104. Heino, TJ, Alm, JJ, Moritz, N, Aro, HT: Comparison of the osteogenic capacity of minipig and human bone marrow-derived mesenchymal stem cells. *J Orthop Res*, 30: 1019-1025, 2012.
105. Kaibuchi, N, Iwata, T, Onizuka, S, Yano, K, Yamato, M, Okano, T, Ando, T: Cytological character of mini pig mesenchymal stromal cells from various tissues and the attempt of cell sheet formation. *Regen Ther*, 6: 83-89, 2017.
106. Linard, C, Busson, E, Holler, V, Strup-Perrot, C, Lacave-Lapalun, JV, Lhomme, B, Prat, M, Devauchelle, P, Sabourin, JC, Simon, JM, Bonneau, M, Lataillade, JJ, Benderitter, M: Repeated autologous bone marrow-derived mesenchymal stem cell injections improve radiation-induced proctitis in pigs. *Stem Cells Transl Med*, 2: 916-927, 2013.
107. Tucker, D, Still, K, Blom, A, Hollander, AP, Kafienah, W, 2020.
108. Liu, X, Quan, N: Immune Cell Isolation from Mouse Femur Bone Marrow. *Bio Protoc*, 5, 2015.
109. Charif, NL, Y., Targa, L, Zhang, L., Li,Y., Mainard, D, Stoltz, J, De Isla, N: Higher Proliferative Potential of Human Mesenchymal Stromal Cells from Wharton’s Jelly Compared to Bone Marrow Is Linked to Decreased Senescence. In: STOLTZ, J. F. (Ed.), IOS Press, 2019 pp 6 - 14.
110. Dominici, M, Le Blanc, K, Mueller, I, Slaper-Cortenbach, I, Marini, F, Krause, D, Deans, R, Keating, A, Prockop, D, Horwitz, E: Minimal criteria for defining

- multipotent mesenchymal stromal cells. The International Society for Cellular Therapy position statement. *Cytotherapy*, 8: 315-317, 2006.
111. McDaniel, JS, Antebi, B, Pilia, M, Hurtgen, BJ, Belenkiy, S, Necsoiu, C, Cancio, LC, Rathbone, CR, Batchinsky, AI: Quantitative Assessment of Optimal Bone Marrow Site for the Isolation of Porcine Mesenchymal Stem Cells. *Stem Cells Int*, 2017: 1836960, 2017.
112. Berg, S, Kutra, D, Kroeger, T, Strahle, CN, Kausler, BX, Haubold, C, Schiegg, M, Ales, J, Beier, T, Rudy, M, Eren, K, Cervantes, JI, Xu, B, Beuttenmueller, F, Wolny, A, Zhang, C, Koethe, U, Hamprecht, FA, Kreshuk, A: ilastik: interactive machine learning for (bio)image analysis. *Nat Methods*, 16: 1226-1232, 2019.
113. Arganda-Carreras, I, Kaynig, V, Rueden, C, Eliceiri, KW, Schindelin, J, Cardona, A, Sebastian Seung, H: Trainable Weka Segmentation: a machine learning tool for microscopy pixel classification. *Bioinformatics*, 33: 2424-2426, 2017.
114. Sommer, C, Hoefler, R, Samwer, M, Gerlich, DW: A deep learning and novelty detection framework for rapid phenotyping in high-content screening. *Mol Biol Cell*, 28: 3428-3436, 2017.
115. Nachtsheim, J, Dursun, G, Markert, B, Stoffel, M: Chondrocyte migration in an acellular tissue-engineered cartilage substitute. *PAMM*, 18, 2018.
116. Nachtsheim, J, Dursun, G, Markert, B, Stoffel, M: Chondrocyte colonisation of a tissue-engineered cartilage substitute under a mechanical stimulus. *Med Eng Phys*, 74: 58-64, 2019.
117. Matziolis, G, Tuischer, J., Kasper, G., Thompson, M., Bartmeyer, B., Krockner, D., Perka, C., Duda, G.: Simulation of Cell Differentiation in Fracture Healing: Mechanically Loaded Composite Scaffolds in a Novel Bioreactor System. *Tissue Eng*, 12, 2006.
118. Ode, A, Kopf, J, Kurtz, A, Schmidt-Bleek, K, Schrade, P, Kolar, P, Buttgeri, F, Lehmann, K, Huttmacher, DW, Duda, GN, Kasper, G: CD73 and CD29 concurrently mediate the mechanically induced decrease of migratory capacity of mesenchymal stromal cells. *European Cells and Materials*, 22: 26-42, 2011.

119. Steadman, JR, Rodkey, WG, Briggs, KK: Microfracture: Its History and Experience of the Developing Surgeon. *Cartilage*, 1: 78-86, 2010.
120. Rodin, S, Antonsson, L, Niaudet, C, Simonson, OE, Salmela, E, Hansson, EM, Domogatskaya, A, Xiao, Z, Damdimopoulou, P, Sheikhi, M, Inzunza, J, Nilsson, AS, Baker, D, Kuiper, R, Sun, Y, Blennow, E, Nordenskjold, M, Grinnemo, KH, Kere, J, Betsholtz, C, Hovatta, O, Tryggvason, K: Clonal culturing of human embryonic stem cells on laminin-521/E-cadherin matrix in defined and xeno-free environment. *Nat Commun*, 5: 3195, 2014.
121. Markert, CD, Guo, X, Skardal, A, Wang, Z, Bharadwaj, S, Zhang, Y, Bonin, K, Guthold, M: Characterizing the micro-scale elastic modulus of hydrogels for use in regenerative medicine. *J Mech Behav Biomed Mater*, 27: 115-127, 2013.
122. Chen, YS, Chen, YY, Hsueh, YS, Tai, HC, Lin, FH: Modifying alginate with early embryonic extracellular matrix, laminin, and hyaluronic acid for adipose tissue engineering. *J Biomed Mater Res A*, 104: 669-677, 2016.
123. Simpliciano, C, Clark, L, Asi, B, Chu, N, Mercado, M, Diaz, S, Goedert, M, Mobed-Miremadi, M: Cross-Linked Alginate Film Pore Size Determination Using Atomic Force Microscopy and Validation Using Diffusivity Determinations. *Journal of Surface Engineered Materials and Advanced Technology*, 03: 1-12, 2013.
124. Wang, N, Adams, G, Buttery, L, Falcone, FH, Stolnik, S: Alginate encapsulation technology supports embryonic stem cells differentiation into insulin-producing cells. *J Biotechnol*, 144: 304-312, 2009.
125. Zraikat, M, Shnyder, S, Sheldrake, H, Patterson, L: The Effect of cRGDfV on Behaviour in 3D Spheroid Invasion Assay and 2D Models. *Journal of Clinical Medicine and Therapeutics*, 2 2017.
126. Chen, Y, Ma, M, Cao, H, Wang, Y, Xu, Y, Teng, Y, Sun, Y, Liang, J, Fan, Y, Zhang, X: Identification of endogenous migratory MSC-like cells and their interaction with the implant materials guiding osteochondral defect repair. *Journal of Materials Chemistry B*, 7: 3993-4007, 2019.

127. Endres, M, Neumann, K, Haupl, T, Erggelet, C, Ringe, J, Sittinger, M, Kaps, C: Synovial fluid recruits human mesenchymal progenitors from subchondral spongioid bone marrow. *J Orthop Res*, 25: 1299-1307, 2007.
128. Lu, J, Shen, X, Sun, X, Yin, H, Yang, S, Lu, C, Wang, Y, Liu, Y, Huang, Y, Yang, Z, Dong, X, Wang, C, Guo, Q, Zhao, L, Sun, X, Lu, S, Mikos, AG, Peng, J, Wang, X: Increased recruitment of endogenous stem cells and chondrogenic differentiation by a composite scaffold containing bone marrow homing peptide for cartilage regeneration. *Theranostics*, 8: 5039-5058, 2018.
129. Ahn, CB, Lee, JH, Han, DG, Kang, HW, Lee, SH, Lee, JI, Son, KH, Lee, JW: Simulated microgravity with floating environment promotes migration of non-small cell lung cancers. *Sci Rep*, 9: 14553, 2019.
130. Wiedemann, MK, F.P.M.; Wolfgang, H.R.; Hanke, R.L.:: Effects of Altered Gravity on the Actin and Microtubule Cytoskeleton, Cell Migration and Neurite Outgrowth. In: *Self-organization and Pattern-formation in Neuronal Systems Under Conditions of Variable Gravity*. Springer, 2011, pp 167-186.
131. Niemeyer, P, Becher, C, Brucker, PU, Buhs, M, Fickert, S, Gelse, K, Gunther, D, Kaelin, R, Kreuz, P, Lutzner, J, Nehrer, S, Madry, H, Marlovits, S, Mehl, J, Ott, H, Pietschmann, M, Spahn, G, Tischer, T, Volz, M, Walther, M, Welsch, G, Zellner, J, Zinser, W, Angele, P: [Significance of Matrix-augmented Bone Marrow Stimulation for Treatment of Cartilage Defects of the Knee: A Consensus Statement of the DGOU Working Group on Tissue Regeneration]. *Z Orthop Unfall*, 156: 513-532, 2018.

8. Appendix

Appendix A

Table A1. Descriptive statistics of hBM-MSCs mobilized into alginate-Ln scaffolds. The SAS software was used to recover descriptive statistics of the cells mobilized into alginate-Ln scaffolds with the help of analysis scripts kindly provided by Mrs. Sylvia Büttner (Department of Medical Statistics, Biomathematics and Information Processing, Medical Faculty of Mannheim of the University of Heidelberg). These calculations correspond to the Fig. 16a.

ANOVA: Comparisons (Alginate)

The GLM Procedure

Dependent Variable: Cells per mm³

Source	DF	Sum of Squares	Mean Square	F Value	Pr > F
Model	3	289.9522917	96.6507639	9.38	<.0001
Error	44	453.3275000	10.3028977		
Corrected Total	47	743.2797917			

R-Square	Coeff Var	Root MSE	Cells per mm ³ Mean
0.390098	87.99030	3.209813	3.647917

Source	DF	Type III SS	Mean Square	F Value	Pr > F
Loading	1	64.1718750	64.1718750	6.23	0.0164
Viability	1	203.7752083	203.7752083	19.78	<.0001
Loading*Viability	1	22.0052083	22.0052083	2.14	0.1510

Table A2. Analytical statistics of hBM-MSCs mobilized into alginate-Ln scaffolds. The SAS software was used to recover descriptive statistics of the cells mobilized into alginate scaffolds with the help of analysis scripts kindly provided by Mrs. Sylvia Büttner (Department of Medical Statistics, Biomathematics and Information Processing, Medical Faculty of Mannheim of the University of Heidelberg). These calculations correspond to the Fig. 16a.

ANOVA: Comparisons (Alginate)

The GLM Procedure

Least Squares Means

Adjustment for Multiple Comparisons: Sidak

Loading	Viability	Cells per mm ³ LSMEAN	LSMEAN Number
+Loading	Non-viable	2.06666667	1
+Loading	Viable	7.54166667	2
-Loading	Non-viable	1.10833333	3
-Loading	Viable	3.87500000	4

Least Squares Means for effect Loading*Viability
Pr > |t| for H0: LSMean(i)=LSMean(j)

Dependent Variable: Cells per mm³

i/j	1	2	3	4
1		0.0008	0.9774	0.6837
2	0.0008		<.0001	0.0447
3	0.9774	<.0001		0.2195
4	0.6837	0.0447	0.2195	

Appendix B

Table B1. Descriptive statistics of hBM-MSCs mobilized into collagen scaffolds. The SAS software was used to recover descriptive statistics of the cells mobilized into collagen scaffolds with the help of analysis scripts kindly provided by Mrs. Sylvia Büttner (Department of Medical Statistics, Biomathematics and Information Processing, Medical Faculty of Mannheim of the University of Heidelberg). These calculations correspond to the Fig. 19c.

ANOVA: Comparisons (Collagen)

The GLM Procedure

Dependent Variable: Cells per mm³

Source	DF	Sum of Squares	Mean Square	F Value	Pr > F
Model	3	456375.4804	152125.1601	173.00	<.0001
Error	40	35173.3612	879.3340		
Corrected Total	43	491548.8417			

R-Square	Coeff Var	Root MSE	Cells per mm ³	Mean
0.928444	41.82135	29.65357		70.90533

Source	DF	Type III SS	Mean Square	F Value	Pr > F
Loading	1	150816.9617	150816.9617	171.51	<.0001
Viability	1	178497.5101	178497.5101	202.99	<.0001
Loading*Viability	1	127061.0086	127061.0086	144.50	<.0001

Table B2. Analytical statistics of hBM-MSCs mobilized into collagen scaffolds. The SAS software was used to recover descriptive statistics of the cells mobilized into collagen scaffolds with the help of analysis scripts kindly provided by Mrs. Sylvia Büttner (Department of Medical Statistics, Biomathematics and Information Processing, Medical Faculty of Mannheim of the University of Heidelberg). These calculations correspond to the Fig. 19c.

ANOVA: Comparisons (Collagen)

The GLM Procedure

Least Squares Means

Adjustment for Multiple Comparisons: Sidak

Loading	Viability	Cells per mm³ LSMEAN	LSMEAN Number
+Loading	Non-viable	12.021037	1
+Loading	Viable	246.882044	2
-Loading	Non-viable	2.404207	3
-Loading	Viable	22.314050	4

Least Squares Means for effect Loading*Viability
Pr > |t| for H0: LSMean(i)=LSMean(j)

Dependent Variable: Cells per mm³

i/j	1	2	3	4
1		<.0001	0.9727	0.9621
2	<.0001		<.0001	<.0001
3	0.9727	<.0001		0.5457
4	0.9621	<.0001	0.5457	

Appendix C

Table C1. Comparison of the counts of cells in alginate-Ln and collagen scaffolds. The SAS software was used to perform a comparison between the cells mobilized into alginate and collagen scaffolds, using t-test with the help of analysis scripts kindly provided by Mrs. Sylvia Büttner (Department of Medical Statistics, Biomathematics and Information Processing, Medical Faculty of Mannheim of the University of Heidelberg). These calculations correspond to the Fig. 21a.

t-Test: Alginate/Collagen with Cells per mm³

The TTEST Procedure

Variable: Cells per mm³

Weight: gewichtung

group	N	Mean	Std Dev	Std Err	Minimum	Maximum
Alginate	48	3.6479	2.2960	0.5740	0	17.5000
Collagen	44	70.4029	63.3738	15.8435	0	378.5
Diff (1-2)		-66.7550	43.8363	15.4985		

group	Method	Mean	95% CL Mean		Std Dev
Alginate		3.6479	2.4932	4.8026	2.2960
Collagen		70.4029	38.4515	102.4	63.3738
Diff (1-2)	Pooled	-66.7550	-97.5454	-35.9645	43.8363
Diff (1-2)	Satterthwaite	-66.7550	-98.7249	-34.7851	

group	Method	95% CL Std Dev	
Alginate		1.9113	2.8759
Collagen		52.3609	80.2963
Diff (1-2)	Pooled	38.2617	51.3274
Diff (1-2)	Satterthwaite		

Method	Variances	DF	t Value	Pr > t
Pooled		Equal 90	-4.31	<.0001
Satterthwaite	Unequal	43.113	-4.21	0.0001

Equality of Variances

Method	Num DF	Den DF	F Value	Pr > F
Folded F	43	47	761.88	<.0001

Table C2. Analytical statistics of the comparison of the counts of cells in alginate-Ln and collagen scaffolds, ANOVA. The SAS software was used to perform an analysis of variance (ANOVA) on the number of cells found into alginate-Ln and collagen scaffolds, using the GLM procedure with the help of analysis scripts kindly provided by Mrs. Sylvia Büttner (Department of Medical Statistics, Biomathematics and Information Processing, Medical Faculty of Mannheim of the University of Heidelberg). These calculations correspond to the Fig. 21a.

ANOVA: Comparisons (Alginate/Collagen)

The GLM Procedure

Dependent Variable: Cells per mm³

Weight: gewichtung

Source	DF	Sum of Squares	Mean Square	F Value	Pr > F
Model	7	196084.3031	28012.0433	188.06	<.0001
Error	84	12511.7009	148.9488		
Corrected Total	91	208596.0040			

R-Square	Coeff Var	Root MSE	Cells per mm ³ Mean
0.940019	32.96239	12.20446	37.02540

Source	DF	Type III SS	Mean Square	F Value	Pr > F
group	1	35649.81445	35649.81445	239.34	<.0001
Loading	1	27555.15549	27555.15549	185.00	<.0001
Viability	1	33674.21779	33674.21779	226.08	<.0001
group*Loading	1	25426.44509	25426.44509	170.71	<.0001
group*Viability	1	29532.38296	29532.38296	198.27	<.0001
group*Loadin*Viability	2	44246.28733	22123.14366	148.53	<.0001

Table C3. Analytical statistics of the comparison of the counts of cells in alginate-Ln and collagen scaffolds, pairwise comparison. The SAS software was used to perform an analysis of variance (ANOVA) on the number of cells found into alginate and collagen scaffolds under loading or no loading, and taking into account the cell viability, using the GLM procedure with the help of analysis scripts kindly provided by Mrs. Sylvia Büttner (Department of Medical Statistics, Biomathematics and Information Processing, Medical Faculty of Mannheim of the University of Heidelberg). These calculations correspond to the Fig. 21a.

ANOVA: Comparisons (Alginate/Collagen)

The GLM Procedure

Least Squares Means

Adjustment for Multiple Comparisons: Sidak

group	Loading	Viability	Cells per mm ³ LSMEAN	LSMEAN Number
Alginate	+Loading	Non-viable	2.066667	1
Alginate	+Loading	Viable	7.541667	2
Alginate	-Loading	Non-viable	1.108333	3
Alginate	-Loading	Viable	3.875000	4
Collagen	+Loading	Non-viable	12.534435	5
Collagen	+Loading	Viable	243.336777	6
Collagen	-Loading	Non-viable	2.634298	7
Collagen	-Loading	Viable	23.106061	8

Least Squares Means for effect group*Loading*Viability

Pr > |t| for H0: LSMean(i)=LSMean(j)

Dependent Variable: Cells per mm³

i/j	1	2	3	4	5	6	7	8
1		1.0000	1.0000	1.0000	0.9993	<.0001	1.0000	0.3791
2	1.0000		1.0000	1.0000	1.0000	<.0001	1.0000	0.8869
3	1.0000	1.0000		1.0000	0.9972	<.0001	1.0000	0.2993
4	1.0000	1.0000	1.0000		1.0000	<.0001	1.0000	0.5553
5	0.9993	1.0000	0.9972	1.0000		<.0001	0.9997	0.9992
6	<.0001	<.0001	<.0001	<.0001	<.0001		<.0001	<.0001
7	1.0000	1.0000	1.0000	1.0000	0.9997	<.0001		0.4315
8	0.3791	0.8869	0.2993	0.5553	0.9992	<.0001	0.4315	

Appendix D

Table D1. Mechanical data of examinations made on hBM-MSCs with alginate-Ln scaffolds. Parameters as piston displacement, force, time and number of periods were calculated for all mechanical examinations for hBM-MSCs and pBM-MSCs. Force values in examinations with pBM-MSCs are given as amplitudes since the offset force of the bioreactor was unknown for this samples. For the force values of hBM-MSCs examinations the offset was subtracted. N= number of examinations performed in the bioreactor. The calculations were made with Origin software.

Data	N	Mean	Std			
			Dev	Min	Median	Max
Force amplitude (N)	12	1.16	0.42	0.69	1.15	2.23
Displacement (μm)	12	277.90	53.01	174.05	287.93	359.01
# periods	12	142.58	16.42	108.00	151.50	156.00
Time (h)	12	24.13	0.08	23.95	24.16	24.21

Table D2. Mechanical data of examinations made on hBM-MSCs with collagen scaffolds. Parameters as piston displacement, force, time and number of periods were calculated for all mechanical examinations for hBM-MSCs and pBM-MSCs. Force values in examinations with pBM-MSCs are given as amplitudes since the offset force of the bioreactor was unknown for this samples. For the force values of hBM-MSCs examinations the offset was subtracted. N= number of examinations performed in the bioreactor. The calculations were made with Origin software.

Data	N	Mean	Std			
			Dev	Min	Median	Max
Force amplitude (N)	11	1.08	0.13	0.88	1.09	1.25
Displacement (μm)	11	202.20	11.10	193.18	199.68	225.73
# periods	11	133.27	10.73	118.00	141.00	143.00
Time (h)	11	23.64	0.86	22.52	23.40	24.95

Appendix E



Fig. 23. Stress on the scaffold after the mechanical stimulation. A trace of mechanical stress was visible as an inner circumference after the scaffold was loaded, which corresponded with the cell reservoir circumference. Image taken from Ref. ⁴ with the permission of PLoS One, license CC-BY.

Appendix F

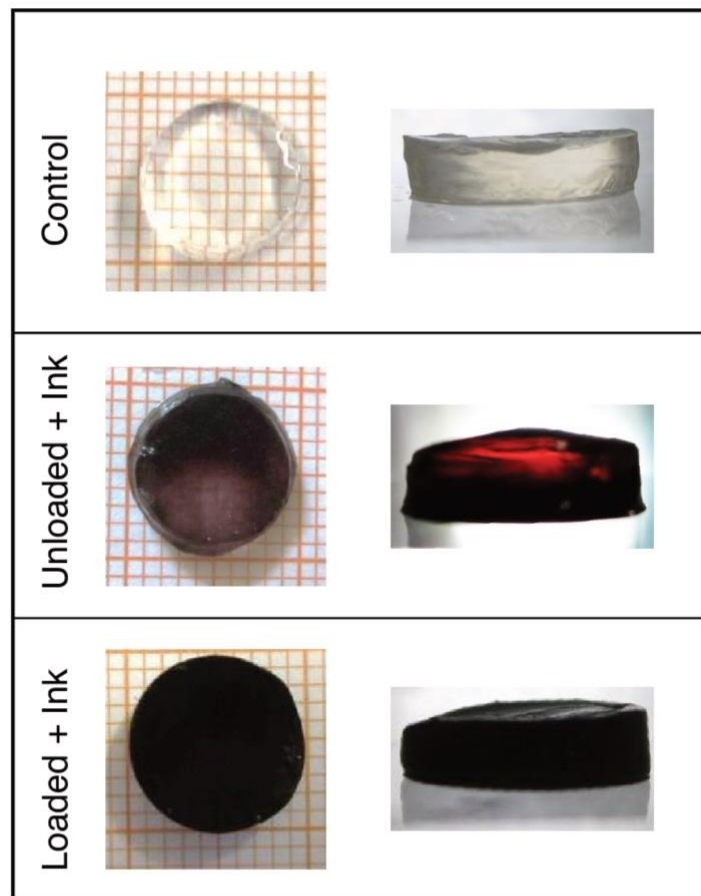


Fig. 24. Mechanical loading enhances the fluid uptake. Dark ink was placed in the cell reservoir compartment to explore whether loading modified the influx of the fluid. The control showed that the ink diffused into the scaffold showing an evident gradient, whereas loaded scaffold was totally stained. This suggested that mechanical loading induced fluid to move toward the scaffold. Image taken from Ref. ⁴ with the permission of PLoS One, license CC-BY.

Appendix G

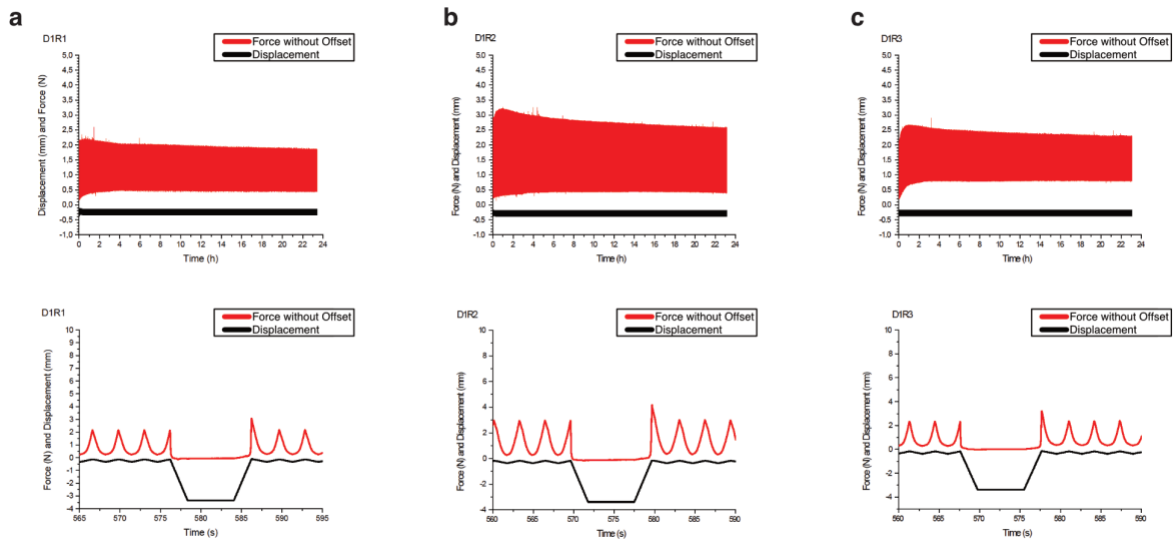


Fig. 25. Biomechanical data of three individual examinations from the same donor. Three independent examinations showed variations in the force and displacement but same behavior along the time. A few abrupt fluctuations were observed for the examinations. The upper panel shows the whole run and the lower the lift maneuver.

9. Curriculum vitae

Personal information

Name: Jeinmy Carolina
Surname: Gámez Villamizar
Date of birth: 05.08.1987
Place of birth: Bogotá, Colombia
Nationality: Colombian
Civil status: Unmarried
Email addresses: Carolina.Gamez@medma.uni-heidelberg.de,
carolina.gamezv@gmail.com

Academic qualifications

September 2016 - Now
Mannheim, Germany

Doctoral studies

Section of Experimental Orthopaedics and Trauma Surgery (OUZ)
Cooperative Research Training Group: Tissue Analytics for Stem Cell Based Diagnostics and Therapy (TACSdT)
Medical Faculty Mannheim of the University of Heidelberg
Thesis: “Mechanical stimulation of mesenchymal stem/stromal cells in a bioreactor system: An approach to mobilize cells into scaffolds”
Doctoral Advisor: Prof. Dr. Markus Schwarz
Heidelberg University

February 2013-August 2016
Bogotá, Colombia

Master in Sciences in Biochemistry

Physiological Sciences Department of the Medicine School
Medicine Faculty
National University of Colombia
Thesis: “Effect of the hypoxia on the redox behavior of carcinoma cell modified with the Na⁺/I⁻ transporter (NIS)”
Final mark: *magna cum laude*
Advisor: Ruth Garzón, Ph.D (University of Rosario)
Bogotá-Colombia

February 2007- April 2012
Bogotá, Colombia

Bachelor in Biology

Biology Department
Sciences Faculty
National University of Colombia
Bogotá-Colombia Exchange trainee
Thesis: “Analysis of internalization capability of the chimeric peptide HKPS in whole peripheral blood and red blood cells infected with *Plasmodium falciparum*”
Advisor: Jean Paul Vernot, Ph.D
Final Mark: Best Research Work of Undergraduate Programs
Graduation

Publications

- **Peer-reviewed publications**

Gamez C, Schneider-Wald B, Schuette A, Mack M, Hauk L, Khan AUM, Gretz N, Stoffel M, Bieback K, Schwarz ML. “Bioreactor for mobilization of mesenchymal stem/stromal cells into scaffolds under mechanical stimulation: Preliminary results”. *PLoS One*. 2020 Jan 10;15(1):e0227553”, doi: <https://doi.org/10.1371/journal.pone.0227553>.

Torres Crigna A., Daniele C, **Gamez C**, Medina Balbuena S, Pastene DO, Nardozi D, Brenna C, Yard B, Gretz N, Bieback K. “Stem/Stromal Cells for Treatment of Kidney Injuries with Focus on Preclinical Models”. *Frontiers Medicine* 2018; 5:179, doi: [10.3389/fmed.2018.00179](https://doi.org/10.3389/fmed.2018.00179).

- **Non peer-reviewed publications**

Gamez C., Schneider-Wald, B., Schuette, A., Mack, M., Hauk, L., Khan, AM., Bieback, K., Schwarz, ML “Intermittent dynamic mechanical stimulation induces recruitment of bone marrow derived-mesenchymal stem/stromal cells”. *German Medical Science*; 2019, doi: [10.3205/19dkou262](https://doi.org/10.3205/19dkou262). German Congress of Orthopedic and Trauma Surgery (DKOU 2019); October 22, 2019, Berlin, Germany.

Gamez C., Khan, AM., Torelli, A., Schneider-Wald, B., Gretz, N., Wolf, I., Bieback, K., Schwarz, ML Image processing workflow to visualize and quantify MSCs in 3D. *German Medical Science*; 2018. doi: [10.3205/18dkou491](https://doi.org/10.3205/18dkou491). German Congress of Orthopedic and Trauma Surgery (DKOU 2018); November 6, 2018, Berlin, Germany.

Patents

Schwarz, M, Bieback, K, Mack, X, Schneider-Wald, B, **Gámez-Villamizar, JC**: Erstellung eine Bioreaktors zur Simulation der in situ Regeneration vom Gelenkknorpel (Gebrauchsmusteranmeldung / amtliches Aktenzeichen: 20 2019 103 387.8)

Abbreviations

AC	Articular cartilage
ACI	Autologous chondrocyte implantation
Alginate-Ln	Alginate laminin scaffolds
BDDGE	1,4-butanediol diglycidyl ether
BM-MSCs	Bone marrow derived-mesenchymal stromal cells
C-AM	Calcein acetoxymethyl
COLA1	Collagen type-I
CTE	Cartilage tissue engineering
Cy7-PEI	Cyanine polyethyleneimine
DMEM	Dulbecco's Modified Eagle's Medium
ECM	Extracellular matrix
EthD-1	Ethidium homodimer-1
FBS	Fetal bovine serum
G	Alpha-L-guluronic acid
hBM-MSCs	Human bone marrow derived-mesenchymal stromal cells
Ln	Laminin
LN521	Human laminin 521
M	Beta-D-mannuronic acid
MACI	Matrix-induced autologous chondrocytes implantation
MSCs	Mesenchymal stromal cells
pBM-MSCs	Porcine bone marrow derived-mesenchymal stromal cells
PBS	Phosphate buffered solution
RT	Room temperature

List of figures

Fig. A1. Histology articular cartilage.

Fig. A2. Blood supply in an osteochondral unit.

Fig. A3. Therapies for articular cartilage regeneration *in situ*.

Fig. A4. Types of sample containers in compression bioreactors.

Fig. A5. Regimes of loading application.

Fig. A6. Chemical structure and ionic gelation of alginate.

Fig. A7. Collagen crosslinking.

Fig. A8. Potential applications of MSCs for AC regeneration.

Fig. A9. 3D migration mechanisms.

Fig. A10. Cell mechanotransduction.

Fig. B1. Problem and experimental question.

Fig. 1. The compression bioreactor.

Fig. 2. Bioreactor system.

Fig. 3. Alginate scaffold casting system.

Fig. 4. Isolation of pBM-MSCs from juvenile pigs.

Fig. 5. Mechanical data processing and analysis.

Fig. 6. Pipeline for cell quantification in 3D.

Fig. 7. Stiffness test of silicone rings.

Fig. 8. Yield of pBM-MSCs isolation.

Fig. 9. Surface markers of pBM-MSCs.

Fig. 10. Immunophenotype of pBM-MSCs isolated from different regions of the same femur.

Fig. 11. Immunophenotype of pBM-MSCs isolated from different legs.

Fig. 12. Staining optimization for cell visualization in 3D.

Fig. 13. Validation of cell quantification in 3D.

Fig. 14. From continuous to intermittent mechanical stimulation.

Fig. 15. pBM-MSCs mobilized into alginate or alginate-Ln scaffolds.

Fig. 16. hBM-MSCs mobilized into alginate-Ln scaffolds.

Fig. 17. Macroscopic observations of collagen and gelatin scaffolds fabrication.

Fig. 18. Microscopic observations of the collagen scaffolds.

Fig. 19. hBM-MSCs mobilized into collagen scaffolds.

Fig. 20. Morphometric of hBM-MSCs in the scaffolds.

Fig. 21. Comparison of counts of cells in alginate-Ln and collagen scaffolds.

Fig. 22. Biomechanical data.

Fig. 23. Stress on the scaffold after the mechanical stimulation.

Fig. 24. Mechanical loading enhances the fluid uptake.

Fig. 25. Biomechanical data of three individual examinations from the same donor.

List of tables

- Table 1. Hardware and software components of the bioreactor.
- Table 2. Collagen and gelatin scaffold fabrication.
- Table 3. Descriptive Statistics of the force at 10 % strain for elastic rings of 3 mm height.
- Table 4. Descriptive Statistics of the force at 10 % strain for elastic rings of 2 mm height.
- Table 5. Descriptive statistics hBM-MSCs in alginate-Ln scaffolds.
- Table 6. Descriptive statistics hBM-MSCs mobilized into collagen scaffolds.
- Table 7. Descriptive statistics of the mechanical stimulation parameters for the examinations with alginate-Ln and collagen scaffolds.
-
- Table A1. Descriptive statistics of hBM-MSCs mobilized into alginate-Ln scaffolds.
- Table A2. Analytical statistics of hBM-MSCs mobilized into alginate-Ln scaffolds.
- Table B1. Descriptive statistics of hBM-MSCs mobilized into collagen scaffolds.
- Table B2. Analytical statistics of hBM-MSCs mobilized into collagen scaffolds.
- Table C1. Comparison of the counts of cells in alginate-Ln and collagen scaffolds.
- Table C2. Analytical statistics of the comparison of the counts of cells in alginate-Ln and collagen scaffolds, ANOVA.
- Table C3. Analytical statistics of the comparison of the counts of cells in alginate-Ln and collagen scaffolds, pairwise comparison.
- Table D1. Mechanical data of examinations made on hBM-MSCs with alginate-Ln scaffolds.
- Table D2. Mechanical data of examinations made on hBM-MSCs with collagen scaffolds.

Acknowledgments

I would like to express my sincere gratitude to my supervisor Prof. Dr. Markus Schwarz, for his supervision, support, guidance, permanent feedback, constructive suggestions and infinite patience along this research process.

I express my deep gratitude to Prof. Dr. Bieback, for her supervision and unrestricted support. For have always being open to listen to me and give advice. She has been pivotal in carrying forward critical experiments for the completion of this thesis work.

I am particularly grateful to Dr. Barbara Schneider for her constructive and valuable suggestions during the planning and development of this thesis, for her excellent guidance and knowledge. I thank her for being unconditional, for her impressive solidarity and kindness to me every day.

I am sincerely grateful to Prof. Dr. Norbert Gretz and Prof. Dr. Mattias Hafner for the enormous and excellent work coordinating the Doctoral Program “Cooperative Research Training Group Tissue Analytics for Stem Cell based Diagnostics and Therapy (TASCDT)” and for the opportunity given to me to take part of this group. In particular, I am deeply grateful to Prof. Gretz for his constant support.

My gratitude is also extended to all my colleagues from the OUZ: Dr. Schneider, Gregor Reising, Andy Schütte, Michael Mack, Ralf Gundling, Dieter Schleicht and Luisa Hauk for their support, constant help and their permanent good mood. I want to thank in particular the engineers Mr. Schütte and Mr. Mack for their huge collaboration and contribution with the bioreactor software and hardware, and Mr. Schleicht for being always ready to build the every new part of the bioreactor.

I would like to thank Mrs. Sina Schwalm for her marvelous organization with the bureaucratic issues of the Graduate Academy, for her good attitude and being always available to listen.

My gratitude to Mrs. Sylvia Büttner and Prof. Dr. Christel Weiß for the excellent statistical support.

My gratitude is also extended to all my colleagues from the TASCDDT graduate academy for their companion- and friendship. In particular to Angelo Torelli for his computational support.

I would especially thank Dr. Arif Khan for his constant support during the whole image analysis, for his friendship and optimism.

I would like also thank all who supported me with any technical or biological supply: Prof. Dr. Norbert Gretz, Prof. Dr. Schmelz, Mrs. Stefanie Uhlig, Adriana Torres Crigna and Stefania Palumbo; and the ZMF, LIMA, and FlowCore facilities.

Last but not least, I am deeply grateful to my family, to my parents and siblings for believing in me and for being always there despite of the distance, and I am especially thankful to Andrés for his remarkable and unconditional support and for being with me through this important journey of my life.

